Title
Parallel and Competitive Processes in Low-Level Vision and Their Impact on Awareness

Author
Denison, Rachel

Publication Date
2013

Peer reviewed|Thesis/dissertation

Parallel and Competitive Processes in Low-Level Vision and Their Impact on Awareness

by

Rachel Nicole Denison

A dissertation submitted in partial satisfaction of the

requirements for the degree of

Doctor of Philosophy

in

Neuroscience

and the Designated Emphasis

in

Computational Science and Engineering

in the

Graduate Division

of the

University of California, Berkeley

Committee in charge:

Professor Michael A. Silver, Chair
Professor Jack Gallant
Professor Stephen Palmer
Professor David Whitney

Fall 2013

Abstract

Parallel and Competitive Processes in Low-Level Vision and Their Impact on Awareness

by

Rachel Nicole Denison

Doctor of Philosophy in Neuroscience

Designated Emphasis in Computational Science and Engineering

University of California, Berkeley

Professor Michael Silver, Chair

Perception consists of the brain's single best interpretation of the sensory world at a given moment in time. Multiple channels of visual input – be they from the two eyes or from the many parallel visual pathways that originate as early as the retina – must be reconciled to arrive at a unified percept. The fact that this must occur in roughly real time as the visual scene changes poses special challenges and constraints. I investigated two classes of visual processes relevant for the perception of time-varying visual stimuli: prediction, with a probable neural substrate in early visual cortical areas, and parallel processing in the magnocellular (M) and parvocellular (P) pathways.

In Chapters 2 and 3, I asked how prediction and parallel pathways, respectively, contribute to perceptual selection using dynamic binocular rivalry stimuli. In binocular rivalry, incompatible images presented to the two eyes result in just one of the images being selected for awareness at any given time. This bistability makes rivalry a useful tool for the study of perceptual selection. In Chapter 2, we found that predictive context in the form of an unambiguous rotating grating biased perceptual selection during subsequent rivalry towards the expected next grating in the rotation sequence, compared to an orthogonal grating. This provided evidence that a prediction-like process influences perceptual selection during rivalry between gratings, which other work has shown is likely resolved at early stages of visual processing.

In Chapter 3, we studied spatial, temporal, luminance, and chromatic factors influencing perceptual selection during interocular switch rivalry. In this type of rivalry, flickering orthogonal gratings are periodically exchanged between the two eyes, resulting in either the perception of a fast, regular alternation between orthogonally oriented gratings (similar to the display presented to a single eye) or a slow, irregular alternation, a percept that requires integration across the two eyes over time. We found that stimuli biased toward the M pathway increased the prevalence of fast, regular alternations, while stimuli biased toward the P pathway increased the prevalence of slow, irregular alternations. This finding suggested that the M and P pathways can make distinct contributions to

perception during binocular rivalry and led us to propose a new framework for understanding perceptual selection during interocular switch rivalry.

Physiological measurement of activity in the M and P pathways can lead to greater understanding of how these pathways contribute to perceptual experience, but methods for measuring functional signals from the M and P pathways of humans have been lacking. Therefore, in Chapter 4, we developed a procedure for functionally mapping the M and P subdivisions of human LGN, the site where these pathways are most clearly segregated, using functional magnetic resonance imaging (fMRI). We observed a gradient of more M-like to more P-like responses across the LGN. Importantly, this gradient had a spatial layout consistent with known LGN anatomical organization. This new method for localizing the M and P subdivisions of the LGN provides a way forward for investigating the function of these pathways in human visual perception, in both healthy and clinical populations.

In summary, prediction and parallel processing are two classes of mechanisms that contribute to perception of dynamic visual stimuli. Here we have shown how such mechanisms operating at low levels of the visual system can help resolve competition between percepts, thereby affecting the contents of visual awareness. In addition, we developed a method for the physiological study of the M and P LGN subdivisions in the human brain, which is a promising technique for the future investigation of the roles of the M and P pathways in human visual perception, among other applications.

To my parents,
Joan and Robert

Table of Contents

Acknowledgments

My thanks, first, to my advisor, Michael Silver. His good humor, open-minded curiosity, and scientific generosity have been both a pleasure and an example. I have benefitted greatly from his clarity and precision as a scientist and his fundamental decency and conscientiousness as a mentor. For five years, he has offered me the twin gifts of space and time and unwavering support to use them.

My graduate education has been enlivened by helpful and thought-provoking discussions, not to mention classes, rotations, and chats during intermission, with the other members of my thesis committee: Jack Gallant, Steve Palmer, and Dave Whitney. I feel privileged to have worked with them.

I would like to thank my fellow Silver Lab members past and present for creating a friendly and supportive lab community. Special thanks to the most important of my teachers in lab: Ariel Rokem, Caterina Gratton, Summer Sheremata, Elise Piazza, David Bressler, and Ayelet Landau. Each of them has given me an example of doing science with joy, integrity, and personal flair, along with practical guidance. Ariel, Caterina, and Summer were the ones I turned to most along the way, and they were unfailingly generous with their expertise, insight, enthusiasm, and sheer hours spent in scientific and moral support. I have been lucky to have all of them as colleagues and friends.

It has been my fortune to work with outstanding collaborators on the projects described in this dissertation. Elise contributed to the experiments of Chapter 2, and I have appreciated her thoughtful and steady approach in our continued collaborations. Joseph Vu, Essa Yacoub, and David Feinberg each offered special expertise and essential support to the experiments of Chapter 4. They deepened my knowledge of fMRI and introduced me to the thrill of working at the edge of scientific technology. Karen De Valois also provided helpful early discussions on this project. I am grateful, too, to the dedication and help of the undergraduate research assistants and graduate rotation students who worked with me over the years, especially RAs Jake Sheynin, Max Schram, and Chris Vasilas.

My experience at Berkeley has been much the richer for the wonderful visual perception community here, including the Whitney, Palmer, Prinzmetal, Robertson, and Gallant labs; outstanding teaching from Bruno Olshausen and rotation mentorship (and beyond) from Rich Ivry; lively discussions with Wendy de Heer and the members of the Time Club journal club; and the lovely combination of inspiration and fun offered by the community of graduate students in the Helen Wills Neuroscience Institute. Within this community, I would especially like to

thank the members of my own class, whose friendship, talents, and good spirits have always made this ride better.

I am indebted to my previous mentors for the exceptional opportunities they provided me: my undergraduate advisor Marvin Chun, at Yale, and the incomparable Jon Driver, at University College London. Thanks to Dave Balota, at Washington University in St. Louis, for his generosity in introducing me to cognitive psychology and treating me like a colleague, even though I still couldn't drive.

Outside of the university, I am deeply grateful for the friendship of so many, and for the myriad ways in which friends are friends. Thanks to Rachel Lesser, Elana Nashelsky, and Miriam Bowring for creating a sense of home in Berkeley; Melody Chan and Amy Katzen for freewheeling talks and good council; and Antony Millner and Lauren Steyn for their keen appreciation and ready sharing of life's finer adventures. For their good music and fellowship, I'd like to thank the members of my string quartet: Rachel, Melody, Andy Eggleston, Serena Le, and Mira Frick. And for their enduring friendship: Emily Kopley, whose steady spirit and generous wit were a beacon across the bay; and Abigail Deutsch, whose wisdom, warmth, humor, and acuity have given me years of solace and delight.

Lastly, my total thanks to Liza Flum for her unflagging support, perceptivity, and camaraderie. And to my family, profound thanks for a lifetime of love and encouragement; and especially to my parents, Joan and Robert Denison, who suggested I could do anything I wanted and have always done whatever they could to help.

Chapter 1

Introduction

Sensory input is often impoverished and ambiguous. A snapshot from the retina may be consistent with many possible interpretations of the state of the world. For example, an image of a shaded surface might correspond to either a convex bump lit from above or a concave dimple lit from below (Figure 1A). However, we don't see a probability distribution over world states: our visual experience is not "70% bump, 30% dimple." The brain picks just one interpretation, and our perceptual experience is typically single and unified. This choice of one out of many interpretations is called perceptual selection.

Perceptual selection has often been studied using bistable (or multistable) images, which have two or more strong but mutually incompatible perceptual interpretations (Blake and Logothetis, 2002; Long and Toppino, 2004). These ambiguous figures are thought to provide a window into the mechanisms of perceptual selection, since the perceptual interpretation can change even while the physical stimuli remain constant. This allows the specific contents of perception to be attributed to the brain instead of to the world.

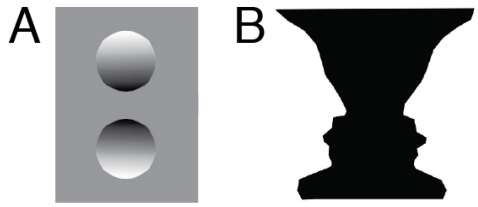

Figure 1. Ambiguous images. (A) A shaded surface can appear as convex or concave, depending on the assumed location of the light source. If light is assumed to be coming from above, the top image is seen as convex and the bottom image as concave. Assuming that light is coming from the bottom would lead to the opposite interpretation. (B) Rubin's bistable face-vase figure can be seen as a black vase on a white background or white faces on a black background, depending on the figure-ground assignment.

The term "bistability" implies the presence of world states that are stable across time. For example, Rubin's bistable face-vase figure (Rubin, 1915) contains the same vase and faces, drawn by the same contours, no matter when you look at it or for how long (Figure 1B). This stability has distinct experimental advantages. For example, changes in brain activity can be related to fluctuations in perception over long presentation durations or repeated trials (Sheinberg and Logothetis, 1997; Andrews et al., 2002; Grunewald et al., 2002). However, unlike the immutable faces and vase of Rubin's figure, actual world states are not so stable – imagine a busy street scene – and due to the movement of our bodies and eyes as we view the world, natural sensory input is even less so.

This thesis considers the problem of visual perceptual selection in the presence of changing visual input. Different mechanisms may govern the selection of dynamic compared to static

input, due both to the potential richness of temporal context in dynamic scenes and to the involvement of neural mechanisms specialized for processing visual changes. In addition, the relationship between brain dynamics and world dynamics must be given particular consideration when sensory input varies over time. These issues have received relatively little attention in studies of perceptual selection, perhaps in part due to the built-in stability of ambiguous images.

In our perceptual selection experiments, we studied a simple ambiguous stimulus in dynamic settings. We employed binocular rivalry, a type of display in which incompatible images presented to the two eyes compete for perceptual dominance (Wheatstone, 1838). When viewing a rivalry display, observers typically do not see an overlay or blend of the two images; rather, over time, perception alternates between the image shown to the left eye and the image shown to the right eye. Rivalry had the advantage, for our purposes, of being one of the most flexible paradigms employing ambiguous stimuli that is commonly used in psychophysics (Kim and Blake, 2005). Any pair of images shown to the two eyes, provided the images are sufficiently different from one another, can engage in rivalry, and the rivalrous images can change over time. To study rivalry in a dynamic context, we either embedded rivalrous images in unambiguous image sequences (Chapter 2) or used rivalry stimuli that were changing over time (Chapter 3).

The problem of perceptual selection given changing visual input should, at the outset, be distinguished from two related questions. The first is the dynamics of perception itself while an observer views a static bistable stimulus – for example, the distribution of percept durations during binocular rivalry (Fox and Herrmann, 1967; Levelt, 1967; Brascamp et al., 2005). The second is perceptual selection of bistable motion stimuli, such as a structure-from-motion rotating cylinder (Treue et al., 1991; Parker and Krug, 2003). Such stimuli, though they are not static, are nevertheless consistent with well-defined perceptual objects that are stable over time.

In contrast, the present work is most closely aligned with studies of basic mechanisms for parsing visual input over space and time. These include studies of low-level visual history effects, such as priming and adaptation, on perceptual selection during binocular rivalry (Blake and Overton, 1979; Pearson and Brascamp, 2008; Bressler et al., 2013), as well as work on the low-level mechanisms of spatiotemporal visual processing, in particular the magnocellular (M) and parvocellular (P) pathways. These pathways, which are most clearly segregated in the M and P subdivisions of the lateral geniculate nucleus (LGN), carry different types of spatial and temporal stimulus information in parallel at early stages of visual processing (Nassi and Callaway, 2009).

In the following chapters, I begin by asking two questions about how a single percept is constructed from dynamic visual input. The first is how recent stimulus history influences perceptual selection. The experiments described in Chapter 2 suggest that, during binocular rivalry, observers are more likely to see an image that is predicted by a preceding, unambiguous image sequence than they are to see the unexpected image (Denison et al., 2011). Second, I ask how different spatiotemporal channels in the visual system – specifically the M and P pathways – mediate perceptual selection of a dynamic stimulus. Chapter 3 provides evidence for distinct contributions of these two pathways to perception during a special, dynamic form of binocular rivalry (Logothetis et al., 1996) and proposes a theoretical alternative to previous hierarchical models of this form of rivalry (Denison and Silver, 2012).

The evidence from Chapter 3 on the contributions of the M and P pathways to perceptual selection points to several questions, including how the two pathways converge or remain segregated in the human visual system (Sincich and Horton, 2005; Nassi and Callaway, 2009) and how activity in the M and P subdivisions of the LGN is related to perceptual experience (Schiller et al., 1990). These questions have proven challenging to study in humans, because answering them requires measurement of activity in the M and P subdivisions of the human LGN, ideally simultaneously with recording from visual cortical areas in order to capture larger-scale pathways. As a first step toward answering such questions and others concerning the function of the M and P pathways in human health and disease, Chapter 4 describes a procedure for functionally mapping the M and P subdivisions of the human LGN for the first time using fMRI (Denison et al., under review).

Together, these studies contribute to our understanding of perceptual selection given changing visual input, demonstrating a new type of integration of past and current input during binocular rivalry, and suggesting new ways of understanding and measuring the contributions of the M and P pathways to perception. This work explores specific mechanisms of what might be described as two general strategies for real-time vision – prediction and parallel processing – which together can hasten the brain's arrival at the best current interpretation of the visual world.

Chapter 2

Predictive context influences perceptual selection during binocular rivalry

2.1 ABSTRACT

Prediction may be a fundamental principle of sensory processing: it has been proposed that the brain continuously generates predictions about forthcoming sensory information. However, little is known about how prediction contributes to the selection of a conscious percept from among competing alternatives. Here, we used binocular rivalry to investigate the effects of prediction on perceptual selection. In binocular rivalry, incompatible images presented to the two eyes result in a perceptual alternation between the images, even though the visual stimuli remain constant. If predictive signals influence the competition between neural representations of rivalrous images, this influence should generate a bias in perceptual selection that depends on predictive context. To manipulate predictive context, we developed a novel binocular rivalry paradigm in which rivalrous test images were immediately preceded by a sequence of context images presented identically to the two eyes. One of the test images was consistent with the preceding image sequence (it was the expected next image in the series), and the other was inconsistent (non-predicted). We found that human observers were more likely to perceive the consistent image at the onset of rivalry, suggesting that predictive context biased selection in favor of the predicted percept. This prediction effect was distinct from the effects of adaptation to stimuli presented before the binocular rivalry test. In addition, perceptual reports were speeded for predicted percepts relative to non-predicted percepts. These results suggest that predictive signals related to visual stimulus history exist at neural sites that can bias conscious perception during binocular rivalry. Our paradigm provides a new way to study how prior information and incoming sensory information combine to generate visual percepts.

2.2 INTRODUCTION

The visual system often receives ambiguous patterns of stimulation that are compatible with multiple interpretations of the visual environment. It therefore must use additional information to construct a single perceptual interpretation of the world. What is the nature of this additional information, and how does the visual system combine this information with incoming sensory signals to determine the contents of perceptual experience at any given moment? One possibility, based on Bayesian accounts of perception, is that prior knowledge about the likely contents of a visual scene influences the interpretation of sensory signals (Helmholtz, 1866; Gregory, 1997; Weiss et al., 2002; Kersten et al., 2004; Knill and Pouget, 2004; Kveraga et al., 2007; Hohwy et

al., 2008). Indeed, expectations arising from repeated presentations of visual stimuli or explicit instructions have been shown to facilitate processing of expected stimuli, resulting in improved visibility (Sekuler and Ball, 1977; Eger et al., 2007; Esterman and Yantis, 2010; Melloni et al., 2011) and both speeded (James et al., 2000; Eger et al., 2007; Esterman and Yantis, 2010) and enhanced (Dolan et al., 1997) recognition of visual stimuli.

Since natural environments are structured in time, one potentially rich source of prior information is patterns of visual stimulation in the recent past. Predictive coding frameworks describe how such a prior might be represented by neural activity, proposing that the brain continuously generates predictions of forthcoming sensory signals (Rao and Ballard, 1999; Friston, 2005). Comparisons of brain activity during expected and unexpected sensory stimulation have provided physiological evidence consistent with these frameworks (Summerfield and Koechlin, 2008; Alink et al., 2010). However, the effects of predictive neural signals on conscious perception have not been well explored. In particular, little is known about how prediction may influence the selection of a specific percept from competing alternatives.

A few studies have used ambiguous stimuli to provide initial insights into this question. For example, it has been shown that pairing secondary cues with rotating stimuli whose direction of rotation is defined by binocular disparity allows these cues to influence perception of rotation direction when disparity information is removed, making the physical rotation direction ambiguous (Haijiang et al., 2006; Sterzer et al., 2008). Specifically, the secondary cues increase the probability that the ambiguous stimuli will be perceived to rotate in the same direction as in the preceding conditioning period, showing that cue-induced expectations can influence perceptual selection. In addition, priming one perceptual interpretation of a binocular rivalry stimulus using either unambiguous low contrast stimuli (Brascamp et al., 2007; Pearson et al., 2008) or mental imagery (Pearson et al., 2008) has been shown to bias perception during subsequent rivalry in favor of the primed percept.

Closer to the question of prediction, Maloney and colleagues (2005) found that recent visual experience influences the perception of an ambiguous apparent-motion quartet. In this study, subjects viewed sequences of quartets with unambiguous rotation directions followed by an ambiguous quartet that could be perceived as rotating either clockwise or counterclockwise. Subjects' perceptual reports were influenced by the pattern of the preceding sequence, with an increased probability of interpreting ambiguous motion in a manner that was consistent with the expectation generated by the sequence.

Binocular rivalry provides a powerful and well-studied paradigm for investigating the effects of predictive context on visual perceptual selection. Binocular rivalry occurs when incompatible images are presented to the two eyes, leading to a perceptual alternation between the images, even though the visual stimuli remain constant. Unlike many other types of multistable percepts (Liebert and Burk, 1985; Peterson, 1986; Toppino, 2003; Shimono et al., 2011), binocular rivalry is often only weakly susceptible to cognitive control (Meng and Tong, 2004). In addition, there is evidence that binocular rivalry can be resolved at stages of visual processing as early as monocular regions of V1 (Polonsky et al., 2000; Tong and Engel, 2001) and the LGN (Haynes et al., 2005; Wunderlich et al., 2005), although this point continues to be debated (Logothetis et al., 1996; Lee and Blake, 1999; Blake and Logothetis, 2002; Tong et al., 2006). Therefore, studying the effects of predictive context on perceptual selection in binocular rivalry may improve understanding of the role of expectation in early visual processing. In one theoretical proposal,

perceptual alternations during binocular rivalry are a product of predictive coding mechanisms (Hohwy et al., 2008), but specific hypotheses arising from this framework have not yet been experimentally tested.

In order to investigate the effects of predictive visual information on perceptual selection, we developed a novel binocular rivalry paradigm. On each trial, we first presented a sequence of identical images to the two eyes that generated an expectation about the next image in the series. We followed this predictive sequence with a rivalry display in which the predicted image was presented to one eye and a non-predicted image was presented to the other eye. We found that subjects were initially more likely to select the predicted image than the non-predicted image. In three additional experiments, we showed that only patterns of visual stimulation in the recent time period before the onset of rivalry contributed to the prediction effect and that prediction of the upcoming stimulus and adaptation to preceding stimuli had separate influences on perceptual selection. We also observed speeded perceptual selection of predicted relative to non-predicted stimuli. Our results suggest that predictive signals exist at neural sites that contribute to perceptual selection during binocular rivalry and emphasize the importance of prior information in determining the contents of conscious visual experience.

2.3 GENERAL METHODS

2.3.1 Subjects

Forty-five subjects participated in one or more of the experiments. Five data sets were excluded from analysis (see Subject exclusion section), resulting in a total of forty-one subjects (aged 18-41 years, 27 female), fifteen of whom participated in Experiment 1, eight in Experiment 2, sixteen in Experiment 3, and thirteen in Experiment 4. Two of the authors participated in two experiments, and one author participated in all four experiments. All subjects provided informed consent, and all experimental protocols were approved by the Committee for the Protection of Human Subjects at the University of California, Berkeley.

2.3.2 Visual stimuli

Stimuli were generated on a Macintosh PowerPC computer using Matlab and Psychophysics Toolbox (Brainard, 1997; Pelli, 1997) and were displayed on two halves of a gamma-corrected NEC MultiSync FE992 CRT monitor with a refresh rate of 60 Hz at a viewing distance of 100 cm. Subjects viewed all stimuli through a mirror stereoscope with their heads stabilized by a chin rest. Visual stimuli were circular patches, 1.8° in diameter, and were surrounded by a black annulus with a diameter of 2.6° and a thickness of 0.2°. Binocular presentation of this annulus allowed it to serve as a vergence cue to stabilize eye position and to ensure that the rivaling stimuli were presented to corresponding retinal locations in the two eyes. All stimuli were presented at 10% contrast on a neutral gray background (luminance of 59 cd/m^2), except in Experiment 4, in which the contrast of the stimuli was varied. All stimuli had the same mean luminance as the background.

On each trial, subjects viewed a stream of items presented identically to both eyes (the "pre-rivalry stream"), followed by a pair of rivalrous stimuli. A brief auditory cue signaled the start of each trial. Each stream item was presented for 300 ms and was followed by a 100 ms blank period. The rivalrous test stimuli were always two monochromatic, sinusoidal grating patches

with a spatial frequency of 3 cycles per degree (cpd) and orthogonal (+/-45°) orientations. Rivalrous stimuli were presented for 4, 5, or 10 seconds in Experiment 1 (fixed stimulus duration for a given subject, with N=4, 5, and 6, respectively), 5 seconds in Experiments 2 and 4, and 10 seconds in Experiment 3.

One of the rivalrous test gratings always had an orientation that was consistent with the preceding predictive context; that is, it was the expected next image following the pre-rivalry stream. We call this the "matching" stimulus, since it matches the predictive context. The orientation of the other rivalrous test grating (the "non-matching" stimulus) was orthogonal to that of the matching stimulus and was inconsistent with the predictive context.

2.3.3 Rivalry task

After passively viewing each pre-rivalry stream, subjects continuously reported their percept during presentation of the rivalrous test stimuli by holding down one of two keys: 1) grating tilted to the left, and 2) grating tilted to the right. Subjects were instructed to begin responding whenever the stimuli stopped moving or changing orientation in a regular fashion, to press a key continuously for as long as the corresponding percept persisted, and not to press any key for ambiguous percepts. Trials in which there was no response during the rivalry period were excluded from the analysis.

2.3.4 Measures of perceptual selection

We expected that predictive context effects would be strongest at the beginning of the rivalry period, so analysis was focused on the initial response to the rivalry stimuli. In particular, we measured the proportion of trials in which the initial percept was the matching versus the non-matching grating. We also measured the latency and duration of the initial response for both matching and non-matching percepts. The experiments were designed to investigate the effects of predictive context on initial rivalry percepts, and the relatively short rivalry presentation durations did not allow these effects to be assessed for subsequent percepts.

2.3.5 Catch trials

To ensure that subjects were following task instructions, approximately 10% of the trials in each experiment were catch trials, in which both eyes viewed identical left- or right-tilted gratings in the "rivalry test" portion of the trial. Catch trials were counterbalanced for grating orientation predicted by the stream (left or right tilt) and direction of tilt of the test stimuli (left or right). Catch trial latencies were used to assess the possibility of response bias, since response bias would be expected to lead to shorter response latencies for catch trial stimuli matching perceptual expectations than for non-matching catch trial stimuli.

2.3.6 Eye dominance screening

Before participating in the study, each subject's eye dominance was measured in a brief pre-test. On each of 24 trials, subjects viewed static orthogonal rivalrous gratings with +/-45° orientation for 10 seconds and continuously reported their percept as described above. Pre-rivalry streams were not presented in these screening trials. Eye dominance was defined as the relative number of trials in which the initial perceptual report corresponded to the grating presented to the left eye versus the right eye.

2.3.7 Subject exclusion

Subjects with strong eye dominance were excluded because a strong bias in favor of the left or right eye during binocular rivalry limits assessment of the effects of experimental manipulations in this study. Subjects whose initial eye dominance in either eye was greater than 85% during the eye dominance screening session were excluded and did not participate in any portion of the study. We also measured eye dominance throughout each experiment by analyzing initial rivalry responses and excluded subjects who had >85% eye dominance for at least half of the experimental session.

In addition to subjects who did not pass the initial eye dominance screen, five data sets from individual subjects were excluded from specific experiments (one from Experiment 1, three from Experiment 3, and one from Experiment 4). In each of Experiments 1 and 3, one subject was excluded for exhibiting excessive eye dominance during the experiment. In Experiment 3, one subject was excluded as an outlier (proportion first response matching was more than 2.5 standard deviations away from the sample mean for one condition comparison). Finally, one subject was excluded in each of Experiments 3 and 4 for using incorrect response keys.

2.4 EXPERIMENT 1

Subjects viewed a predictive stimulus stream consisting of a series of oriented gratings presented identically to the two eyes. This stream generated a percept of rotating apparent motion, thereby establishing an expectation regarding the orientation of the next image in the series (Figure 2A). We measured the effect of this predictive context on subsequent perceptual selection during rivalry between orthogonal gratings. We hypothesized that predictive and sensory information would be integrated, increasing the likelihood of selecting the predicted percept. In this framework, predictive context functions as a prior that influences perceptual interpretation of the ambiguous visual stimuli.

2.4.1 Methods

The pre-rivalry stream consisted of a sequence of monochromatic sinusoidal grating patches with a spatial frequency of 3 cpd. Orientations of successive stream items either increased or decreased by 45˚, generating an apparent motion percept of rotation in either the clockwise or counterclockwise direction (Figure 2A). In the subsequent rivalry test, one of the two static gratings (the “matching” grating) had the orientation that came next in the apparent motion series, and the other grating (the “non-matching” grating) had an orientation orthogonal to that predicted by the stream. The orientation of the first pre-rivalry stream stimulus was selected so that the rivalrous gratings would always have oblique (+/-45°) orientations.

There were four pre-rivalry stream conditions: number of stream items (between 0 and 15), the grating orientation predicted by the stream (left or right tilt), the eye to which the “matching” rivalrous grating was presented (left or right eye), and stream rotation direction (clockwise or counterclockwise). The four stream conditions were fully counterbalanced across trials, resulting in a 16 x 2 x 2 x 2 design. Subjects completed either 24 or 32 trials for each stream length, and all conditions were randomly intermixed.

2.4.2 Results: Perceptual selection is biased in favor of the predicted percept

A rotation stream of variable length (0-15 stream items; Figure 2A) was followed by presentation of a rivalrous pair of test gratings. The rotation stream generated a consistent percept of rotating apparent motion in either a clockwise or counterclockwise direction, and one of the rivalrous stimuli was consistent with this apparent motion percept (the "matching" stimulus), while the other (the "non-matching" stimulus) was not.

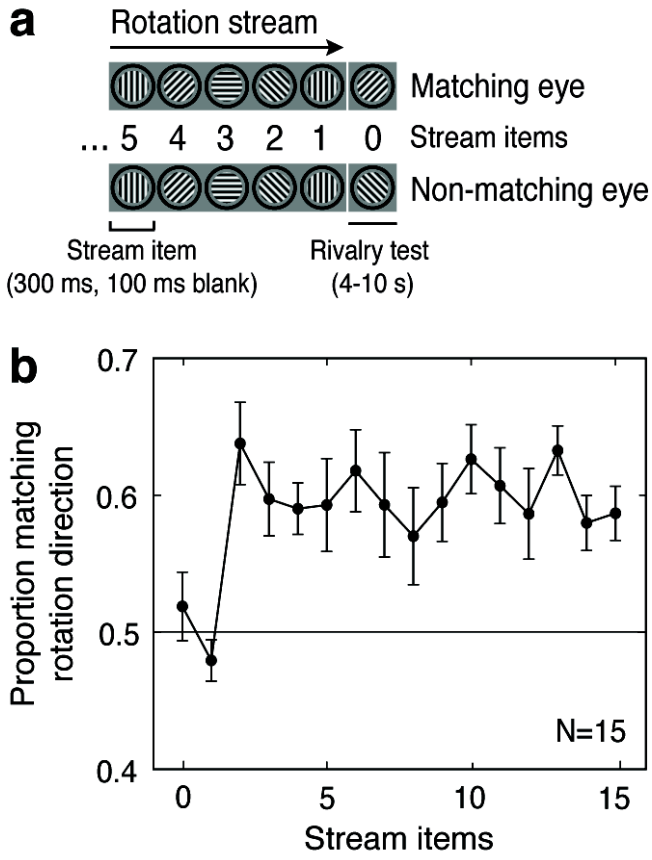

Figure 2. Experiment 1: Predictive context in a pre-rivalry rotation stream influences initial perceptual selection in binocular rivalry. (A) Schematic of the stimuli (pre-rivalry stream and rivalry test). This example stream has clockwise rotation and five stream items shown. Stream items were always presented identically to both eyes, and rivalry items were always a pair of gratings with orthogonal +/-45° orientations, with one of the two gratings matching the rotation direction (i.e., it was the expected next item in the rotation stream). (B) Subjects initially perceived the rivalrous grating that matched the rotation direction more often than they initially perceived the non-matching grating whenever the number of stream items was sufficient to define a rotation direction (two or more stream items). The size of this effect was similar for all stream durations from 2-15 items. Error bars are s.e.m.

The results provide clear support for our hypothesis that prediction would influence perceptual selection: for rotation streams with two or more items (the minimum number needed to establish an apparent motion percept), perceptual selection in binocular rivalry was consistently biased in favor of the matching grating. Specifically, the matching grating was initially selected on about 60% of trials, regardless of the number of items in the stream (Figure 2B).

2.5 EXPERIMENT 2

In Experiment 1, the predictive context provided by rotation streams with 2-15 items enhanced selection of the matching grating, but the size of this effect did not depend on the length of the stream. We therefore asked in Experiment 2 whether very recent stimulus history (only the two items immediately preceding the rivalry test) was sufficient to bias perceptual selection, even for longer stream conditions.

2.5.1 Methods

Half of the streams were composed of gratings that rotated either clockwise or counterclockwise (as in Experiment 1), and the other half were scrambled such that each orientation in the rotation stream was presented in a random position in the scrambled stream sequence (Figure 3A). However, for both rotation and scrambled trials, the final two stream items preceding the rivalrous test stimulus were always consistent with a particular rotation direction. This rotation direction defined the "matching" and "non-matching" rivalrous test grating. For scrambled streams, we ensured that there were no complete rotations in the stream by requiring at least two items in the first part of the stream to be different from the original rotation sequence. There were five stream conditions which were fully counterbalanced across trials: stream type (scramble or rotation), number of stream items (between 4 and 7), and the same final three conditions as in Experiment 1 (grating orientation predicted by the stream, the eye to which that matching grating was presented, and stream rotation direction). Subjects completed 24 trials for every combination of stream type and number of stream items, and all conditions were randomly intermixed.

2.5.2 Results: Recent stimulus history drives predictive effects on perceptual selection

We compared initial perceptual selection for rivalrous test stimuli presented after streams with either a scrambled sequence of orientations in the initial part of the stream or with fully coherent rotation throughout (Figure 3A). If consistent predictive stimulus history over an extended viewing period is required for the rotation matching effect, then disruption of predictive context in the early part of the stream in the scrambled condition should reduce the size of this effect, compared to the full rotation condition. However, if only recent stimulus history is responsible for the rotation matching effect, then the size of the effect should be identical in the rotation and scrambled conditions, and this is the result that was obtained.

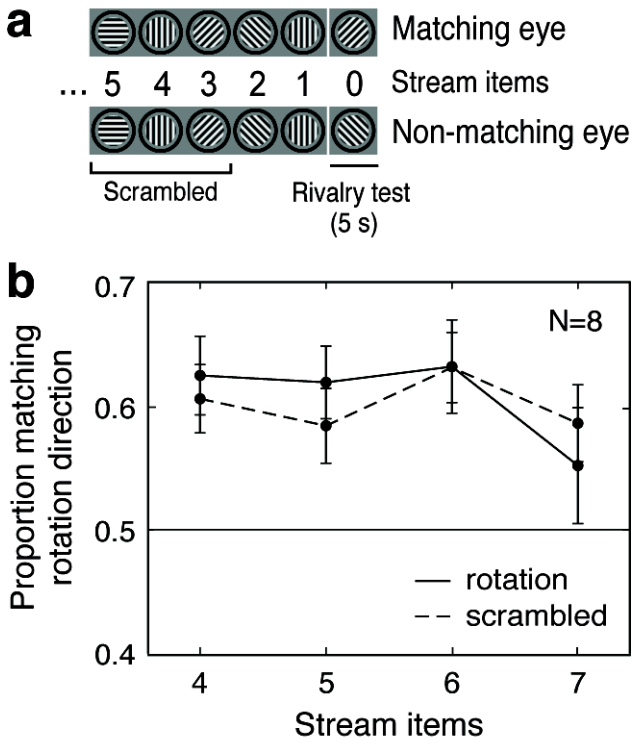

Figure 3. Experiment 2: Effects of predictive context depend only on recent stimulus history. (A) Schematic of the stimuli. For the scrambled condition, the order of the gratings in the first part of the rotation stream (preceding the final two items) was randomized so that the first part of the stream did not contain a consistent rotation. However, the two stream items immediately before the rivalry test were always consistent with a particular rotation direction (in this example, clockwise) for both rotation and scrambled trials. (B) Scrambling the sequence of orientations in the stream prior to the final two stream items did not diminish the rotation matching effect. Error bars are s.e.m.

For rotation streams, we found increased selection of the predicted percept (combining all stream lengths), replicating the results of Experiment 1 ($t(7) = 21.28$, $p < 0.001$; Figure 3B). Scrambled streams also generated a significant rotation matching effect ($t(7) = 29.77$, $p < 0.001$; Figure 3B), suggesting that consistent rotation throughout the stream was not required for the effect. Moreover, there was no significant difference between the rotation and scrambled conditions in the size of the mean matching effect across all stream lengths (paired t-test, $t(7) = 0.19$, n.s.; Figure 3B). Together, these results show that the predictive context provided by only the two items immediately preceding the rivalry test was sufficient to maximally bias perceptual selection in this paradigm.

2.6 EXPERIMENT 3

Orientation-specific adaptation to stream gratings might have contributed to the rotation matching effects observed in Experiments 1 and 2. The stimuli in these experiments controlled for adaptation to the final stream item, because the angular difference between the final stream grating and each of the rivalrous gratings (both matching and non-matching) was always 45°. However, it was still possible that the rotation matching effect was influenced by orientation-specific adaptation to the second-to-last stream item (Figure 4A). This grating always had the same orientation as the non-matching rivalry grating, so it was possible that adaptation to this grating biased perceptual selection against the non-matching grating orientation (e.g., Blake and Overton, 1979; but also see Brascamp et al., 2007), perhaps contributing to the rotation matching effect. We conducted Experiment 3 to compare the effects of prediction and adaptation on perceptual selection in this paradigm.

2.6.1 Methods

Subjects viewed two pre-rivalry stream items on all trials, based on our finding from Experiments 1 and 2 that two stream items were sufficient to produce the rotation matching effect. The first stream item was always a sinusoidal grating with an orientation of either +45˚ or -45˚, presented to both eyes. The second stream item, also presented binocularly, was one of the following: a vertical or horizontal grating (generating, together with the first stream item, apparent clockwise or counterclockwise rotation, as in Experiment 1), a blank (mean luminance), a bullseye pattern of 3-cpd sinusoidal concentric circles, or a plaid pattern formed by superimposing vertical and horizontal 3-cpd gratings.

The blank, bullseye, and plaid stimuli were designed to disrupt rotational apparent motion perception of the pre-rivalry stream, compared to the rotation stimulus. In all trials, the orientation of the first stream item determined the orientation of the test grating that would be consistent with perceived rotational motion and therefore defined which rivalrous test grating was "matching" and which was "non-matching". Each trial had four fully counterbalanced conditions: stream type (the four types described above) and the same final three conditions as in the earlier experiments (grating orientation predicted by the stream, the eye to which that matching grating was presented, and stream rotation direction). Each subject completed 48 trials for each stream type, and all conditions were randomly intermixed.

2.6.2 Results: Separate effects of prediction and adaptation on perceptual selection

To determine the contribution of adaptation to the matching effect, we created streams that preserved the second-to-last stream item, thereby maintaining orientation-specific adaptation, but that altered the final item in the stream, thereby reducing or eliminating the perception of stream rotation (Figure 4A). Perceptual selection for these reduced predictive context streams was compared to that for a full rotation condition.

This experiment included a total of four stream conditions (Figure 4B). Matching effects in the *rotation* condition could be due to prediction, adaptation, or some combination of these factors. In the *blank* and *bullseye* conditions, there was no apparent motion percept (and therefore no predictive information available), so any bias in perceptual selection for this condition could only be due to adaptation. Finally, the *plaid* condition was an intermediate condition in which the presence of both vertical and horizontal grating components in the plaid may have interfered with the perception of apparent motion in the stream without abolishing it altogether. This is because both vertical and horizontal components were consistent with the same "matching" rivalry grating. For example, a left-tilted grating followed by a plaid could be seen as clockwise apparent motion if the vertical plaid component were emphasized or as counterclockwise apparent motion if the horizontal plaid component were emphasized, but both of these apparent rotation percepts predict a right-tilted matching grating during the rivalry test. The plaid condition therefore contains some predictive context but presumably generates a weaker apparent motion percept than the rotation condition.

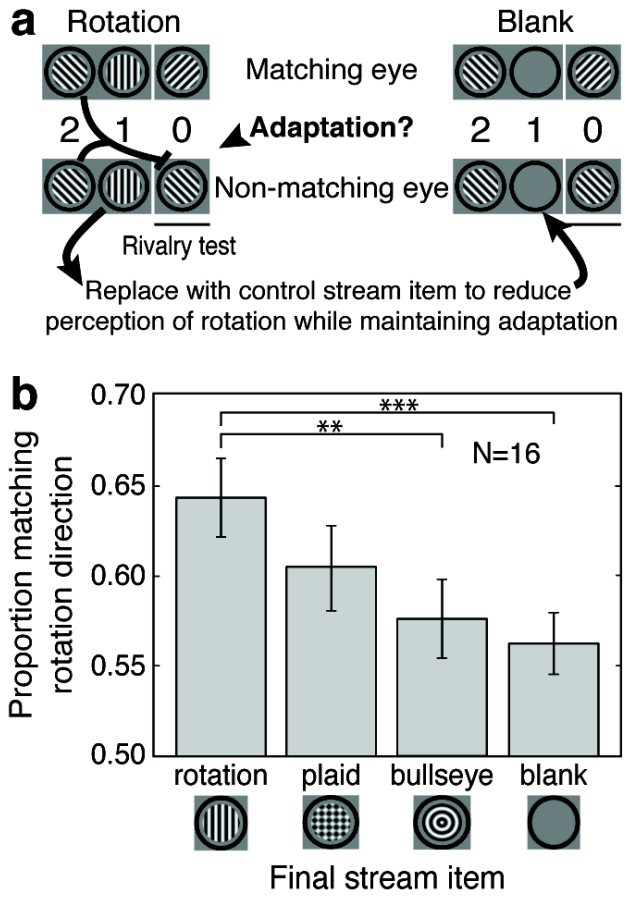

Figure 4. Experiment 3: Separate contributions of prediction and adaptation to the matching effect. (A) Schematic of the stimuli. Left: An example rotation stream showing how adaptation to the second-to-last stream item could bias selection toward the matching stimulus. Right: To control for adaptation, the final stream item was replaced with one of three other stimuli (plaid, bullseye, or blank; the blank condition is shown here). These alternative final stream items reduced the perception of rotation while maintaining any orientation-specific adaptation to the second-to-last stream item. (B) The size of the rotation matching effect decreased with increasing disruption of rotation perception. The bullseye and blank conditions quantify the effects of adaptation alone, as no perception of rotation was possible for these conditions. The matching effect for the rotation condition was significantly larger than that for the bullseye or blank condition, indicating an effect of predictive context that cannot be accounted for by adaptation. Error bars are s.e.m. **, $p < 0.01$; ***, $p < 0.005$.

The results of Experiment 3 revealed separate effects of adaptation and prediction on perceptual selection (Figure 4B). There were reliable matching effects in the adaptation-only conditions (blank and bullseye), indicating that orientation-specific adaptation to the second-to-last stream item biased selection against the non-matching (adapted) grating. However, the matching effect for the rotation condition (resulting from both adaptation and prediction effects) was significantly larger than the adaptation-only effects (rotation vs. blank, $t(15) = 3.36$, $p < 0.005$; rotation vs. bullseye, $t(15) = 2.96$, $p < 0.01$), indicating that prediction enhances the rotation matching effect beyond what is found for adaptation alone. The size of the matching effect for the plaid was in between that of the rotation condition and the adaptation-only conditions, as expected if this stimulus produced intermediate levels of apparent motion perception. Thus, the effects of pre-rivalry stream rotation on perceptual selection of binocular rivalry stimuli reflect a combination of adaptation and prediction effects that can be experimentally dissociated.

2.7 EXPERIMENT 4

The strength of orientation-selective adaptation depends on stimulus contrast (Blakemore and Nachmias, 1971), while predictive context is provided for any contrast for which the stream items are visible. We therefore conducted Experiment 4 to measure the contrast dependence of the adaptation and prediction effects described above.

2.7.1 Methods

The rotation and blank stream conditions from Experiment 3 were used, and the items in the streams had 5%, 25%, or 100% contrast. The contrast of the rivalrous gratings was also 5%, 25%, or 100%, independent of the stream contrast. Thus, each trial had six fully counterbalanced conditions: stream type (rotation or blank), stream item contrast, rivalrous stimuli contrast, and the final three conditions as in the earlier experiments. "Matching" and "non-matching" rivalrous test gratings were defined as in Experiment 3. Each subject completed 32 trials for every combination of stream type, stream item contrast, and rivalrous stimuli contrast, and all conditions were randomly intermixed.

2.7.2 Results: Effects of stimulus contrast dissociate prediction and adaptation

We independently varied the contrast of the stream items and of the rivalrous stimuli for both the rotation and blank conditions from Experiment 3 and observed a main effect of stream contrast (ANOVA, $F(2,48) = 11.95$, $p < 0.001$; Figure 5), with increasing stream contrast causing a dramatic increase in the magnitude of the matching effect in the blank (adaptation-only) condition. However, increasing stream contrast led to a smaller increase in the matching effect in the rotation condition (stream contrast x stream type interaction, $F(2,48) = 10.74$, $p < 0.001$), mainly due to the significantly larger matching effect for the rotation compared to the blank condition at the lowest stream contrast (ANOVA for 5% stream contrast condition, main effect of stream type, $F(1,24) = 7.31$, $p < 0.05$). At this low contrast, adaptation is weak, and prediction effects dominate.

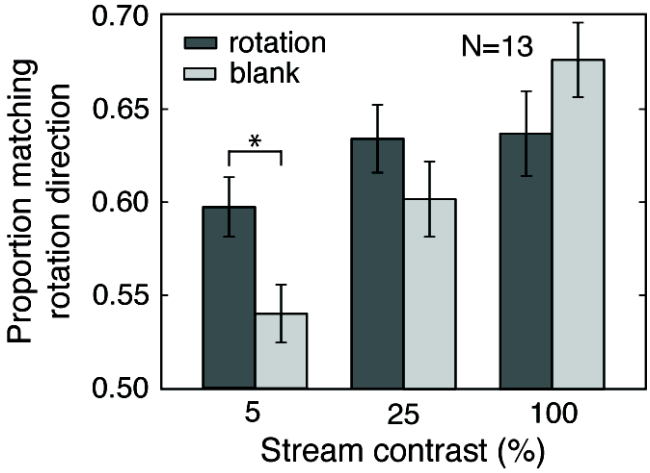

Figure 5. Experiment 4: Effects of stream contrast on prediction and adaptation. Increasing the contrast of the stream items increased the size of the matching effect for the blank condition more than for the rotation condition. The prediction effect corresponds to the difference between the rotation and blank values and was greatest at the lowest stream contrast. The blank condition quantifies the effects of adaptation alone, and these effects were larger for higher stream contrasts. Error bars are s.e.m. *, $p < 0.05$.

We also observed a main effect of contrast of the rivalrous test gratings ($F(2,48) = 8.65$, $p < 0.005$), with the size of the matching effect decreasing as rivalry stimulus contrast increased, for both rotation and blank conditions (no interaction between rivalry stimulus contrast and stream type: $F(2,48) = 0.01$, n.s.). This effect of rivalry stimulus contrast could be because competition between higher contrast rivalry stimuli is less affected by either prediction or adaptation. Because the blank condition represents only adaptation effects, while the rotation condition includes effects of both adaptation and prediction, the lack of a significant interaction indicates that adaptation was the more important factor in the effect of rivalry stimulus contrast. Figure 5 displays data for each stream contrast condition, collapsed across rivalry stimulus contrast.

The different effects of stream contrast in the rotation and blank conditions provide an additional dissociation of prediction and adaptation effects. This experiment showed a robust prediction effect even for a very low (but still above the visibility threshold) stream contrast of 5%, while adaptation effects were minimized at this contrast. These results suggest that low contrast stimuli can be used to reduce adaptation effects, providing a strategy for emphasizing prediction effects that could be employed in future studies of predictive context. Experiments 1-3 used 10% contrast for both pre-rivalry stream and rivalry stimulus items, and this relatively low contrast may have helped to reveal prediction effects in these experiments.

2.8 ADDITIONAL RESULTS

2.8.1 Prediction speeds perceptual selection as measured by latency to report initial percept

So far we have demonstrated that predictive context affects which percept is initially selected during binocular rivalry. We also analyzed the effects of predictive context on the latency and duration of the initial response to the rivalrous test stimuli. We present latency data for Experiment 3 because it contains the most effective experimental control of adaptation effects. For the conditions that contain predictive context (rotation and plaid), response latencies were shorter for matching than for non-matching initial percepts, while no differences between matching and non-matching initial percepts were observed for the bullseye and blank conditions, which lack predictive context (Figure 6) (rotation, $t(15) = 4.26$, $p < 0.001$; plaid, $t(15) = 3.06$, $p < 0.01$; bullseye, $t(15) = 1.73$, n.s.; blank, $t(15) = 1.63$, n.s.). Therefore, adaptation effects alone do not reliably speed perceptual report, while prediction does. Similar results were also obtained in Experiments 1, 2, and 4: we found shorter response latencies for matching than for non-matching initial percepts, indicating that predictive context speeded perceptual report for predicted stimuli.

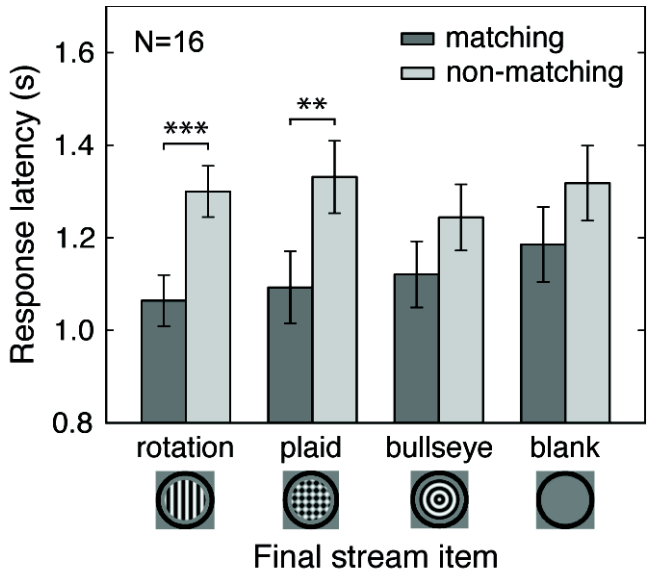

Figure 6. Effects of prediction and adaptation on latency of initial response. Results from Experiment 3 are shown. Response latencies were shorter for initially reported matching compared to non-matching rivalry stimuli. This effect was observed only in the rotation and plaid conditions, suggesting that prediction but not adaptation speeded perceptual report. Error bars are between-subject standard errors of the difference between matching and non-matching percept response latencies. **, $p < 0.01$; ***, $p < 0.001$.

We observed less consistent effects of prediction on the duration of the initial response across the experiments. Our ability to accurately estimate the initial response duration may have been affected by the duration of the rivalry test period, which was 10 seconds or shorter, depending on the experiment. Because of this limited response window, some initial responses were maintained until the end of the trial and terminated at that point. When we excluded those

truncated responses, we found a longer mean duration of initial responses for matching than for non-matching stimuli in the rotation condition for all four experiments. In Experiment 3, the difference in mean first response duration between matching and non-matching trials with non-truncated initial responses was significant only in the rotation condition (rotation, $t(15) = 2.82$, $p < 0.05$; plaid, $t(15) = 0.19$, n.s.; bullseye, $t(15) = 0.19$, n.s.; blank, $t(15) = 1.11$, n.s.). This suggests that prediction prolongs the predicted initial percept compared to the non-predicted percept.

2.8.2 Possible contribution of response bias to predictive context effects

In principle, the effects of predictive context we report could be due to perceptual selection of matching stimuli and/or a response bias in favor of these stimuli. However, data from catch trials argue against a simple response bias as the source of our predictive context effects. Every experiment contained catch trials, in which the pre-rivalry stream sequences were the same as in the experimental trials, but instead of a rivalrous pair of gratings, the same grating was presented to both eyes. For these unambiguous test stimuli, there were no significant effects of predictive context in any experiment, either on the initially selected percept (proportion of responses matching the rotation direction) or on the initial response latency (matching vs. non-matching responses). These findings suggest that predictive context did not result in errors in perceptual report that led subjects to report the matching percept when they did not actually see it and did not result in subjects responding to a matching stimulus more quickly, given identical perceptual latencies for matching and non-matching stimuli.

2.9 DISCUSSION

Our experiments provide the first evidence that predictive information influences perceptual selection during binocular rivalry: stimuli that were consistent with the established predictive context tended to dominate over inconsistent stimuli in initial perceptual selection. We further characterized three key aspects of the effects of predictive information on perceptual selection in our paradigm. First, we showed that only recent visual stimulus history contributed to the prediction effect. As few as two stream items (the minimal number required to establish a rotation direction) produced the maximal rotation matching effect (Experiment 1), and introducing random sequences of grating orientation prior to these two stream items did not change the size of the matching effect (Experiment 2). Second, prediction and orientation-specific adaptation separately contributed to the matching effect (Experiment 3), and the results of Experiment 4 suggest a strategy for minimizing the influence of adaptation, namely using a low stream contrast. Adaptation effects were reduced for low stream contrasts, while prediction effects were robust for all tested contrasts. Third, subjects were faster to report initial percepts that matched the predictive context compared to those that did not. In Experiment 3, this effect was specific to the prediction conditions and was not found in the adaptation-only conditions.

2.9.1 Predictive context and response latency

We found that the latency of the first response was shorter for percepts that matched the expectations established by predictive context. Physiological studies also suggest that prediction may reduce the latency of neural responses to expected stimuli. Melloni and colleagues (2011) found that EEG activity differentiating seen and unseen stimuli occurred about 100 ms earlier when the visual stimulus was expected compared to when it was unexpected. In addition, James

and colleagues (2000) showed that BOLD responses peaked earlier for primed than for unprimed visual stimuli in a manner that correlated with behavioral report. Finally, latencies of single cell responses to images embedded in natural sequences are shorter than response latencies for the same images presented in isolation (Perrett et al., 2009).

2.9.2 Effects of priming on perceptual selection

Perceptual history has previously been shown to contribute to perceptual selection during binocular rivalry in various priming paradigms. Intermittent presentations of rivalry stimuli tend to stabilize the perceptual interpretation, such that the perceptual alternations characteristic of continuous rivalrous viewing are markedly slowed (Leopold et al., 2002; Pearson and Brascamp, 2008). In this case, priming arises from a neural signal associated with the previous perceptual decision and not the stimulus per se, since the stimulus is always ambiguous. Unambiguous primes can also increase the likelihood that the primed stimulus will be selected during subsequent rivalry. This effect depends strongly on contrast, with lower contrast primes facilitating subsequent selection of the prime, and higher contrast primes suppressing it as a result of adaptation (Brascamp et al., 2007; Pearson et al., 2008). Mental imagery can also bias subsequent selection during rivalry toward the previously imagined percept (Pearson et al., 2008).

In the present study, the rotating pre-rivalry stream could be considered a prime for the predicted rivalry stimulus. However, our experiments are importantly different from previous binocular rivalry priming studies in that the predicted ("primed") orientation never appeared immediately before the rivalry period and indeed was often not presented at any time during the pre-rivalry stream. Therefore, the effects of predictive context in our study could not be due to a residual memory trace from a previously presented stimulus but instead were due to a predictive signal specific to the expected grating orientation. Likewise, our predictive effects were likely not due to subjects imagining the expected next stimulus, since imagery effects are negligible for brief imagery durations (Pearson et al., 2008), and the rivalry stimuli were always presented immediately after the pre-rivalry stream in our experiments. Nonetheless, it is possible that selection biases due to stimulus priming, imagery, and prediction share common neural and/or psychological substrates, a question which will be of interest in future research.

2.9.3 Attention and predictive context

It is possible that increased allocation of attention to the features of the expected stimulus may have played a role in the prediction effects we observed. Exogenously cueing attention to one of two superimposed stimuli has been shown to increase the likelihood that the cued stimulus will initially dominate when the two stimuli are made rivalrous (Ooi and He, 1999; Mitchell et al., 2004; Chong and Blake, 2006; Hancock and Andrews, 2007). Similar effects on initial dominance have been found when endogenous attention is directed toward one of the stimuli during a difficult task prior to binocular rivalry (Chong and Blake, 2006).

It should be noted, however, that in these studies, a cue draws attention to a currently visible stimulus, thereby increasing the likelihood that the cued stimulus perceptually dominates in a subsequent rivalry period. This is different from our study, in which the grating presented immediately before the rivalry display (the final stream item) has equal angular distance from the

two rivalrous gratings. If attention were simply cued to the features of the final grating in the pre-rivalry stream, it would not favor either of the rivalrous gratings.

In creating predictive context that generates an expectation about the appearance of a future stimulus, our study should also be distinguished from previous studies of expectation that have used instructions to generate an attentional set for a particular kind of stimulus (Summerfield et al., 2006; Summerfield and Koechlin, 2008; Summerfield and Egner, 2009). In these studies, many types of stimuli appear with equal likelihood, but only one type (the "expected" stimulus) is relevant for performing the task. We might call expectations of this type "attentional expectations." In our study, on the other hand, subjects presumably expect that a stimulus rotating in a particular direction will continue to rotate in that direction, but the predicted and non-predicted stimuli (matching and non-matching orientations) are equally task relevant. Such expectations about the likely future state of the stimulus are "perceptual expectations." An important task for future research will be to understand how these two types of expectations are represented in the brain and how they influence the processing of sensory signals (Summerfield and Egner, 2009).

Finally, attention and predictive coding mechanisms are thought to have different effects on sensory responses in the brain, with attention facilitating (Carrasco, 2011) and predictive coding mechanisms suppressing responses at early stages of visual processing (Summerfield and Koechlin, 2008; Garrido et al., 2009; Alink et al., 2010; Melloni et al., 2011; but see Spratling, 2008; Spratling, 2010, for an attempt to reconcile effects of attention and predictive coding in a single model). An attention-based account of our predictive context effects would postulate enhanced responses in neurons representing the predicted stimulus at lower hierarchical levels of the visual system, while reduced responses in these areas would be consistent with predictive coding models.

2.9.4 Relationships with other effects of predictive visual motion context on perception

The prediction effects we describe may share mechanisms with recently reported effects of predictive motion extrapolation on a visual detection task (Roach et al., 2011). In this study, detection performance for patterned targets at the leading edge of a moving grating was measured, and the results suggest that the visual system generates a predictive signal resembling a low-contrast extrapolation of the grating in the direction of motion. The effects depended on the spatial phase of the gratings and extended over only about 1° of visual angle, leading the authors to speculate that they could be mediated by cortical area V1. A similar weak but pattern-specific representation generated by extrapolation of rotational motion could also account for the predictive rivalry effects we observed. Our results suggest that this type of motion signal extrapolation could influence not only visual sensitivity but also perceptual selection during ambiguous visual stimulation.

Our findings may also be related to the phenomenon of representational momentum—the observation that memory for the final position of a moving target is mislocalized in the direction of motion (Freyd and Finke, 1984; Hubbard, 2005). Representational momentum can be observed following presentation of a series of discrete views of a rotating target, in which motion was implied (as in our study) (Freyd and Finke, 1984; Freyd and Johnson, 1987). The spatiotemporal continuity of motion may be a particularly strong prior that could play a role in a range of perceptual and neural effects (Watamaniuk and McKee, 1995; Doherty et al., 2005).

2.9.5 Priors and perception

An important question for future research is the extent to which the predictive effects we report generalize to other types of priors. Although they are not always discussed in a Bayesian framework, other rivalry studies have also documented what may be the effects of priors on perceptual selection. For example, images with natural image statistics tend to dominate over more artificial images (Baker and Graf, 2009), upright faces tend to dominate over inverted faces (Engel, 1956; Zhou et al., 2010), and images of floors tend to dominate over images of ceilings (Ozkan and Braunstein, 2009). These findings, including our own, can be interpreted as empirical evidence for a long-standing notion, that perception is an inference process (Helmholtz, 1866; Gregory, 1997; Kersten et al., 2004; Kveraga et al., 2007). Bayesian modeling of perception of ambiguous visual displays has been a particular focus of theoretical work in this vein (Dayan, 1998; Schrater and Sundareswara, 2007; Hohwy et al., 2008; Sundareswara and Schrater, 2008; Gershman et al., 2009), and recent empirical work shows that Bayesian cue combination can explain perception of a bistable depth stimulus (Moreno-Bote et al., 2011).

2.9.6 Predictive coding and neural mechanisms of binocular rivalry

In predictive coding models of the visual system (Mumford, 1992; Rao and Ballard, 1999; Friston, 2005; Friston and Kiebel, 2009), higher levels of the visual hierarchy predict upcoming responses in lower levels, and these predictions are compared with actual responses in the lower levels via an inhibitory mechanism. Residual signal in the lower levels therefore serves as an error signal that is then transmitted to higher levels in order to improve future predictions. According to this model, posterior information about the percept is represented at higher hierarchical levels, and the dominant percept corresponds to the perceptual hypothesis with the highest posterior probability. Top-down predictions therefore explain away predicted bottom-up signals, and so the representation of a stimulus at the lower levels should have reduced error-related activity while that stimulus is perceived (Murray et al., 2002; Friston, 2005; Hohwy et al., 2008; Summerfield and Koechlin, 2008; Alink et al., 2010).

Neurophysiological studies during binocular rivalry have yielded mixed results regarding correlations between perception and activity in different visual areas. Few (if any) neurons in early visual areas such as the LGN (Lehky and Maunsell, 1996; Wilke et al., 2009) and V1 (Leopold and Logothetis, 1996) have spiking responses that vary as a function of perception during binocular rivalry. In contrast, later visual cortical areas such as V4, MT, and IT have more neurons with perceptually-correlated responses (Logothetis and Schall, 1989; Leopold and Logothetis, 1996; Sheinberg and Logothetis, 1997). This increase in the proportion of neurons whose activity reflects the perceptual interpretation of a rivalry stimulus at increasingly higher levels of the visual processing hierarchy is consistent with predictive coding frameworks, in that the highest levels of predictive coding hierarchies should most closely reflect the final perceptual interpretation. That being said, these neurophysiological studies all employed stimuli that were matched to the response preferences of the recorded neurons in each visual area, raising the possibility that perception-related neural modulation depends on stimulus complexity, as neurons in higher-order areas respond preferentially to more complex stimuli than those in lower-order areas. However, even for similar rivalrous grating stimuli, the proportion of neurons with perceptually-modulated responses is higher in V4 than in V1/V2, making it unlikely that stimulus complexity is the only factor accounting for differences between visual areas in percept-related modulations (Leopold and Logothetis, 1996).

In predictive coding frameworks, lower hierarchical levels should carry an error signal for suppressed percepts, and the existence of neurons in V4 (Leopold and Logothetis, 1996) and MT (Logothetis and Schall, 1989) that show enhanced responses during rivalry suppression of their preferred stimulus may be consistent with this. On the other hand, Leopold and Logothetis (1996) did not find V1/V2 neurons that showed enhanced responses when their preferred stimulus was perceptually suppressed, which is at odds with predictive coding models and may be an interesting avenue for further investigation.

In contrast to single cell activity, fMRI and low frequency (<30 Hz) LFP signals have been shown to correlate strongly with perception during binocular rivalry in visual areas as early as V1 (fMRI: Polonsky et al., 2000; Tong and Engel, 2001; Lee and Blake, 2002; Lee et al., 2005; LFP: Wilke et al., 2006) and the LGN (fMRI: Haynes et al., 2005; Wunderlich et al., 2005; LFP: Wilke et al., 2009). In the context of predictive coding, these responses could be interpreted as reflecting top-down predictive feedback from higher cortical regions (Hohwy et al., 2008), particularly if BOLD and LFP signals primarily reflect synaptic inputs to a given population of neurons (Logothetis et al., 2001; Logothetis, 2008).

2.9.7 Conclusions

The extent to which the resolution of binocular rivalry is driven by competition between representations at lower levels, higher levels, or multiple hierarchical levels in the visual system has been the subject of much debate (Logothetis et al., 1996; Lee and Blake, 1999; Blake and Logothetis, 2002; Tong et al., 2006). Our approach of experimentally manipulating top-down priors on perceptual selection could help to clarify this question by providing experimentally distinguishable hypotheses about how prior information and sensory information combine within neural circuits. Such studies could be especially informative when psychophysical manipulations of prior information are combined with physiological measures of neural activity at different hierarchical levels in the visual system.

Here, we have demonstrated predictive effects on perceptual selection during binocular rivalry. Therefore, predictive context influences what is often thought to be a low-level competitive process in a manner consistent with theories of predictive coding. Our findings suggest that the visual system uses recently encountered visual information to help construct a single perceptual interpretation of a scene. Thus, predictive information may play an important role in natural vision by helping to constrain perceptual interpretations of the visual world to those that are most consistent with the recent past.

Chapter 3

Distinct contributions of the magnocellular and parvocellular visual streams to perceptual selection

3.1 ABSTRACT

During binocular rivalry, conflicting images presented to the two eyes compete for perceptual dominance, but the neural basis of this competition is disputed. In interocular switch (IOS) rivalry, rival images periodically exchanged between the two eyes generate one of two types of perceptual alternation: 1) a fast, regular alternation between the images that is time-locked to the stimulus switches and has been proposed to arise from competition at lower levels of the visual processing hierarchy, or 2) a slow, irregular alternation spanning multiple stimulus switches that has been associated with higher levels of the visual system. The existence of these two types of perceptual alternation has been influential in establishing the view that rivalry may be resolved at multiple hierarchical levels of the visual system. We varied the spatial, temporal, and luminance properties of IOS rivalry gratings and found, instead, an association between fast, regular perceptual alternations and processing by the magnocellular stream and between slow, irregular alternations and processing by the parvocellular stream. The magnocellular and parvocellular streams are two early visual pathways that are specialized for the processing of motion and form, respectively. These results provide a new framework for understanding the neural substrates of binocular rivalry that emphasizes the importance of parallel visual processing streams, and not only hierarchical organization, in the perceptual resolution of ambiguities in the visual environment.

3.2 INTRODUCTION

Ambiguous visual displays, in which multiple perceptual interpretations of a single display are possible, dissociate visual percept from visual stimulus, thereby providing an opportunity to study the neural selection processes that lead to visual awareness (Blake and Logothetis, 2002). Binocular rivalry is a powerful example of an ambiguous visual display (Alais and Blake, 2005). During binocular rivalry, conflicting images presented to the two eyes result in a visual percept that alternates between the two images, even though the visual stimuli remain constant. Since stimulus-related visual information is represented in multiple brain regions and at multiple levels of the visual processing hierarchy, an important goal for visual neuroscience is the identification of the neural substrates of perceptual selection.

In the case of binocular rivalry, studies have provided evidence for perceptual selection both at the level of monocular representations (the “eye level”) and at higher levels of the visual

hierarchy that contain binocular representations of visual stimuli (the "stimulus level"). In support of perceptual selection at the eye level, psychophysical studies have shown that the detection of a probe stimulus is impaired if it is presented to the eye containing the currently suppressed stimulus (Fox and Check, 1966, 1968; Wales and Fox, 1970; Blake and Fox, 1974; Blake et al., 1998) and that a single interocular exchange of rivalrous stimuli causes the previously dominant eye to remain dominant, leading to the sudden dominance of the previously suppressed stimulus (Blake et al., 1980).

Brain imaging studies using fMRI in humans have likewise shown fluctuations in eye-specific activity that are time-locked to perceptual alternations during binocular rivalry, both in the monocular blind spot in V1 (Tong and Engel, 2001) and in regions of the LGN showing strong eye preference (Haynes et al., 2005; Wunderlich et al., 2005). Interestingly, electrophysiological recordings from monocular cells of macaque V1 during binocular rivalry have revealed very little modulation of spike rate as a function of perceptual alternation (Leopold and Logothetis, 1996), although such modulations are more common in higher-order areas in both the ventral (area V4, Leopold and Logothetis, 1996; inferotemporal cortex, Sheinberg and Logothetis, 1997) and dorsal cortical processing streams (area MT, Logothetis and Schall, 1989).

In support of perceptual selection at the stimulus level, various binocular rivalry paradigms result in visual percepts that require integration of information from the two eyes. For example, when parts of two meaningful images are distributed between the eyes, subjects may perceive alternation between the coherent images instead of between the monocular inputs (Diaz-Caneja, 1928 (translated into English in Alais et al., 2000); Kovács et al., 1996; see also Lee and Blake, 2004, for an eye-based rivalry interpretation of these results). Logothetis et al. (1996) introduced the interocular switch (IOS) rivalry paradigm, in which conflicting stimuli are exchanged between the two eyes about three times per second (Figure 7) and contain on-off flicker at a higher frequency (Logothetis et al., 1996). IOS rivalry can elicit two types of percepts. The first is a fast, regular perceptual alternation that is time-locked to the stimulus switches. Because this alternation corresponds to the sequence of stimuli presented to one eye, it has been proposed to arise from interocular competition, or "eye rivalry" (Lee and Blake, 1999). We will call this type of percept *fast, regular alternation rivalry*, or *FRA rivalry*. The second possible percept is a slow, irregular alternation in which perception of a single stimulus can persist over several interocular stimulus switches. Because both stimuli are presented to each eye during a period of stable perception of just one of the stimuli, this alternation has been considered to result from competition between binocular stimulus representations in the brain, or "stimulus rivalry" (Logothetis et al., 1996). We will call this type of percept *slow, irregular alternation rivalry*, or *SIA rivalry*.

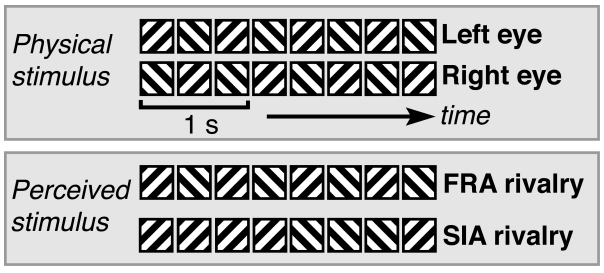

Figure 7. IOS rivalry stimuli and percepts. Orthogonal gratings are exchanged between the eyes three times per second. These stimuli give rise to two types of visual percepts: fast, regular alternations in perceived orientation that are time-locked to the stimulus exchanges (FRA rivalry), or slow, irregular orientation alternations that span multiple interocular switches (SIA rivalry).

Given the compelling evidence for perceptual selection at both eye and stimulus levels, a consensus view has emerged in which perceptual selection may occur at multiple levels in the visual hierarchy, perhaps simultaneously (Blake and Logothetis, 2002; Nguyen et al., 2003; Freeman, 2005; Tong et al., 2006; Pearson et al., 2007). However, this synthesis offers little explanation as to why perceptual selection may occur at different levels and currently does not specify the factors that determine the level(s) at which perceptual selection is resolved for a given visual display.

In the IOS rivalry paradigm, the prevalence of FRA and SIA rivalry is highly dependent on the properties of the visual stimuli that are shown (Lee and Blake, 1999; Bonneh et al., 2001; Silver and Logothetis, 2007; Kang and Blake, 2008; van Boxtel et al., 2008). This makes it an attractive paradigm for the study of how perceptual selection is governed by the specific visual information present in a display. In order to better understand the influence of spatial, temporal, and luminance factors on perceptual selection, we measured the proportions of FRA and SIA rivalry for IOS rivalry gratings over a range of spatial frequencies, flicker frequencies, and luminance conditions. Our findings suggest a new framework for understanding perceptual selection during IOS rivalry in which the type of perceptual alternation depends on distinct contributions from the magnocellular (M) and parvocellular (P) visual streams.

In Experiment 1, we found a strong spatiotemporal interaction between stimulus factors that affected the type of perceptual alternation in IOS rivalry, with different effects of flicker frequency for high and low spatial frequency stimuli. The pattern of this interaction correlates with the well-studied physiological response properties of the M and P streams. Specifically, it is consistent with the M stream being important for FRA rivalry and the P stream being preferentially associated with SIA rivalry. In Experiment 2, we tested this hypothesis by using isoluminant red/green gratings in IOS rivalry in order to reduce the M stream response to the stimuli. We observed more SIA rivalry when subjects viewed isoluminant IOS rivalry gratings compared to monochromatic black/white gratings, as predicted by the M/P framework. In Experiment 3, we probed the specific M stream mechanisms that could account for the effects of flicker frequency by varying the flicker frequency as well as the duration of a pre-switch blank period for non-flickering stimuli. We found similar effects of flicker frequency and pre-switch blank duration, suggesting that if M responses to successive presentations of orthogonal gratings are sufficiently separated in time, SIA rivalry is more likely to occur. These results suggest that transient M stream neuronal responses are a critical determinant of the type of perceptual alternation that occurs in IOS rivalry.

The M/P framework suggested by our findings provides a novel conceptual model for perceptual selection during binocular rivalry, incorporating distinct contributions from the M and P streams. This framework accounts for a number of stimulus dependencies either previously described in the IOS rivalry literature or investigated here for the first time, including spatial frequency, temporal frequency, luminance contrast, and color contrast. Unlike the distinction between lower and higher levels of the visual processing hierarchy, which is consistent with a variety of neural substrates, the M/P framework is based on fundamental physiological and anatomical subdivisions of the visual system. It is therefore amenable to further testing using a variety of neurophysiological methods and suggests new approaches for the investigation of the neural mechanisms of perceptual selection.

3.3. METHODS

3.3.1 Subjects

Twenty-three subjects participated in the experiments. Five of these subjects participated in two of the experiments, and two participated in all three (one was an author). Seven subject data sets from individual experiments were excluded from analysis (see Subject exclusion section below). This left a total of seventeen subjects (aged 19-32 years, 10 female), six of whom participated in Experiment 1, eight in Experiment 2, and eleven in Experiment 3. All subjects provided informed consent, and all experimental protocols were approved by the Committee for the Protection of Human Subjects at the University of California, Berkeley.

3.3.2 Visual stimuli

IOS rivalry displays were generated on a Macintosh PowerPC computer using Matlab and Psychophysics Toolbox (Brainard, 1997; Pelli, 1997) and were displayed on two halves of a gamma-corrected NEC MultiSync FE992 CRT monitor with a refresh rate of 60 or 90 Hz at a viewing distance of 100 cm. Subjects viewed the rivalrous stimuli through a mirror stereoscope with their heads stabilized by a chin rest. Rivalry stimuli were circular grating patches 1.8° in diameter. Each grating was surrounded by a black annulus with a diameter of 2.6° and a thickness of 0.2°. Binocular presentation of this annulus allowed it to serve as a vergence cue to stabilize eye position.

In Experiments 1 and 3, IOS rivalry stimuli were sinusoidal gratings with 4 or 7 cycles per degree (cpd), presented at 25% contrast on a neutral gray background (luminance of 59 cd/m^2). The two gratings were orthogonally oriented with +/-45° tilts and were simultaneously flickered on and off, with a 50% duty cycle, at different frequencies on different trials. Gratings had the same mean luminance as the background. Flicker frequencies were 0 (no flicker), 6, 9, 15, 22.5, and 30 Hz in Experiment 1 and 6, 9, 15, and 22.5 Hz in Experiment 3. The two grating orientations were exchanged between the eyes three times per second (except in the 22.5 Hz flicker frequency condition, in which the orientations were exchanged at 2.8 Hz in order to have an integral number of flicker cycles in each IOS period, given a 90 Hz monitor refresh rate).

In Experiment 2, IOS rivalry gratings were presented on a 23% gray background (luminance of 27 cd/m^2), which was selected based on pilot testing as a luminance level that could be perceptually matched to both red and green without saturating either color. Rivalry stimuli were circular patches of 4 cpd square-wave gratings and were either black/white monochrome or red/green isoluminant. Flicker frequencies were 0 (no flicker), 3, 6, 9, 15, 22.5, and 30 Hz. Monochrome gratings varied from dark to bright around the background gray level, with 46% contrast and the same mean luminance as the background. Red and green luminance values for the isoluminant gratings were psychophysically matched to the background gray level individually for each subject using flicker photometry (see below).

In Experiment 3, trials were either *continuous-flicker* (identical to those in Experiment 1) or *blank-only*. In blank-only trials, rivalry gratings were always on except for a brief off period (replaced with gray background luminance) just before each interocular switch. The duration of this blank period was matched to the duration of the final off period in a corresponding continuous-flicker trial. For example, in a continuous-flicker trial with 15 Hz flicker frequency, a

full flicker cycle has a duration of 67 ms, so each on and off portion of the flicker lasts 33 ms. Therefore, in the corresponding blank-only trial, the 333 ms IOS period consisted of a 300 ms on interval followed by a 33 ms off interval, followed immediately by the interocular switch.

3.3.3 Task

In all experiments, subjects viewed rivalry displays for one minute per trial. They continuously indicated their percept by holding down one of three keys: 1) fast, regular switching of perceived grating orientation, 2) slow, irregular switching (grating tilted left), or 3) slow, irregular switching (grating tilted right). Subjects were instructed to continuously press a key for as long as the corresponding percept was predominant and to not press any key for ambiguous percepts that were not one of the three response categories. Subjects completed three trials in each condition, with trials from all conditions randomly intermixed. In Experiment 2, two subjects viewed the rivalry displays for 30 s per trial. Excluding these subjects did not qualitatively change any of the results, so we included them in the analyses presented here.

3.3.4 Flicker photometry

Before completing the rivalry task of Experiment 2, subjects performed flicker photometry to determine their psychophysical red and green isoluminant values for use in the rivalry task. Subjects completed two flicker photometry sessions consisting of three runs each. The first session served as practice in order to acclimate participants to the task. The results of the second session were used to determine the isoluminant red and green intensity values that were then used in Experiment 2.

During each run, two disk colors flickered back and forth at a rate of 20 Hz while participants used key presses to increase or decrease the luminance value of the variable-luminance disk until it matched the constant-luminance disk in perceived luminance. In the first run of each session, subjects matched a green disk to the gray background. In the second run, subjects matched a red disk to the green disk, using the green luminance value determined in the first run. Finally, subjects matched a red disk to the gray background. This allowed us to estimate the consistency of the red/green isoluminant match. All disks were surrounded by black annuli, were the same dimensions as the grating stimuli used in the rivalry task, and were viewed through the stereoscope using the same setup as in the rivalry task.

Each flicker photometry run contained four trials: in two of these, the variable-luminance disk started at a high luminance value, while in the other two, the variable-luminance disk started at a low luminance value. The mean red and green color values selected for the variable-luminance disk across all trials were used as the isoluminant red and green values for an individual subject in the rivalry task.

3.3.5 Data analysis

3.3.5.1 IOS rivalry index

The “IOS rivalry index” is defined as the difference between the total time in which subjects reported SIA rivalry (sum of tilted left and tilted right response durations) and the total time they reported FRA rivalry, normalized by the sum of these values:

$$\text{IOS rivalry index}_{(\text{subject, condition})} = \frac{\text{time("SIA rivalry")} - \text{time("FRA rivalry")}}{\text{time("SIA rivalry")} + \text{time("FRA rivalry")}}$$

3.3.5.2 Normalization and statistical testing

Since we were interested in within-subject differences across the experimental conditions, we normalized each subject's IOS rivalry index values using the group mean. To do this, we first calculated the group mean IOS rivalry index across all conditions from the raw data and then added a constant to the mean of each individual subject's data across conditions so that it was equal to the group mean. This procedure does not change the mean values of the group data or the relationships among data points for single subjects, but it corrects for overall differences between subjects that would affect responses in all conditions, such as a general tendency toward experiencing SIA or FRA rivalry. All statistics and error bars were calculated using normalized data using between-subjects variance.

Statistical testing in Experiments 1 and 2 did not include the no flicker data (all trials in Experiment 3 had flicker). This is because it was not clear where to place "no flicker" stimuli on a flicker frequency continuum: although they have a flicker frequency of zero, they are perceptually more similar to the 30 Hz flicker frequency stimuli (which appeared as non-flickering, lower contrast stimuli as a result of flicker fusion) than to the 6 Hz flicker frequency stimuli (for which the slow flicker with long blank durations was easily perceived).

3.3.5.3 Flicker vs. blank-only comparison

In Experiment 1, high flicker frequencies were associated with reduced SIA rivalry for low spatial frequency stimuli, with a roughly inverse linear relationship between flicker frequency and IOS rivalry index values. In Experiment 3, we tested whether this effect held for "blank-only" stimuli. To do this, we fit linear functions to the continuous-flicker and blank-only data. These linear functions were generated in each condition for each subject, and we tested whether, across subjects, the slopes of these lines were different from zero using a two-tailed t-test on the individual subject slopes.

3.3.6 Subject exclusion

A total of seven subjects were excluded from the analysis (one subject from Experiment 2 and six subjects from Experiment 3). In Experiment 2, the subject was excluded because of inconsistent flicker photometry performance. Both when matching green to the background gray level and when matching red to gray and to green, the variance of this subject's flicker photometry values was greater than two standard deviations above the mean variance of all subjects. It is therefore likely that the isoluminant values for this subject were inaccurate; however, the results do not qualitatively change if this subject is included in the analysis.

In Experiment 3, five subjects were excluded because their IOS rivalry index was at floor or ceiling in one or more of the flicker type / spatial frequency conditions. Therefore, it was not possible to test the effects of flicker frequency for these subjects with accuracy. A subject's data was considered to be at floor or ceiling when the mean IOS rivalry index value across flicker frequencies for any flicker type / spatial frequency combination was below -0.95 or above 0.95 (the index ranges from -1 to 1). One additional subject was excluded from Experiment 3 because

in the 4 cpd, blank-only condition, this subject's fitted slope was greater than 2.5 standard deviations from the group mean. However, all reported effects do not change if this subject is included in the analysis.

3.4 RESULTS

3.4.1 Spatiotemporal interactions in IOS rivalry

Previous studies have examined the influence of spatial and temporal stimulus factors on the type of perceptual alternation during IOS rivalry. These factors include the spatial frequency of the stimuli (Lee and Blake, 1999), the temporal frequency of the interocular switches (Lee and Blake, 1999), and the duty cycle of the stimulus flicker (van Boxtel et al., 2008). However, there is currently no unified physiological explanation for these dependencies. Further, flicker of the IOS rivalry stimuli facilitates SIA rivalry (Logothetis et al., 1996; Lee and Blake, 1999), but the neural basis of this phenomenon remains unclear. Flicker has been proposed to disrupt the normal processes underlying conventional binocular rivalry (Lee and Blake, 1999) and plays a key role in a computational model of IOS rivalry (Wilson, 2003). In this model, stimulus flicker prevents the build-up of inhibition between monocular neurons, allowing perceptual competition to bypass the eye level and to be resolved instead at the stimulus level. However, van Boxtel et al. (2008) found that a short blank period immediately preceding the interocular stimulus switch was sufficient to cause SIA rivalry and that flickering the stimuli was not required.

To investigate the spatiotemporal properties of IOS rivalry and to better understand the role of flicker in facilitating SIA rivalry, we varied the spatial frequency and flicker frequency of IOS rivalry gratings and measured the proportions of FRA and SIA rivalry. Six subjects viewed IOS rivalry gratings for periods of one minute and held down keys to continuously report their percept: 1) fast, regular switching of perceived grating orientation, 2) slow, irregular switching (grating tilted left), or 3) slow, irregular switching (grating tilted right). Subjects withheld their response for ambiguous percepts that did not correspond to any of the three response categories.

We calculated an IOS rivalry index for each subject and each experimental condition, defined as the difference between the average amount of time per trial in which subjects reported SIA rivalry and the average amount of time they reported FRA rivalry, divided by the average amount of time they reported either SIA or FRA rivalry. This index ranges from 1 to -1, with 1 indicating only SIA rivalry, -1 indicating only FRA rivalry, and 0 indicating equal amounts of SIA and FRA rivalry.

The IOS rivalry index was calculated from the total time subjects reported the SIA rivalry or FRA rivalry percept, but there was also a certain amount of time in each trial during which subjects made no response at all, indicating that their percept did not match any of the response categories. We found no significant effects on the average amount of "no response" time for any of the experimental manipulations we report here. Thus, all changes in the IOS rivalry index resulted from trade-offs between SIA rivalry and FRA rivalry. (Figure 11, Supplement, shows SIA and FRA total response durations plotted separately for each experiment.)

Flicker frequency affected the proportions of FRA and SIA rivalry for IOS rivalry gratings at both spatial frequencies tested (4 and 7 cpd) (Figure 8, see also Figure 11A, Supplement). In accordance with previous findings (Logothetis et al., 1996; Lee and Blake, 1999), we observed

more SIA rivalry with flicker than without it. At high spatial frequencies without flicker, we observed more SIA rivalry than reported in previous studies (Lee and Blake, 1999), perhaps because of our longer trial duration and our method of continuous response collection. We also observed more SIA rivalry for high spatial frequency than for low spatial frequency stimuli, consistent with previous reports (Lee and Blake, 1999).

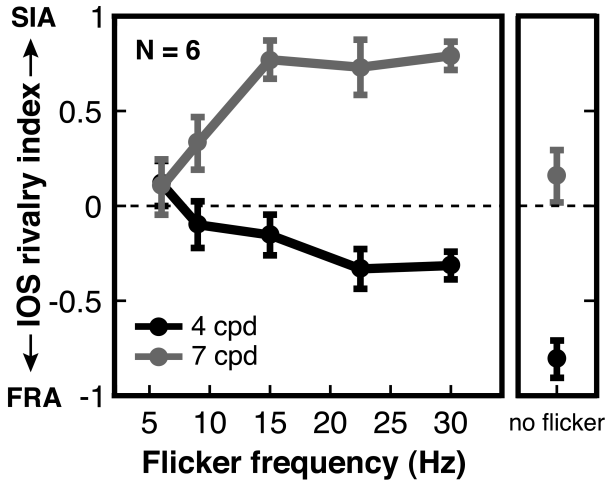

Figure 8. Results of Experiment 1: Spatiotemporal interaction in IOS rivalry. IOS rivalry gratings with high or low spatial frequencies and different on-off flicker frequencies were presented on a gray background. As flicker frequency increased, the predominance of SIA rivalry increased for high spatial frequency gratings (7 cpd, gray line) but decreased for low spatial frequency gratings (4 cpd, black line). Error bars are s.e.m.

Importantly, we found a strong interaction between flicker frequency and spatial frequency (2-way ANOVA, $F(4,50) = 8.71$, $p < 0.0001$). As flicker frequency increased, SIA rivalry increased for high spatial frequency gratings, but FRA rivalry increased for low spatial frequency gratings (Figure 8). We first consider the flicker frequency effect for high spatial frequency gratings. This effect could reflect changes in effective stimulus contrast, since effective contrast decreases with increasing flicker rate (Robson, 1966) and stimuli with lower physical contrast have been reported to enhance SIA rivalry (Lee and Blake, 1999). If effective contrast acts like physical contrast in IOS rivalry, the reduced effective contrast at higher flicker frequencies could lead to more SIA rivalry, as we observed. Indeed, we found qualitative support for this account in separate experiments in which we psychophysically measured the effective contrast of flickering high spatial frequency gratings for individual observers and then repeated the IOS rivalry experiment using 1) non-flickering gratings with physical contrasts set to the measured effective contrasts for each subject, and 2) flickering gratings with physical contrasts set to equate effective contrast across flicker frequencies (Figure 12, Supplement).

Effective contrast differences may also contribute to the relatively higher proportion of FRA rivalry observed for zero-flicker stimuli, which have higher effective contrast than their flickering counterparts. To emphasize this difference between flickering and non-flickering stimuli, as well as the perceptual similarity of non-flickering to fast-flickering stimuli (which can appear as non-flickering due to flicker fusion), we place no-flicker data points to the right of the flicker data points in all figures (except Figure 12, Supplement, which shows data from experiments in which we explicitly manipulated contrast).

Although effective contrast could explain the effect of flicker frequency on IOS rivalry for high spatial frequency gratings, the increase in FRA rivalry with increased flicker frequency for low spatial frequency gratings (Figure 8) is *inconsistent* with (and in fact is in the opposite direction

of) the effect expected from changes in effective contrast alone. Likewise, an increase in FRA rivalry with increased flicker frequency would not be predicted by a model in which flicker allows a monocular competition stage to be bypassed (Wilson, 2003), since in this model, high flicker rates are proposed to reduce inhibitory interactions among monocular neurons, leading to increased SIA rivalry.

The spatiotemporal interaction in IOS rivalry observed here cannot be explained by existing models of rivalry. What physiological mechanisms could account for these results? The P and M visual streams have spatial and temporal frequency selectivities that correlate with the stimulus parameters that promote SIA and FRA rivalry, respectively. In our data, high spatial frequencies were preferentially associated with SIA rivalry, while low spatial frequencies led to relatively more FRA rivalry. In the lateral geniculate nucleus (LGN) of the thalamus, P neurons have smaller receptive fields (Derrington and Lennie, 1984) and higher spatial resolution (Kaplan and Shapley, 1982) compared to M neurons, consistent with an association of P neurons with high spatial frequencies and M neurons with low spatial frequencies. While both spatial frequencies tested here (4 and 7 cpd) are likely to evoke some response from neurons in the P stream, neurophysiological results suggest that the M stream would respond more weakly to the 7 cpd rivalry stimuli than to the 4 cpd stimuli (Derrington and Lennie, 1984). Therefore, processing of 4 cpd stimuli is likely to be biased toward the M stream, relative to processing of 7 cpd stimuli. For these low spatial frequency stimuli, higher temporal frequencies promoted FRA rivalry. This pattern of results correlates with the temporal properties of the M stream, where higher temporal frequencies evoke larger responses in M neurons in the LGN, up to about 20 Hz (Derrington and Lennie, 1984). The association of SIA rivalry with the P stream and FRA rivalry with the M stream is also generally consistent with the canonical functions of these two visual streams, with slow, sustained processing of visual form occurring in the P stream, and rapid processing of transient, moving stimuli occurring in the M stream (Livingstone and Hubel, 1988).

3.4.2 Effects of isoluminance on IOS rivalry

To test the hypothesis that the M stream promotes FRA rivalry and the P stream is associated with SIA rivalry using a different type of stimulus manipulation, we conducted Experiment 2, in which we used red/green isoluminant stimuli to reduce responses of M stream neurons. Single-cell recordings from macaque LGN have shown that P neurons have color-opponent center-surround receptive fields, while the center and surround portions of M neuron receptive fields are not as selective for color (Schiller and Malpeli, 1978). In addition, the magnitude of the reduction in response to red/green isoluminant stimuli compared to luminance-defined stimuli is greater for M than for P LGN neurons in the macaque (Hubel and Livingstone, 1990), although this has not always been found (Logothetis et al., 1990). Finally, lesions of the P layers of the LGN cause severe deficits in perception of heterochromatic red/green flicker, while M lesions have no effect on performance of this task (Schiller et al., 1990). Isoluminant stimuli containing only color contrast are therefore commonly used to decrease the contribution of the M stream in psychophysical tasks (e.g., Livingstone and Hubel, 1987, 1988).

We used flicker photometry to determine each subject's isoluminant red and green values with respect to a standard gray background. We compared IOS rivalry for 4 cpd monochrome gratings, like those used in Experiment 1, to red/green isoluminant gratings with the same spatial frequency. This spatial frequency should activate both the M and P streams, leading to a bias in favor of the P stream in the isoluminant condition, relative to the monochrome condition.

As predicted by our M/P model of perceptual selection in IOS rivalry, reducing the contribution of the M stream using isoluminant stimuli increased SIA rivalry. A two-factor analysis of variance with flicker frequency and isoluminance as factors showed a main effect of isoluminance on the IOS rivalry index ($F(1,84) = 9.14$, $p < 0.005$), with subjects reporting more SIA rivalry in the isoluminant condition (Figure 9, see also Figure 13, Supplement).

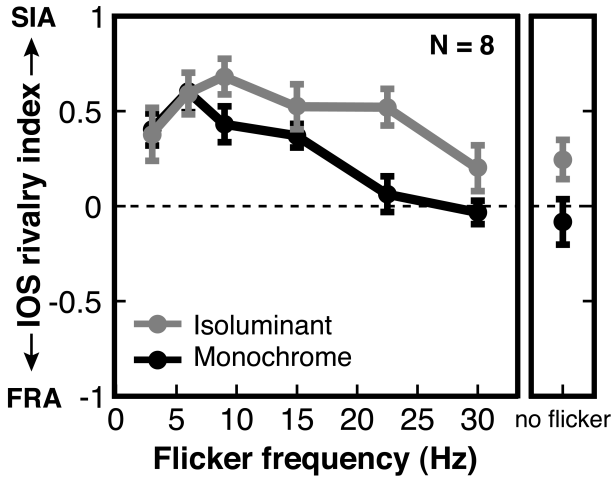

Figure 9. Results of Experiment 2: Isoluminance increases the amount of SIA rivalry in IOS rivalry. Monochrome (black/white) or isoluminant (red/green) gratings with different flicker frequencies were presented on a gray background. Subjects perceived more SIA rivalry for isoluminant gratings (gray line) than for monochrome gratings (black line). Error bars are s.e.m.

Because there was less SIA rivalry at higher flicker frequencies for both the monochrome and isoluminant conditions, the interaction between flicker frequency and isoluminance condition did not reach significance in this group of subjects. However, those subjects who showed a strong flicker frequency effect for isoluminant stimuli were also those who had a negligible main effect of isoluminance. It is possible that luminance contrast was not sufficiently minimized in the red/green stimuli presented to these subjects, possibly due to error in the flicker photometry measurements. Therefore, we selected a subset of subjects for further analysis that showed a significant effect of isoluminance at one or more flicker frequencies, as measured by paired t-tests of total time per trial reporting SIA or FRA rivalry in the monochrome compared to the isoluminant condition. Like the full sample of eight subjects, the group of six subjects who met this criterion exhibited a main effect of isoluminance ($F(1,60) = 13.74$, $p < 0.001$), with more SIA rivalry for isoluminant stimuli. In addition, this subset of subjects exhibited an interaction between flicker frequency and isoluminance condition ($F(5,60) = 2.79$, $p < 0.05$), with higher flicker frequency leading to more FRA rivalry in the monochrome condition but not in the isoluminant condition (Figure 13, Supplement). This interaction is analogous to the spatiotemporal interaction observed in Experiment 1 and is again consistent with the M/P framework.

The results from Experiment 2 corroborate those from Experiment 1 by using isoluminance, a manipulation of the relative contributions of the M and P streams that is wholly orthogonal to the spatial and temporal frequency manipulations employed in Experiment 1. In both experiments, a reduction in the ability of the IOS rivalry gratings to engage the M stream, through the use of high spatial frequency, low temporal frequency (for low spatial frequency stimuli), or isoluminant stimuli, resulted in an increase in SIA rivalry.

3.4.3 M stream temporal properties and the flicker frequency effect

Experiment 1 showed that the prevalence of FRA rivalry increases with increasing flicker frequency only for low spatial frequency gratings (Figure 8), suggesting that the M stream contributes to this flicker frequency effect. In Experiment 2, we replicated this effect and found it to be weaker when the stimuli were isoluminant (Figures 9 and 13, Supplement), again pointing to a role for the M stream in mediating the perception – and specifically the temporal frequency dependence – of FRA rivalry. In Experiment 3, we test which temporal properties of the M stream might account for the observed flicker frequency dependence of the IOS rivalry percept. We consider two hypotheses, both based on the known temporal properties of M neurons. Magnocellular neurons in the LGN exhibit larger responses to higher temporal frequencies, up to about 20 Hz (Derrington and Lennie, 1984). Therefore, in Experiments 1 and 2, the increase in FRA rivalry with increasing flicker frequency could have been due to greater activation of the M stream by higher flicker frequencies. We will call this the *temporal frequency hypothesis*. Second, neurons in the M layers of the LGN have more transient responses, in contrast to the more sustained responses of P stream neurons (Schiller and Malpeli, 1978). Extracellular recordings from the LGN show that the duration of the majority of M responses is less than 50 ms, while P responses are sustained for more than 200 ms (Maunsell et al., 1999). If interactions between M stream responses to successive stimuli (i.e., at the time of the interocular stimulus switch) are required to generate a switch in perceived grating orientation in IOS rivalry, then orthogonal gratings presented closer together in time may result in more FRA rivalry. In this case, higher flicker rates contain shorter blank intervals between successive stimulus presentations at the time of the interocular switch, facilitating interactions between successive M responses to these stimuli and leading to more FRA rivalry. We will call this the *response transiency hypothesis*.

Experiment 3 tests whether the temporal frequency tuning of the M stream or its response transiency is more likely to explain the flicker frequency effect on IOS rivalry observed in Experiments 1 and 2. Two flicker conditions were employed. One of these conditions (the *continuous-flicker condition*) replicated the continuous, 50% duty cycle on/off flicker used in Experiments 1 and 2. In the other condition (the *blank-only condition*), the rivalry gratings were presented for the entire interocular switch period without flicker but were removed from both eyes just before each switch, creating a short pre-switch blank period (van Boxtel et al., 2008). The duration of this blank period was matched to the duration of the flicker off period (i.e., one half of the flicker cycle) for one of the frequencies in the continuous-flicker conditions (Figure 10A). Thus, continuous-flicker trials and their corresponding blank-only trials were identical during the off period just before the interocular switch. However, they differed with respect to the presence or absence of flicker prior to this off period. If the temporal frequency hypothesis is correct, the proportions of FRA and SIA rivalry should be independent of the duration of the pre-switch blank period in the blank-only trials, as these trials do not contain any flicker. On the other hand, if the response transiency hypothesis is correct, the variation in the duration of the pre-switch blank period should produce a pattern of results similar to that caused by changes in flicker frequency in Experiments 1 and 2.

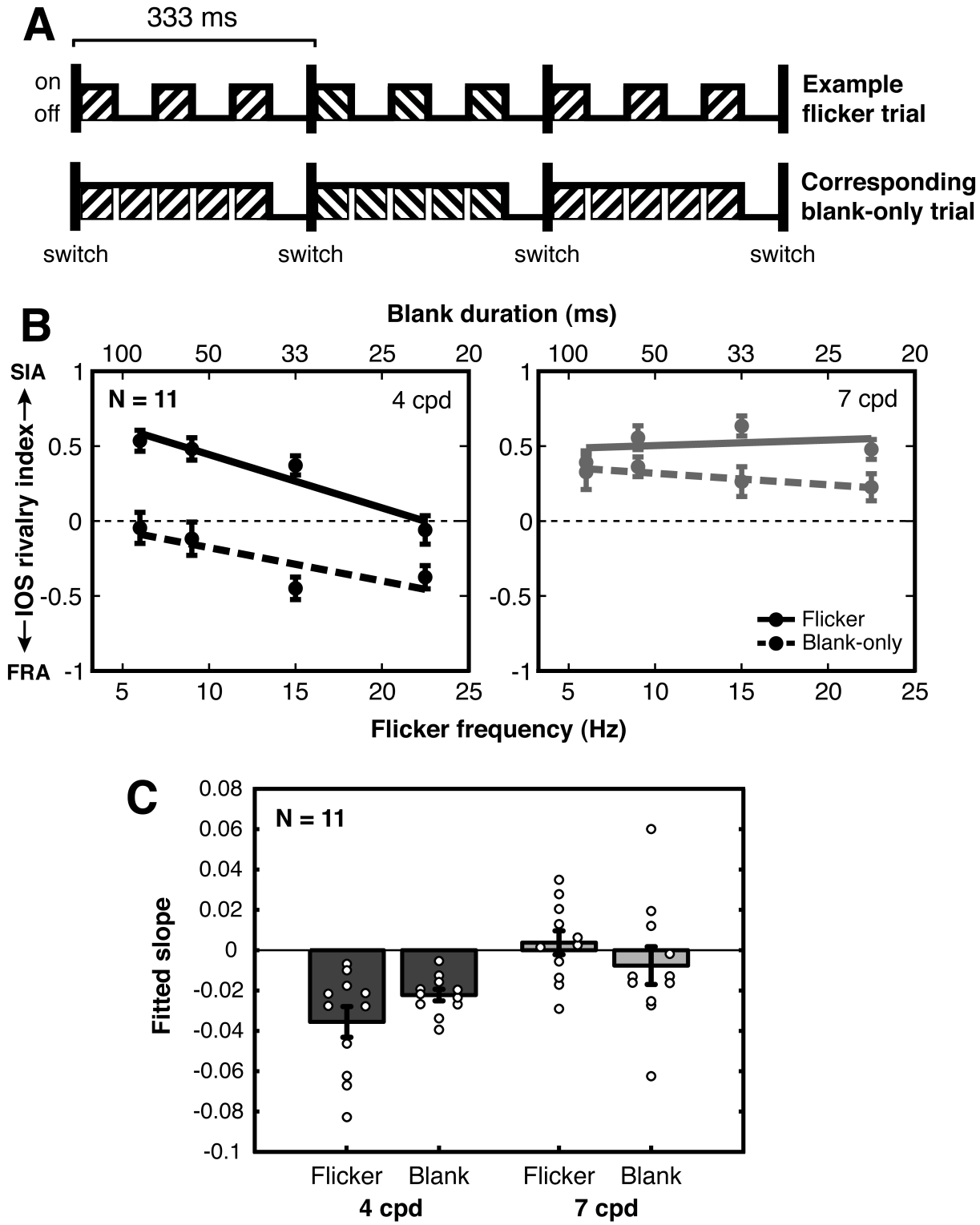

Figure 10. Stimulus design and results for Experiment 3: Short pre-switch blanks promote FRA rivalry for low spatial frequency IOS rivalry gratings. (A) Two types of stimuli were constructed. The stimulus sequence is shown for only one of the eyes. Continuous-flicker stimuli flickered on and off with a 50% duty cycle at one of four flicker frequencies in different trials. For each flicker frequency, a corresponding blank-only stimulus was constructed in which gratings were always on except during a short blank period immediately preceding the interocular switch. The duration of this blank period was the same as the duration of the pre-switch off period in the corresponding

continuous-flicker condition. In the example shown here, the flicker frequency is 9 Hz, and the corresponding blank duration is 56 ms. (B) Two spatial frequencies and four flicker frequencies were tested for both the continuous-flicker (solid lines) and blank-only (dotted lines) conditions. For low spatial frequency stimuli (4 cpd, left, black lines), increases in flicker frequency and decreases in blank duration both resulted in increased FRA rivalry. High spatial frequency stimuli (7 cpd, right, gray lines) showed no effect of either flicker frequency or blank duration on the IOS rivalry index. (C) Linear functions were fit to individual subject data for each spatial frequency / flicker condition. Means of the fitted slopes for each condition are plotted as bars (dark = low spatial frequency, light = high spatial frequency). Error bars are s.e.m. Fitted slopes for individual subjects are shown as white circles.

We tested rivalry gratings with spatial frequencies of 4 and 7 cpd in the continuous-flicker and blank-only conditions (Figure 10B, see also Figure 11C, Supplement). In the continuous-flicker condition, we replicated the spatiotemporal interaction between spatial frequency and flicker frequency found in Experiment 1 (2-way ANOVA, $F(3,80) = 7.50$, $p < 0.0005$). We also observed a significant main effect of flicker condition, with more SIA rivalry for continuous-flicker trials than for blank-only trials (3-way ANOVA, $F(1,160) = 88.8$, $p < 0.0001$). This effect of flicker condition may have been due to lower effective contrast for continuous-flicker trials compared to blank-only trials (Robson, 1966).

To test the temporal frequency and response transiency hypotheses, we fit linear functions to individual subject data from continuous-flicker and blank-only trials (Figure 10C). For low spatial frequency, the slopes of the linear fits were significantly different from zero for both the continuous-flicker and blank-only conditions (t-test, continuous-flicker, $t(10) = 4.67$, $p < 0.001$; blank-only, $t(10) = 7.74$, $p < 0.0001$). In both cases, increased flicker frequency (or reduced blank duration) resulted in more FRA rivalry. We also fit linear functions to the high spatial frequency data and found that neither the continuous-flicker nor the blank-only trials had slopes that were significantly different from zero (t-test, continuous-flicker, $t(10) = 0.63$, $p > 0.5$; blank-only, $t(10) = 0.82$, $p > 0.1$). Thus, for high spatial frequency gratings that preferentially activate the P stream, there was no detectable effect of either flicker frequency or blank duration on perception during IOS rivalry. On the other hand, clear and similar effects of flicker frequency and blank duration were observed specifically for the low spatial frequency gratings that are biased toward M stream processing.

These findings support the response transiency hypothesis – that interactions between responses to successive orthogonal stimuli in the M stream are important for the perception of FRA rivalry. They also counter the notion that flicker per se is required to generate SIA rivalry (Lee and Blake, 1999; Wilson, 2003), since changes in the duration of the pre-switch blank period for non-flickering stimuli were sufficient to influence the proportion of SIA rivalry. A similar point was made by van Boxtel et al. (2008), who observed increased levels of SIA rivalry when a blank was inserted before interocular switches in non-flickering IOS rivalry stimuli. Our results confirm this finding and further show that the dependence of this effect on blank duration is only present for the spatial frequency that is relatively biased toward M stream processing. Lastly, the effect of blank duration is similar in size to the flicker frequency effect in the same subjects.

3.5 DISCUSSION

The neural sites at which binocular rivalry are resolved is a fundamental question in the study of visual awareness and has been the topic of much debate (Blake and Logothetis, 2002; Tong et al., 2006). A centerpiece of this debate has been the demonstration of “stimulus rivalry” during

IOS rivalry: a pair of rivalrous stimuli that are periodically exchanged between the two eyes can generate slow, irregular alternations of percepts that require visual information to be combined across the two eyes over multiple interocular stimulus switches (SIA rivalry) (Logothetis et al., 1996). This observation has been used to argue that high-level stimulus representations, as opposed to low-level, eye-specific ones, compete for perceptual selection during rivalry (Logothetis et al., 1996; Sengpiel, 1997; Logothetis, 1998). It has also influenced models in which binocular rivalry is resolved at multiple hierarchical levels in the visual system (Logothetis et al., 1996; Dayan, 1998; Ooi and He, 1999; Bonneh et al., 2001; Freeman, 2005; Tong et al., 2006; Pearson et al., 2007).

Although the existence of SIA rivalry has been interpreted as evidence for high-level perceptual selection, it has also been shown that these alternations occur only under specific stimulation conditions (Lee and Blake, 1999). Computational models in which rivalry may either occur at the "eye level" or at a higher "stimulus level" can account for some of these dependencies, such as the increase in SIA rivalry for flickering stimuli (Wilson, 2003). However, no existing model provides a unified account of the various documented stimulus factors that promote FRA or SIA rivalry.

Our findings provide new evidence regarding the stimulus properties that govern perception during IOS rivalry and suggest a physiologically-grounded framework that accounts for many of the findings in the IOS rivalry literature. The M/P framework provides an alternative to the eye level/stimulus level dichotomy in that it does not require the FRA percept to result from selection at a lower level in the visual hierarchy than the SIA percept. Rather, the type of perceptual alternation is determined by the preferential processing of IOS rivalry stimuli in either the M or P stream. Combined with previous findings from physiological and lesion studies in the LGN, our results demonstrate an association between the temporal and spatial frequencies that generate FRA rivalry and activate the M stream and between those that generate SIA rivalry and activate the P stream (Table 1). Although we consider human IOS rivalry data alongside physiology and lesion results from macaque monkeys, a number of studies have shown that humans and macaques have very similar flicker detection thresholds (De Valois et al., 1974b), contrast sensitivity functions (De Valois et al., 1974a), and perceptual alternations during binocular rivalry (Leopold and Logothetis, 1996).

Relationships between perception during IOS rivalry and properties of the P and M processing streams

Parallels between P stream properties and stimulus properties leading to more SIA rivalry

Stimulus attribute	Parvocellular LGN physiology (macaques)	Effects of parvocellular LGN lesions (macaques)	SIA rivalry (humans)
Spatial frequency	Small receptive fields [1], high spatial resolution [1,2]	Decrease in visual acuity [3], reduction in contrast sensitivity especially for spatial frequencies >2 cpd [4]	Higher spatial frequency [5, present study]
Temporal frequency	Optimal temporal frequency ~10 Hz [1,6]	No effect on flicker detection [4]	Lower flicker rates [present study]
Transience	Sustained responses [7,8]	N/A	Longer blank between successive orthogonal stimuli [9, present study]
Color contrast	Color-opponent receptive fields [7], strong responses to colored gratings [10]	Reduction in color contrast sensitivity [3] and heterochromatic flicker sensitivity [4]	Isoluminant red/green stimuli [present study]
Luminance contrast	Weak contrast sensitivity [1,2]	Reduction in contrast sensitivity [3,4]	Lower contrast [5,11, present study]

Parallels between M stream properties and stimulus properties leading to more FRA rivalry

Stimulus attribute	Magnocellular LGN physiology (macaques)	Effects of magnocellular LGN lesions (macaques)	FRA rivalry (humans)
Spatial frequency	Large receptive fields [1], low spatial resolution [1,2]	No effect on visual acuity [4]	Lower spatial frequency [5, present study]
Temporal frequency	Optimal temporal frequency ~20 Hz [1,6]	Impairment of flicker detection [12], especially >15 Hz [4]	Higher flicker rates [present study]
Transience	Transient responses [7,8]	N/A	Shorter blank between successive orthogonal stimuli [9, present study]
Color contrast	No color-opponent receptive fields [7], poor responses to chromatic gratings [10]	No effect on color contrast sensitivity [3] or heterochromatic flicker sensitivity [4]	Monochrome black/white stimuli [present study]
Luminance contrast	Strong contrast sensitivity [1,2]	No effect on contrast sensitivity [4] except at high temporal frequencies [3]	Higher contrast [5,11, present study]

Table 1. Top, properties of P pathway and stimulus conditions leading to SIA rivalry. Bottom, properties of M pathway and stimulus conditions leading to FRA rivalry. Both physiological and lesion results from the M and P pathways are in correspondence with the stimulus conditions favoring FRA and SIA rivalry in all cases where data are available, with the partial exception of luminance contrast (see Discussion). References cited in the table are as follows: 1. Derrington and Lennie, 1984; 2. Kaplan and Shapley, 1982; 3. Merigan et al., 1991; 4. Schiller et al., 1990; 5. Lee and Blake, 1999; 6. Hicks et al., 1983; 7. Schiller and Malpeli, 1978; 8. Maunsell et al., 1999; 9. van Boxtel et al., 2008; 10. Hubel and Livingstone, 1990; 11. Logothetis et al., 1996. 12. Merigan and Maunsell, 1990.

The M/P framework not only accounts for effects of spatial frequency, temporal frequency, and color contrast on IOS rivalry, but it may account for the effects of luminance contrast as well. Lee and Blake (1999) showed that lower contrast stimuli are more likely to generate SIA rivalry than higher contrast stimuli (see also Logothetis et al., 1996 and Figure 12, Supplement). In the M/P framework, these findings would be consistent with an association between the P stream and low contrast vision. However, the physiology and lesion data diverge on the question of whether the processing of low contrast stimuli relies more on the P or the M stream (Table 1). Individual P cells exhibit weak contrast sensitivity, while individual M cells are highly sensitive to contrast (Kaplan and Shapley, 1982; Derrington and Lennie, 1984). However, P layer lesions result in reductions in contrast sensitivity, as measured behaviorally, while M layer lesions do not (except at high temporal frequencies), suggesting that the P stream supports processing of low contrast stimuli (Schiller et al., 1990; Merigan et al., 1991). This discrepancy between the physiological and lesion data for luminance contrast may be explained by the fact that there are many more retinal inputs to the P than to the M layers of the LGN (Perry et al., 1984), and behavioral detection of low contrast stimuli near threshold results from significant averaging across neurons. Therefore, both physiological and lesion results from the M and P pathways are in correspondence with the stimulus conditions favoring FRA and SIA rivalry in all cases where data are available, with the partial exception of luminance contrast – where the physiology and lesion data disagree and the M/P framework is consistent with results from lesion studies, which assess contrast sensitivity of the entire visual system.

In Experiment 2, we used isoluminant stimuli to decrease the relative contribution of M stream processing (Livingstone and Hubel, 1987, 1988) and found more SIA rivalry for isoluminant gratings, consistent with the M/P framework. However, it should be noted that red/green gratings have both lower luminance contrast and higher red/green color contrast than monochromatic gratings. It is therefore possible that the results from Experiment 2 could be due to differences in luminance contrast (see also Lee and Blake (1999) and Figure 12, Supplement) that are not related to differential contributions of the M and P streams. However, color stimuli with minimal luminance contrast are strongly biased towards P stream processing, and importantly, contrast effects alone cannot account for all of the results we report. Specifically, they cannot explain the decrease in SIA rivalry with increasing flicker frequency for 4 cpd, luminance-defined stimuli (Figures 8-10), while these results are predicted by the M/P framework.

Our results suggest that stimuli that are more likely to elicit M stream responses lead to the perception of fast, regular alternations, whereas stimuli that are preferentially processed by the P stream result in slow, irregular alternations of sustained form percepts, with rivalry dynamics similar to conventional, static binocular rivalry. These changing and sustained form percepts are consistent with the general roles of the dorsal and ventral cortical processing streams in the perception of transient events and stimulus motion, and the perception of sustained form information, respectively. The dorsal and ventral cortical streams, in turn, have been proposed to

depend on the functions of the M and P systems. (Ungerleider and Mishkin, 1982; Livingstone and Hubel, 1988).

Although the M/P framework is based on correlations between stimulus factors that produce either FRA or SIA rivalry and the results of physiological and lesion studies in the M and P layers of the LGN, the framework does not require that binocular rivalry be resolved in the LGN. In fact, orthogonal rivalrous stimuli and congruent grating pairs produce identical responses in LGN neurons of awake macaque monkeys performing a visual fixation task (Lehky and Maunsell, 1996). The amount of segregation of the M and P streams in visual cortex is controversial (Livingstone and Hubel, 1988; Merigan and Maunsell, 1993; see Nassi and Callaway, 2009, for a recent review), but the complementary effects of lesions of the M and P layers of the LGN on visual perception suggest significant functional segregation of the two systems (Schiller et al., 1990). We propose that processing of visual stimuli in IOS rivalry is preferentially routed into distinct cortical circuits based on the relative responses of M and P LGN neurons and that the resulting perceptual alternations take place in these cortical circuits. Physiological studies will be required to assess this possibility directly.

Studies that compare motion to color and form during conventional binocular rivalry viewing are also consistent with the M/P framework. Rivalry between face stimuli strongly reduces sensitivity to the appearance of face probes presented to the suppressed eye but has no effect on the detection of probes containing visual motion (Alais and Parker, 2006). Analogous results have been obtained for motion rivalry and face probes (Alais and Parker, 2006), suggesting a high level of independence of rivalry for motion (associated with the M and dorsal cortical streams) and visual form rivalry (associated with the P and ventral cortical streams). Other studies have shown that rivalrous stimuli containing incongruent motion signals and incongruent form or color simultaneously generate a perception of binocular integration of motion and perceptual alternations of form or color (Carney et al., 1987; Andrews and Blakemore, 1999; Carlson and He, 2000; Andrews and Blakemore, 2002). These findings have led to the suggestion that rivalry may be primarily a product of the P pathway (Carlson and He, 2000; He et al., 2005).

On the other hand, Livingstone and Hubel (1988) have suggested that binocular rivalry, like stereopsis, depends on the M stream, since it breaks down at high spatial frequencies (>10 cpd) and at isoluminance. In line with this view, rivalry can be generated by interocular differences in motion direction for stimuli that are otherwise identical (Enoksson, 1963; Logothetis and Schall, 1990). Our results suggest a possible reconciliation of these views, namely that rivalry may occur within either the M or P stream, depending on the relationship between stimulus properties and the selectivities of the two streams. This view is supported by the findings that large interocular differences in spatial (Yang et al., 1992) or temporal (van de Grind et al., 2001) stimulus properties do not produce binocular rivalry but instead result in a percept of transparency. Likewise, in random-dot stereograms, stereopsis may be mediated by one spatial frequency channel, while rivalry simultaneously occurs in another (Julesz and Miller, 1975). One possibility is that two stimuli that are separately processed by the M and P streams cannot engage in rivalry and that rivalry can only occur within either the M or P stream.

Our third experiment suggests that the transient nature of M stream neuronal responses may underlie the relative predominance of FRA rivalry at high flicker frequencies for low spatial frequency gratings. We observed that successive, orthogonally oriented gratings presented closer

together in time were more likely to lead to FRA rivalry than orthogonal gratings presented further apart in time. This effect was present only for low spatial frequency stimuli, implicating the M stream. This finding can also be viewed in the context of the role of the M stream in motion perception. One perceptual interpretation of FRA rivalry is that of a single grating apparently moving between left- and right-tilted orientations, either alternating between the two orientations or rotating clockwise or counterclockwise. Previous studies have found that perception of apparent motion is strongly dependent on the duration of the blank interval between successive stimulus presentations. Specifically, apparent motion perception is most sensitive to small changes in temporal interval in the range of 20-100 ms, with stronger apparent motion for shorter intervals and weaker apparent motion for longer intervals (Baker and Braddick, 1985; Bours et al., 2007). This interval range is similar to that of the pre-switch blank durations in our Experiment 3, where we observed a similar pattern of sensitivity to temporal interval between successive stimulus presentations, with shorter intervals leading to increased perception of FRA rivalry (for low spatial frequency stimuli only). Therefore, one interpretation of the results from Experiment 3 is that the inter-stimulus interval-dependent mechanisms responsible for motion perception also contribute to the perception of FRA rivalry.

Previous studies have shown increases in SIA rivalry in the presence of on-off flicker in IOS rivalry (Logothetis et al., 1996; Lee and Blake, 1999; Knapen et al., 2007; van Boxtel et al., 2008). One prominent explanation of this effect has been that flicker reduces interocular inhibition between monocular neuronal populations, resulting in perceptual selection at a higher, binocular level in the visual hierarchy. This explanation has been applied to the finding that stimulus flicker increases both SIA rivalry in IOS rivalry (van Boxtel et al., 2008) and interocular grouping of Diaz-Caneja-type "horseshoe" stimuli (Knapen et al., 2007). Wilson (2003) explicitly modeled this hypothesis using a two-level neural network in which stimulus flicker prevents the build-up of inhibition between left eye and right eye neurons at the lower, monocular level, resulting in competition between incompatible stimulus representations at the higher, binocular level. Our data are not consistent with this model in three ways. First, we found that varying flicker frequency had different effects for high and low spatial frequency stimuli, a result that would not be predicted by a general model of this type. Second, we showed, in agreement with van Boxtel et al. (2008), that flicker is not required to increase the prevalence of SIA rivalry: a short blank before each orientation switch is sufficient. Third, we observed a substantial amount of SIA rivalry for high spatial frequency stimuli, even with no flicker and no blanks. Therefore, even when there is ample time for the build-up of monocular inhibition to occur, SIA rivalry can still take place.

One appealing aspect of the M/P framework is that it is amenable to physiological testing. Electrophysiology, brain imaging, lesion, and patient studies could all help to confirm or refute the validity of this framework. In addition, future physiological as well as psychophysical investigations could potentially refine the framework by testing specific mechanisms by which M stream activity might lead to FRA rivalry and P stream activity to SIA rivalry. Finally, the M pathway is selectively impaired in dyslexia (Demb et al., 1998) and schizophrenia (Butler and Javitt, 2005). A better understanding of the contributions of the M and P systems to perceptual selection will be useful for characterizing the consequences of M stream dysfunction in these diseases.

The M/P framework for interpreting experimental results from IOS rivalry brings together psychophysical and physiological results to shed light on the neural basis of perceptual selection. As an alternative to the eye level/stimulus level dichotomy, this framework raises important questions regarding how parallel visual processing pathways and the hierarchical organization of the visual system interact to generate perception. With its sensitivity to multiple physiologically-relevant stimulus dimensions, IOS rivalry offers a powerful paradigm for continued exploration of these questions.

3.6 SUPPLEMENT

3.6.1 Total response durations for Experiments 1-3

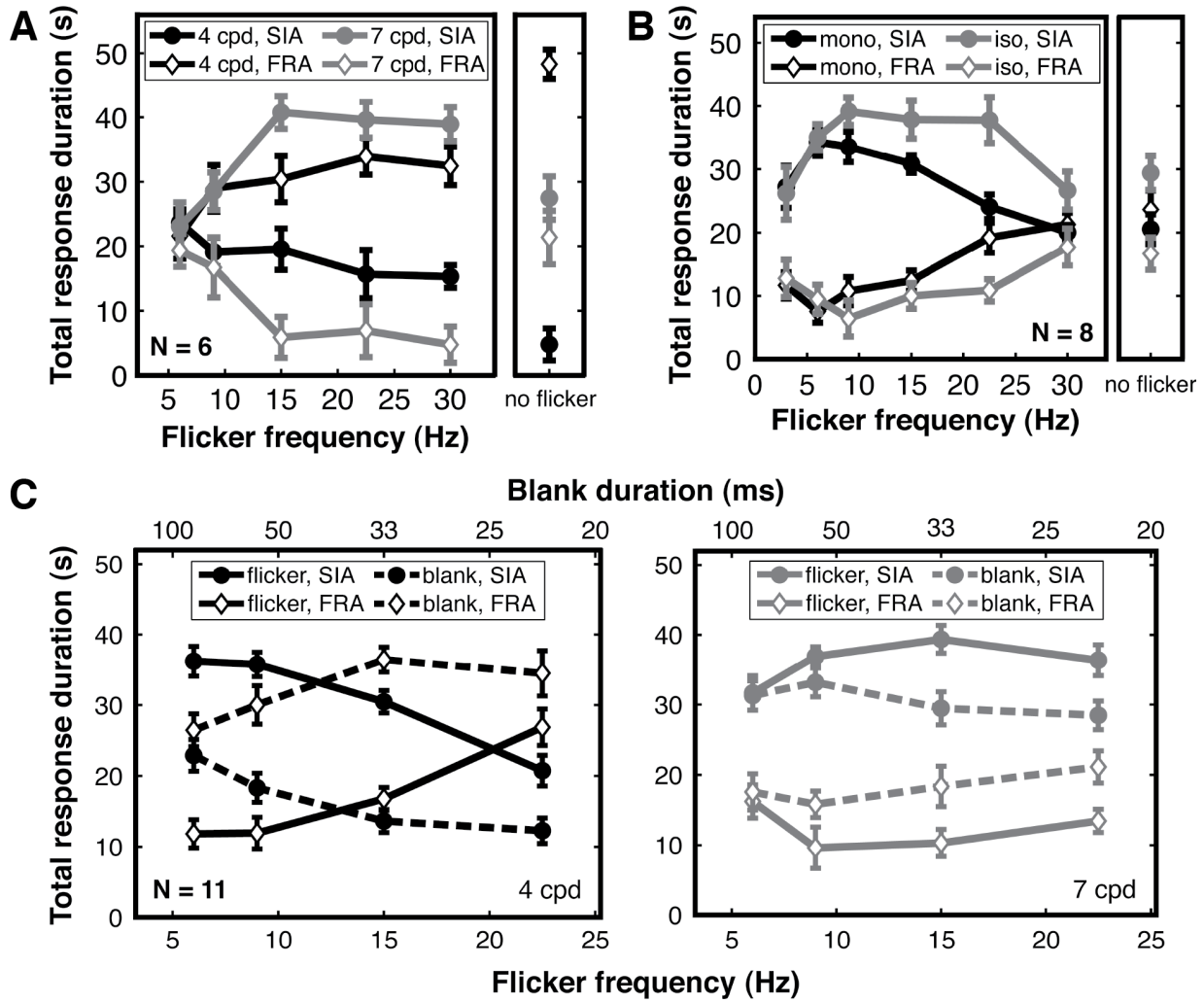

Figure 11. (A) Experiment 1: Mean total duration of SIA and FRA rivalry responses. Each trial duration was 60 s. For high spatial frequency gratings (7 cpd, gray), SIA rivalry (filled circles) increases while FRA rivalry (empty diamonds) decreases with increasing flicker frequency. The opposite pattern holds for low spatial frequency gratings (4 cpd, black). Error bars show s.e.m. across subjects. (B) Experiment 2: Mean total duration of SIA and FRA rivalry responses. Each trial duration was 60 s. Isoluminant stimuli (gray) resulted in increased SIA rivalry (filled circles) and reduced FRA rivalry (empty diamonds) compared to monochrome stimuli (black). Error bars show s.e.m. across subjects. (C) Experiment 3: Mean total duration of SIA and FRA rivalry responses. Each trial duration was 60 s. Overall, less SIA rivalry (filled circles) and more FRA rivalry (empty diamonds) was observed for blank-only trials (dashed lines) compared to flicker trials (solid lines). However, the effects of flicker frequency were

similar for blank-only and flicker trials. This was the case for both the low spatial frequency (4 cpd, left, black lines) and high spatial frequency (7 cpd, right, gray lines) conditions. Error bars show s.e.m. across subjects.

3.6.2 Effective contrast experiments

In Experiment 1, we observed an increase in SIA rivalry with increasing flicker frequency for high spatial frequency IOS rivalry gratings. While this effect of flicker frequency on perception of high spatial frequency stimuli is not incompatible with the M/P framework, it is also not predicted by this framework. We hypothesized that decreases in effective contrast with increasing flicker frequency could explain this effect, since reducing physical stimulus contrast has been shown to increase the predominance of SIA rivalry in IOS rivalry (Lee and Blake, 1999). Therefore, in Supplemental Experiment 1 (SE1), we tested whether non-flickering gratings that were matched in effective contrast to gratings with different flicker frequencies would yield IOS rivalry percepts similar to those observed with flickering gratings that had the same effective contrast. In Supplemental Experiment 2 (SE2), we tested whether equating effective contrast for gratings with different flicker frequencies would eliminate the effect of flicker frequency on the IOS rivalry index. Two subjects participated in these experiments; both had also participated in Experiment 1 (Subject 1 was an author). Both experiments consisted of a contrast matching session and an IOS rivalry session.

3.6.2.1 Methods

Contrast matching. Two pairs of gratings with the same properties as those used in Experiment 1 were arranged vertically on a screen, one pair on top of the other, and viewed through a mirror stereoscope. The display setup was identical to that described in Experimental Procedures in the main text. The gratings had a spatial frequency of 7 cpd and were oriented with +/- 45˚ tilt from vertical. Because the two gratings comprising each pair were identical, they were binocularly fused when viewed through the stereoscope, yielding a percept of two tilted gratings, one on top of the other.

The top grating pair was the "standard" and always had a physical contrast of 25%, corresponding to the contrast of the gratings in Experiment 1. The bottom grating pair was the "adjusted" stimulus – that is, subjects adjusted the physical contrast of this stimulus to match the perceived contrast of the fixed standard. In SE1 contrast matching runs, the standard flickered and the adjusted stimulus did not flicker. In SE2 runs, the adjusted stimulus flickered, while the standard did not flicker. Flicker frequencies of 0 (no flicker), 6, 9 15, 22.5, or 30 Hz were tested, and flicker was on/off with a 50% duty cycle. Each run contained four trials: in two of these, the adjusted stimulus started at a high contrast, while in the other two, the adjusted stimulus started at a low contrast. The "matched contrast value" for each run was taken to be the mean of the values from the four trials. Thus, SE1 contrast matching produced estimates of the effective contrast of a 25% physical contrast grating flickering at different frequencies, while SE2 contrast matching produced estimates of the physical contrast of a grating flickering at different frequencies required to have an effective contrast equal to a non-flickering 25% contrast grating.

IOS rivalry. IOS rivalry stimuli were presented for periods of 60 s while subjects held down keys to report fast-switch, slow-switch (tilted left), or slow-switch (tilted right) percepts. Stimuli and procedures were identical to those used in Experiment 1, except for the following: 1) All stimuli

had a spatial frequency of 7 cpd. 2) In SE1, gratings did not flicker but were presented at six different contrasts in different trials. Each flicker frequency was presented at a different contrast that was derived from the contrast matching portion of SE1. In SE2, IOS rivalry gratings flickered on and off with a 50% duty cycle at frequencies of 0, 6, 9, 15, 22.5, and 30 Hz in different trials. Gratings with each of these flicker frequencies were set to the corresponding matched contrast values measured in the contrast matching portion of SE2. Three trials in each condition were presented in SE1 and six trials in each condition were presented in SE2, with three trials per condition in each of two blocks. All conditions were randomly intermixed within a block.

3.6.2.2 Results

Contrast matching. Both subjects showed the expected pattern of results in both SE1 and SE2 contrast matching sessions: a decrease in effective contrast as flicker frequency increased. In SE1, in which the standard was flickering, matched contrast values for the adjusted stimulus decreased with increasing flicker frequency (Figure 12A, top), while in SE2, in which the adjusted stimulus was flickering, matched contrast values for that stimulus increased with increasing flicker frequency (Figure 12A, bottom).

IOS rivalry. In the IOS rivalry portion of SE1, both subjects showed increases in SIA rivalry as the contrast of the gratings was reduced, even though none of the gratings were flickering (Figure 12B, middle). This increase was similar to the effect of flicker frequency for high spatial frequency gratings in Experiment 1 (Figure 12B, top). In SE2, when effective contrast was equated for stimuli with different flicker frequencies, the flicker frequency effect seen in Experiment 1 was not apparent for either subject (Figure 12B, bottom). Together, these experiments suggest that the increase in SIA rivalry for high spatial frequency IOS rivalry gratings in Experiment 1 may be accounted for by changes in effective contrast and not by changes in flicker frequency per se.

Figure 12. IOS rivalry effective contrast experiments. (A) Contrast matching results. In SE1 (top), two subjects adjusted the contrast of a non-flickering grating to perceptually match it to a 25% contrast standard grating that flickered on and off at one of six flicker frequencies. In SE2 (bottom), the same subjects adjusted the contrast of a flickering grating (same flicker frequencies) to match the contrast of a non-flickering standard with 25% contrast. Error bars are s.e.m. of the four contrast matching trials in each condition. In all cases, increasing flicker frequency reduced effective contrast. (B) Results of IOS rivalry experiments with matched contrast. Top: Individual subject data from Experiment 1 for Subjects 1 and 2. These subjects are representative of the group that participated in Experiment 1. Middle: In SE1, subjects viewed non-flickering IOS rivalry stimuli with contrast that was matched to a 25% contrast stimulus flickering at different frequencies ("Equivalent flicker frequency"). Both subjects reported more SIA rivalry for lower contrast (higher equivalent flicker frequency) gratings. Bottom: In SE2, subjects viewed flickering IOS rivalry stimuli for which effective contrast was equated across flicker frequencies. There was no apparent change in the IOS rivalry index as a function of flicker frequency.

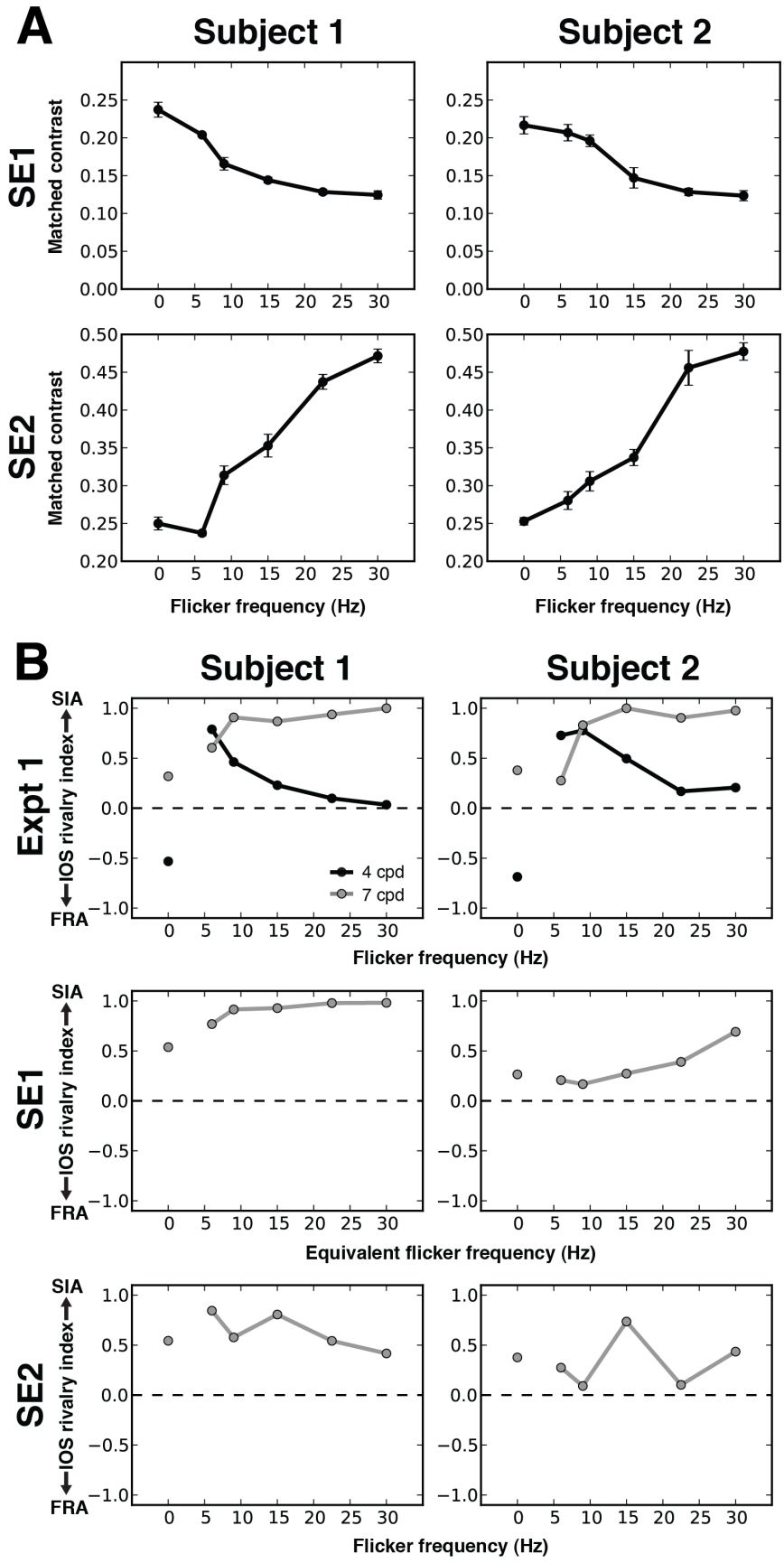
A
Subject 1
Subject 2
SE1
Matched contrast
SE2
Matched contrast
Flicker frequency (Hz)
Flicker frequency (Hz)
B
Subject 1
Subject 2
Expt 1
SIA
IOS rivalry index
FRA
4 cpd
7 cpd
Flicker frequency (Hz)
SE1
Equivalent flicker frequency (Hz)
SE2
Flicker frequency (Hz)

3.6.3 Interaction between flicker frequency and isoluminance condition

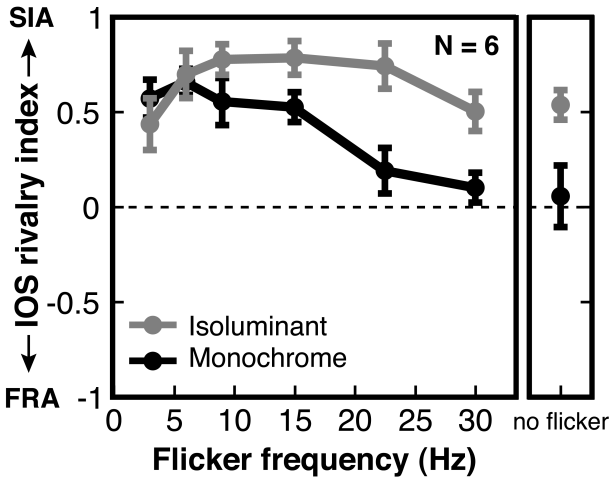

Figure 13. Results of Experiment 2: Interaction between flicker frequency and isoluminance condition for a subset of subjects who showed a main effect of isoluminance. Data are plotted from six subjects who reported more SIA or less FRA rivalry for the isoluminant compared to the monochrome stimuli at one or more flicker frequencies. As flicker frequency increased, SIA rivalry decreased for monochrome stimuli, but there was no significant effect of flicker frequency on the IOS rivalry index for isoluminant stimuli.

Chapter 4

Functional mapping of the magnocellular and parvocellular subdivisions of human LGN

4.1 ABSTRACT

The magnocellular (M) and parvocellular (P) subdivisions of primate LGN are known to process complementary types of visual stimulus information, but a method for noninvasively defining these subdivisions in humans has proven elusive. As a result, the functional roles of these subdivisions in humans have not been investigated physiologically. To functionally map the M and P subdivisions of human LGN, we used high-resolution fMRI at high field (7T and 3T) together with a combination of spatial, temporal, luminance, and chromatic stimulus manipulations. We found that stimulus factors that differentially drive magnocellular and parvocellular neurons in primate LGN also elicit differential BOLD fMRI responses in human LGN and that these responses exhibit a spatial organization consistent with the known anatomical organization of the M and P subdivisions. In test-retest studies, the relative responses of individual voxels to M-type and P-type stimuli were reliable across scanning sessions on separate days and across sessions at different field strengths. The ability to functionally identify magnocellular and parvocellular regions of human LGN with fMRI opens possibilities for investigating the functions of these subdivisions in human visual perception, in patient populations with suspected abnormalities in one of these subdivisions, and in visual cortical processing streams arising from parallel thalamocortical pathways.

4.2 INTRODUCTION

Parallel processing, the simultaneous analysis of different sensory features in different brain areas, enables the efficient representation of a huge variety of sensory properties (Nassi and Callaway, 2009). An important early site of parallel processing in the mammalian visual system is the lateral geniculate nucleus (LGN) of the thalamus, the primary thalamic relay between the retina and visual cortex (Sherman and Guillery, 2006). In primates, the LGN is composed of magnocellular (M), parvocellular (P), and koniocellular (K) layers. Monkey electrophysiological studies have demonstrated that M and P neurons, which dominate primate vision (Schiller et al., 1990; Nassi and Callaway, 2009), have distinct and complementary spatial, temporal, luminance, and chromatic stimulus preferences (Schiller and Malpeli, 1978; Kaplan and Shapley, 1982; Hicks et al., 1983; Derrington and Lennie, 1984; Hubel and Livingstone, 1990; Shapley, 1990; Reid and Shapley, 2002) and response dynamics (Schiller and Malpeli, 1978; Maunsell et al., 1999). As a result, M neurons are well suited for the detection of motion and other rapid visual

changes occurring at large spatial scales, while P neurons are well suited for detailed form and color processing.

Although the functions of the M and P subdivisions have been well characterized in the macaque monkey LGN, their study in the human LGN has proven challenging. In particular, the LGN's small size and location deep within the brain has made it difficult to measure distinct signals from the M and P subdivisions using noninvasive techniques. However, there are strong motivations to study these subdivisions in humans, including: understanding their roles in human visual perception, attention, and awareness (Livingstone and Hubel, 1988; Yeshurun and Levy, 2003; Denison and Silver, 2012); characterizing their interactions with large-scale cortical networks; and evaluating their involvement in human disorders such as dyslexia (Stein and Walsh, 1997) and schizophrenia (Butler and Javitt, 2005). Importantly, given the lack of functional data from human M and P subdivisions, the degree to which their functional properties have been conserved across humans and other primates remains an open question. While conservation is expected based on similarities in both visual system anatomy and visual perception between monkeys and humans (De Valois et al., 1974a; De Valois et al., 1974b; de Courten and Garey, 1982; Merigan, 1989; see Livingstone and Hubel, 1987, 1988), perfect homology between the species cannot be assumed (Hickey and Guillery, 1979).

Here we report the first robust demonstration of functional maps of the M and P subdivisions of human LGN using fMRI at 7T and 3T, employing stimuli based on the response properties of monkey M and P neurons. Maps with the anatomically correct spatial organization were observed in nearly all hemispheres, and individual subjects' maps were reliable across separate scanning sessions.

4.3 METHODS

4.3.1 Subjects

Six adult subjects (25-27 years of age; 1 male, 5 females) participated in the study. Three subjects were scanned in multiple sessions, and two of the subjects were authors. All subjects provided written informed consent, and all experimental protocols were approved by the Committee for the Protection of Human Subjects at the University of California, Berkeley, or the Institutional Review Board for human subjects research at the University of Minnesota, as appropriate. Subjects had normal or corrected-to-normal visual acuity.

4.3.2 Visual display

The stimuli were generated on Macintosh computers using MATLAB (The MathWorks Inc., Natick, MA), Psychophysics Toolbox (Brainard, 1997; Pelli, 1997), and Python with Vision Egg (Straw, 2008) and displayed using gamma-corrected projection systems. In Minnesota, stimuli were projected from a NEC NP4000 (NEC Display Solutions, Tokyo) liquid crystal display projector located outside the scanner room and reflected via a mirror onto a translucent screen positioned over the subject's chest. The screen was viewed via a mirror mounted over the subject's eyes, with a total viewing distance of 23-31 cm. The screen height subtended 20-29 degrees of visual angle, and the screen width subtended 47-70 degrees of visual angle, with variability across subjects arising from differences in screen positioning. In Berkeley, stimuli were projected from an Avotec SV-6011 (Avotec, Inc., Stuart, FL) liquid crystal display

projector onto a translucent screen located at the end of the scanner bore behind the subject's head. The screen was viewed via a mirror mounted over the subject's eyes, with a total viewing distance of 29 cm. The screen height subtended 34-37 degrees of visual angle, and the screen width subtended 44-48 degrees of visual angle.

4.3.3 Visual stimulus

An alternating hemifield stimulus (Figure 14A) was used to localize the LGN (Figure 14B). This stimulus consisted of a 100% contrast flickering checkerboard pattern that reversed contrast polarity at a frequency of 4 Hz (for the full flicker cycle). This checkerboard had a radial check pattern with a check size of 15° polar angle and an eccentricity that was scaled according to the formula $s = 0.05 \times r^{0.8}$, where s is check size and r is distance from fixation in degrees of visual angle. The checkerboard pattern covered half of the screen except for the central 0.6° of visual angle, which contained background gray luminance (50% contrast, luminance 105 cd/m^2 (3T) or 1019 cd/m^2 (7T)). The other half of the screen also contained the gray background. A white fixation point subtending 0.2° of visual angle appeared at the center of the screen throughout the run, and subjects were instructed to maintain fixation while passively viewing the stimuli. For each run, the checkerboard pattern alternated between the left and right halves of the screen, 16 s (7T) or 13.5 s (3T) per side, and was presented for 8 (7T) or 11 (3T) left-right cycles.

An M/P localizer stimulus (Figure 14C) was designed to elicit differential responses from voxels with greater M-layer representation and voxels with greater P-layer representation, based on findings from monkey electrophysiology (see Kleinschmidt et al., 1996; Liu et al., 2006, for related approaches). The M/P localizer consisted of 16-s (7T) or 18-s (3T) blocks of "M stimuli", "P stimuli", and blank (fixation point only) stimuli. The M and P stimuli were both full-field sinusoidal gratings with sinusoidal counterphase flicker. The outer borders of the stimulus faded into gray to avoid sharp visual edges at the stimulus boundaries. The gratings were presented at one of 6 orientations (0°, 30°, 60°, 90°, 120°, or 150°) and changed to a new random orientation every 3 s, in order to drive different populations of LGN neurons with different spatial receptive fields throughout the block.

The M stimulus was a 100% luminance contrast, black-white grating with a spatial frequency of 0.5 cpd and a flicker frequency of 15 Hz. The P stimulus was a low luminance-contrast, high color-contrast red-green grating with a spatial frequency of 2 cpd and a flicker frequency of 5 Hz. A spatial frequency of 2 cpd was selected for the P stimulus because contrast sensitivity for isoluminant stimuli is attenuated at high spatial frequencies (De Valois and De Valois, 2000). The blank stimulus was a gray screen of mean luminance.

The red and green levels of the P stimulus were set to be near-isoluminant by performing heterochromatic flicker photometry outside the scanner. Specifically, subjects adjusted the luminance of a green disk to match a 100% red disk on a neutral gray background by minimizing the perception of flicker as the two disks alternated at a frequency of 7.5 Hz. Two subjects (S2 and S3) performed flicker photometry, and the average green value (39%) from these subjects was used for all scanning sessions.

Although we did not perform flicker photometry in the scanner for all subjects (due to time constraints as well as a concern about adapting subjects to the red and green stimuli before the M/P localizer scans), we verified that the green luminance value obtained outside the scanner

was reasonable for both scanner displays by obtaining flicker photometry data from two subjects on the 7T display (mean of 41% green) and one subject on the 3T display (49% green). Since the values needed to achieve isoluminance vary across subjects and across the visual field, our main objective was to create a standard low luminance contrast stimulus that would enable relative activation of the M vs. P subdivisions.

On each run, 15 blocks (6 M, 6 P, and 3 blank) were presented in pseudorandom order, with the constraint that the same stimulus type could not appear in adjacent blocks in order to minimize adaptation to the M or P stimuli. A white fixation point subtending 0.2° visual angle appeared at the center of the screen throughout the stimulus blocks, and subjects were instructed to maintain fixation throughout the run.

Subjects performed a target detection task during the M and P stimulus blocks to encourage them to attend to the visual stimuli throughout the run (Figure 14C). Targets were contrast decrement 2D Gaussians presented for 300 ms. We used luminance contrast decrements (fade to gray) for M blocks and color contrast decrements (fade to yellow) for P blocks, since luminance contrast was already minimal for the P stimuli. Target size was linearly scaled with eccentricity by adjusting the sigma parameter of the Gaussian. The overall target size was set individually for each subject, separately for the M and P stimulus conditions, to attempt to equate task difficulty in the M and P blocks.

During each stimulus block, 0, 1, 2, or 3 targets appeared on the screen, and subjects were asked to count the number of targets in each block. Targets appeared at random times throughout the block and could appear at any location within the stimulus. At the end of a stimulus block, the screen turned gray and the fixation point turned black for 1.5 s (7T) or 1.75 s (3T), indicating the response period. During this time, subjects pressed a button to report how many targets they had seen during the previous stimulus block. The fixation point then turned white for 500 ms, indicating the start of the next stimulus block. Therefore, the total block duration (including stimulus, response, and cue periods) was 18 s (7T) or 20.25 s (3T), corresponding to 9 TRs in both cases. At the beginning of each run (before the stimulus blocks), an 8 s (7T) or 9 s (3T) blank stimulus was presented, which the subject viewed passively while maintaining fixation. In the 7T sessions, an 8-s blank stimulus was also shown at the end of each run. M/P localizer runs were about 5 minutes in length, with 4-12 (median 8) runs collected per session (Table 2).

M/P mapping methods by session

	Session	Subject	Paired sessions for cross-session reliability	Number of M/P runs	Voxel size	Matrix size	IPAT	MB	Partial Fourier	Number of slices	TE (ms)	Flip angle (deg)	Echo spacing (ms)	Notes
7T	1	1	7T 2 and 3	7	1.5 mm isotropic	128 x 128	3	-	6/8	38	18	80	0.82	-
	2	1	7T 1	4	1.5 mm isotropic	128 x 128	3	-	6/8	40	17	78	0.82	Sessions 2 and 3 were collected contiguously
	3	1	7T 1	4	1.25 x 1.25 x 1.2 mm	154 x 154	3	-	6/8	38	16	80	0.76	Sessions 2 and 3 were collected contiguously. Hemifield localizer from session 2.
	4	2	3T 1 and 2	8	1.5 mm isotropic	128 x 128	3	-	6/8	38	17	78	0.72	-
	5	3	3T 3	11	1.5 mm isotropic	128 x 128	3	-	6/8	38	18	80	0.82	12 runs were collected, but one was excluded due to an artifact
	6	4	-	8	1.3 mm isotropic	160 x 160	2	2	5/8	64	17	70	0.74	ROIs from GLM, not hemifield localizer
	7	5	-	6	1.3 mm isotropic	160 x 160	2	2	5/8	64	17	70	0.74	-
3T	1	2	7T 4, 3T 2	8	1.75 x 1.75 x 1.5 mm	128 x 128	-	-	6/8	21	40	75	0.78	-
	2	2	7T 4, 3T 1	8	1.75 x 1.75 x 1.5 mm	128 x 128	-	-	6/8	21	40	75	0.78	-
	3	3	7T 5	12	1.75 x 1.75 x 1.5 mm	128 x 128	-	-	6/8	21	40	75	0.78	-
	4	6	-	7	1.75 x 1.75 x 1.5 mm	128 x 128	-	-	6/8	21	40	75	0.78	-

Table 2. M/P mapping methods for each experimental session showing parameters that varied across sessions. iPAT = in-plane parallel imaging factor. MB = multiband slice parallel imaging factor. TE = echo time.

4.3.4 MRI data acquisition

7-Tesla MRI anatomical and functional images were acquired at the University of Minnesota on a whole-body scanner driven by a Siemens console with a head RF coil (Nova Medical; single transmit, 24 receive channels). BOLD data were acquired using a T2*-weighted single-shot gradient-echo echo planar imaging sequence that included both parallel imaging and fat suppression. Slices were near axial and were oriented to cover LGN and the occipital lobe as well as parts of the parietal and temporal lobes. TR was 2000 ms, with 144 volumes acquired per run. The phase encoding direction was anterior-to-posterior, and the slice acquisition order was interleaved. Other acquisition parameters varied across sessions, as detailed in Table 2. These parameters included: parallel imaging methods (in-plane phase-encode acceleration factors (iPAT) of 2 or 3 and a multiband (MB) slice acceleration factor (Feinberg et al., 2010; Moeller et al., 2010; Setsompop et al., 2012) of 2), partial Fourier of 5/8 or 6/8, number of slices (38, 40, or 64), slice thickness (1.2-1.5 mm, 0 mm gap), in-plane resolution (1.25 x 1.25 mm – 1.5 x 1.5 mm), TE (16-18 ms), flip angle (70-80°), and echo spacing (0.72-0.82 ms). Matrix size ranged from 128 x 128 to 160 x 160, and in-plane FOVs ranged from 192 x 192 mm to 208 x 208 mm. A high-resolution T1-weighted MPRAGE anatomical volume with a spatial resolution of 1 x 1 x 1 mm was acquired for each subject, sometimes in a separate session. Subjects lay head first, supine, in the scanner, with foam padding around the head to reduce head motion.

3-Tesla MRI data were acquired at the University of California, Berkeley, using a Siemens Trio scanner equipped with a 32-channel head coil. BOLD data were acquired using a T2*-weighted single-shot gradient-echo echo planar imaging sequence with 6/8 partial Fourier acquisition and fat suppression. 21 near-axial slices (1.5 mm thickness, 0.075 mm gap) were acquired with a 128 x 128 matrix and in-plane FOV of 224 x 224 mm for a spatial resolution of 1.75 x 1.75 x 1.575 mm, covering LGN and parts of the occipital lobe, including the calcarine sulcus. TR was 2250 ms, with 139 volumes acquired per run. TE = 40 ms, flip angle = 75°, the phase encoding direction was anterior-to-posterior, and echo spacing = 0.78 ms. The slice acquisition order was interleaved. A Siemens prescan normalize filter was applied to the functional images at the time of acquisition to reduce spatial inhomogeneities. This filter normalizes the functional images by the receive field of the head RF coil, which is calculated from separate scans.

Before the 3T functional runs, 21 slices (1.5 mm thickness, 0.075 mm gap) of an in-plane anatomical volume were acquired with a 256 x 256 matrix and in-plane FOV of 225 mm x 225 mm, for a spatial resolution of 0.88 x 0.88 x 1.575 mm. This volume had the same slice thickness and positioning as the functional scans and was used to facilitate the alignment of the functional scans to a high-resolution T1-weighted MPRAGE anatomical volume with a spatial resolution of 1 x 1 x 1 mm (which was sometimes acquired in a separate session). Subjects lay head first, supine, in the scanner, with foam padding around the head to reduce head motion.

4.3.5 Data analysis

4.3.5.1 fMRI preprocessing

To correct for subject motion, all functional volumes from each run were aligned to the first volume of the session using FSL MCFLIRT (Jenkinson et al., 2002). The first volume was selected because it was acquired closest in time to the in-plane anatomical volume (which was collected only in 3T sessions). To assess subject head motion, we calculated the maximum

translational and rotational displacements across each session from the 6 motion parameters (3 translation, 3 rotation) obtained from MCFLIRT. Total translational displacements were defined as the square root of the sum of squared *x*, *y*, and *z*-direction displacements. Total rotational displacements were defined as the sum of the absolute values of the rotational displacements in the three orthogonal directions. The maximum difference between these referenced displacements across the session was then calculated. Because small but frequent head motion can have different effects on data quality than large but infrequent head motion while producing similar levels of total head displacement over the course of a scan, we also calculated the mean framewise displacement (FD), which summarizes translational and rotational head motion between adjacent frames, with rotational displacements converted from degrees to mm by assuming a spherical surface with radius 50 mm (Power et al., 2012). This overestimates the rotational displacement of the LGN, since it is less than 50 mm from the center of the brain, but we used this value in order to facilitate comparison with other reports of FD. Head motion values are reported in Table 3.

Estimated head motion

	Max translational displacement (mm)	Max rotational displacement (deg)	Mean FD (mm)
7T	2.8 (1.2-4.4)	2.4 (1.5-3.7)	0.12 (0.08-0.15)
3T	1.5 (0.8-2.5)	2.3 (1.7-3.0)	0.14 (0.13-0.17)

Table 3. Head motion estimates, giving the mean and range (in parentheses) of each metric across subjects. Max displacement is the difference between the two head positions that were farthest from one another during the session. FD = framewise displacement.

Next, volumes at the beginnings and ends of functional runs were discarded. For hemifield localizer runs, volumes corresponding to half of a stimulus alternation cycle (7T sessions 6 and 7: 8 volumes, 3T: 6 volumes) or a full alternation cycle (7T sessions 1-5: 16 volumes) were discarded from the beginning of each run. Volumes were also discarded from the ends of runs in some sessions (7T session 6: 8 volumes; session 7: 64 volumes; 3T: 1 volume). In all hemifield localizer runs, 128 volumes (7T) or 132 volumes (3T) were retained for the analysis. For M/P localizer runs, either 4 volumes at the beginning of each run (3T) or 4 volumes at the beginning and 5 volumes at the end of each run (7T) were discarded. These discarded volumes corresponded to initial and final blank periods, which were presented in addition to the three blank stimulus blocks in each M/P localization run. In all M/P localizer runs, 135 volumes were retained for analysis.

For all functional runs, the time series for each voxel was then detrended to remove low-frequency noise and slow drift (Zarahn et al., 1997; Smith et al., 1999). Finally, each voxel time series was divided by its mean to convert the arbitrary image intensity units into percent signal change.

4.3.5.2 Alignment to high-resolution anatomical

For each subject, the in-plane anatomical volume (3T) or mean volume of the first functional run (following motion correction) (7T) was aligned to the high-resolution anatomical volume through the combined use of an automatic alignment tool (Nestares and Heeger, 2000) and manual adjustment in the VISTA software package mrVista (http://white.stanford.edu/software/).

Conversion of anatomical coordinates into Talairach space was performed within mrVista by selecting anatomical landmarks on the high-resolution anatomical volume and applying a coordinate transformation for each subject based on these landmarks.

4.3.5.3 LGN ROI definition

ROIs corresponding to the entire LGN (including both M and P subdivisions) were defined by identifying voxels responding to contralateral visual stimulation using Fourier analysis of the hemifield localizer runs. Coherency (coherence magnitude and phase) was calculated between the average time series of hemifield-alternation runs in each voxel and a sinusoid with a frequency equal to that of the hemifield alternation cycles.

The LGN region was identified as a cluster of voxels in the appropriate anatomical location having high coherency magnitudes and phases corresponding to contralateral visual responses. Specifically, the coherency magnitude threshold was adjusted to retain bilateral clusters of voxels with similar phases in the LGN regions while reducing the presence of noisy voxels with heterogeneous phases elsewhere. Because signal-to-noise differered across sessions, this adjustment was done separately for each session. Thresholds ranged from C>0.19 to C>0.21 for 7T sessions and from C>0.17 to C>0.19 for 3T sessions. ROI borders were manually drawn around these clusters in functional space. In uncertain cases, voxels were checked for survival across a range of thresholds. Occasionally, voxels that did not meet the threshold were included in order to preserve the convexity of the structure, with the knowledge that ROIs would be subsequently restricted based on further functional criteria.

For one session (7T session 6), the hemifield localizer runs did not have sufficiently high coherence values, perhaps due to eye movements during the runs. For this session, the LGN ROIs were defined based on the GLM analysis (see below), from the clusters of voxels for which the time series variance explained by the GLM exceeded 2%. This variance explained threshold was selected using thresholding heuristics similar to those used for setting coherence thresholds in the other sessions (i.e., to reveal bilateral LGN clusters while reducing noisy voxels elsewhere). For 7T session 3, which was conducted consecutively with session 2 (the subject remained in the scanner but was tested with different scanning parameters), a separate hemifield localizer was not collected; instead the ROIs from session 2 were used. All ROIs were defined before conducting the M/P mapping analysis.

4.3.5.4 Estimation of responses to M and P stimuli

A GLM analysis was performed to estimate the responses of each LGN voxel to M and P stimuli. A design matrix was constructed with an M regressor (1 when the M stimulus was on and zero otherwise), a P regressor (1 when the P stimulus was on and zero otherwise), and one regressor for each run (1 during a given run and zero otherwise). Each regressor was then convolved with a gamma function HRF (Boynton et al., 1996) to generate the final design matrix. This model was fit to the time series (a concatenation of all M/P runs in a session) of each voxel using mrVista. The estimated responses of each voxel to the M and P stimuli correspond to $beta_M$ and $beta_P$, respectively. The relative response of each voxel to M vs. P stimuli was defined as the difference between $beta_M$ and $beta_P$ ($beta_{M-P}$) for that voxel. Negative $beta_M$ or $beta_P$ values likely indicate a poor (noisy) response to that stimulus, though in principle they could reflect suppression compared to the blank stimulus.

4.3.5.5 Spatial analyses

To quantify the spatial organization of the M/P functional maps, we divided LGN voxels into M and P groups and compared the spatial centers of the two groups. We classified each functional voxel as belonging to either the M or P group based on its $beta_{M-P}$ value. Since human histological studies have found that, on average, 20% of the volume of the LGN is made up of M layers and 80% is made up of P layers (Andrews et al., 1997; Selemon and Begovic, 2007), we considered the 20% of voxels with the highest $beta_{M-P}$ values to be the M group and the remaining 80% of voxels to be the P group. The 3D spatial center of each group in each LGN was defined as the mean voxel coordinate in each spatial dimension (anterior-posterior, dorsal-ventral, and medial-lateral). These center coordinates were then transformed into Talairach space to provide a unified spatial reference frame with a canonical brain orientation, which facilitated comparison across subjects.

4.3.5.6 Map consistency across thresholds

To assess map consistency across a range of voxel selection criteria, we repeated the spatial centers analysis procedure for many levels of thresholding, based on the proportion of variance explained by the GLM for each voxel. Only voxels in the LGN ROIs defined from the hemifield localizer were considered. Thresholding by proportion of variance explained is an unbiased procedure, as this measure reflects voxel responses to both M and P stimuli. Voxels that did not meet the variance explained threshold were excluded from the LGN ROI for that threshold level. We then repeated the spatial centers analysis in each ROI for each threshold level. Different threshold ranges were used for 7T (0-0.05) and 3T (0-0.01) data, due to the overall higher proportions of variance explained at 7T. Threshold levels were spaced at intervals of 0.001 proportion variance explained.

4.3.5.7 Reliability analyses

In order to assess consistency of LGN M/P maps across scans, we performed cross-session and within-session reliability analyses on the $beta_{M-P}$ values for each voxel. Cross-session reliability was evaluated for M/P mapping data collected from the same individual scanned on two different days. Table 2 shows all the sessions performed in this study and lists the paired comparison sessions (if any) for each one. For subjects who participated in multiple sessions, all pairwise combinations of sessions were compared, with the exception of 7T sessions 2 and 3, since these sessions were conducted during the same scanning period (i.e., the subject was continuously in the magnet), not on separate days.

Cross-session reliability was measured as the correlation between $beta_{M-P}$ maps collected from the same subject on two different days. The two $beta_{M-P}$ maps were projected from functional space to an aligned high-resolution anatomical image and then resampled to the resolution of the anatomical volume using nearest neighbor interpolation. The intersection between the LGN ROIs defined from the two sessions was then computed in anatomical space. Only voxels that were common to both ROIs were considered for the reliability analysis. We then computed the Pearson correlation coefficient between the $beta_{M-P}$ values from the two days. For each LGN ROI comparison pair, we calculated the proportion overlap of the two ROIs as the ratio of the volume of their intersection to the volume of their union.

Within-session reliability was defined as the inter-run correlation in $beta_{M-P}$ values across voxels. Separate GLMs were performed for each M/P mapping run, resulting in separate $beta_{M-P}$ estimates for each run for every voxel. The Pearson correlation of these $beta_{M-P}$ values across voxels in each LGN ROI was calculated for all pairwise comparisons of runs, and the inter-run correlation corresponded to the mean of these pairwise correlations. This measure indicates the map quality obtained from a single functional run, allowing comparisons across sessions with different numbers of runs.

4.3.5.8 Functional SNR

To quantify functional SNR of M/P runs, we performed a one-way ANOVA of the mean response amplitudes of each voxel during M, P, and blank stimulus blocks. F statistics were calculated for each run and then averaged across voxels and across runs for each hemisphere. Time series segments contributing to calculation of a block mean response had the same total duration as the block but were delayed with respect to the start of the block to account for the hemodynamic delay. We tested delays of 0, 1, 2, and 3 TRs, and we report F statistics for a delay of 1 TR, since the mean of the F statistic across all sessions was maximal at this delay for both 3T and 7T session groups.

4.4 RESULTS

We measured fMRI BOLD responses from the human LGN with high spatial resolution (ranging from 1.25x1.25x1.2 mm at 7T to 1.75x1.75x1.5 mm at 3T) in order to resolve M and P layers within the LGN. We functionally localized the boundaries of human LGN with a flickering checkerboard stimulus that alternated between the left and right hemifields (Figure 14A and B; Figure 15A). LGN volumes ranged between 287-456 mm^3 for 3T sessions and 144-368 mm^3 for 7T sessions, similar to past studies (O'Connor et al., 2002; Kastner et al., 2004).

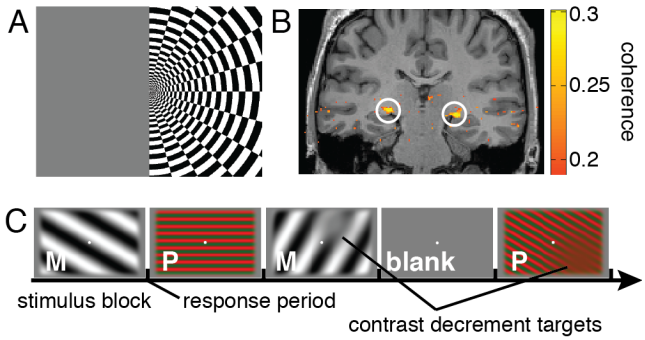

Figure 14. LGN M/P localization methods. (A) A flickering checkerboard stimulus that alternated between the left and right visual hemifields was used to localize the LGN. (B) Voxels were selected that responded selectively to contralateral visual field stimulation. Coherence threshold = 0.19 in this example (see Methods). LGN regions are indicated by white circles. (C) M-type (monochrome, low spatial frequency, high temporal frequency, high luminance contrast) and P-type (high color contrast, high spatial frequency, low temporal frequency, low luminance contrast) grating stimuli were designed to elicit differential BOLD responses from the M and P subdivisions of human LGN. Subjects maintained fixation at the center of the screen while viewing blocks of full-field M and P stimuli that were interleaved with blocks of blank stimuli. Concurrently, subjects performed a contrast decrement detection task during the M- and P-stimulus blocks, counting the number of luminance contrast (M blocks) or color contrast (P blocks) targets that appeared in each block.

We then used M-type (monochrome, low spatial frequency, high temporal frequency, high luminance contrast) and P-type (high color contrast, high spatial frequency, low temporal frequency, low luminance contrast) stimuli (Figure 14C) to elicit differential BOLD responses from the M and P subdivisions of the LGN. Stimulus parameters were selected based on the known response properties of M and P neurons from macaque electrophysiological recordings. Subjects performed an attention-demanding contrast decrement detection task during stimulus presentation, with similar behavioral accuracy for M blocks and P blocks (M: 75%, P: 71%; $t(10) = 1.07$, $p = 0.31$, n.s.). We then employed a general linear model (GLM) to measure each LGN voxel's response to the M and P stimuli and defined the relative M vs. P response in each voxel as the difference of the M and P response amplitudes.

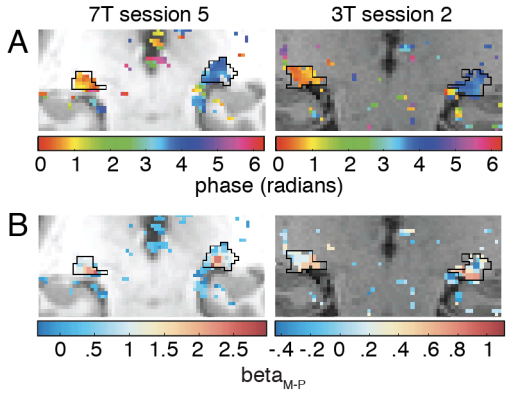

Figure 15. ROI definition and M/P maps overlaid on anatomical images. (A) For each voxel, coherency was computed for the voxel response and the time course of left-right hemifield alternation of a flickering checkerboard. Coherency phases of the best-fit responses, thresholded by coherency magnitude, are displayed on coronal slices through the LGN from two example subjects (left: 7T, C>0.21; right: 3T, C>0.17). Phases between 0 and π (orange-yellow) reflect voxel preferences for right visual field stimulation, while phases between π and 2π (blue) reflect voxel preferences for left visual field stimulation. LGN ROIs are outlined in black. Note that data were analyzed and ROIs were defined in functional space, and both functional data and ROIs have been interpolated to anatomical space in this figure for visualization. (B) Relative responses to M vs. P stimulus blocks for each voxel (betaM-P) for the two subjects and slices shown in panel A (left: 7T; right: 3T), with maps thresholded based on the hemifield localizer, as in A.

The resulting M, P, and M-P maps of the LGN exhibited a gradient of more M-like to more P-like voxels at field strengths of both 7T and 3T (Figure 15B; Figure 16). Specifically, we found that M-like voxels were concentrated in the more ventral and medial portions of the LGN, while P-like voxels were concentrated in the more dorsal and lateral portions. Importantly, this result matches the known relative positions of human M and P layers from human histology (Figure 16, inset) and thus validates our approach.

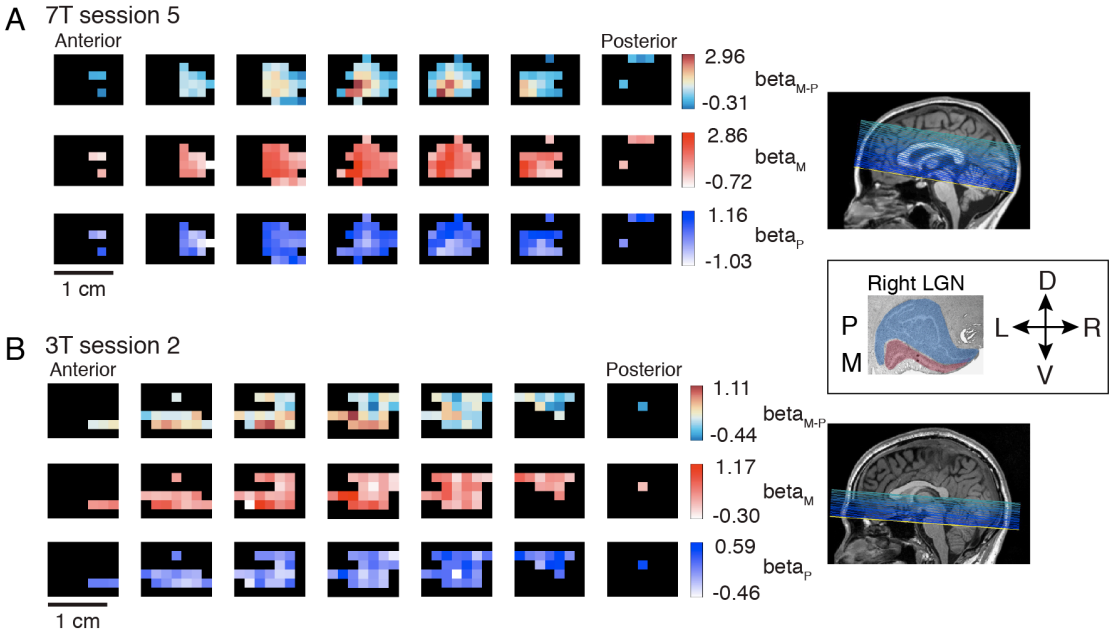

Figure 16. LGN M/P maps. (A) Right LGN maps acquired at 7T from an example subject (subject 3, session 5). Maps are shown as serial coronal slices in functional space (cross-sections through the original axial slices), with no resampling. Only LGN ROI voxels are shown. Top row: relative responses to M vs. P stimulus blocks for each voxel ($beta_{M-P}$). Middle row: responses to M stimulus blocks ($beta_M$). Bottom row: responses to P stimulus blocks ($beta_P$). At right is shown the slice prescription for this session overlaid on a midline sagittal anatomical image. The inset shows a reference coronal histological section of a right human LGN with the M and P layers colored red and blue, respectively (modified from Selemon and Begovic, 2007). Consistent with the anatomical section, the functional maps show stronger M-type responses medially and ventrally and stronger P-type responses laterally and dorsally. D, dorsal; V, ventral; L, left (medial in this example); R, right (lateral in this example). (B) Right LGN maps acquired at 3T from an example subject (subject 2, session 2). All other aspects of this panel are the same as in panel A.

To quantify the spatial distribution of M-like and P-like voxels across the LGN, we classified voxels as either "more M" or "more P" based on their relative responses to the two stimulus types (M-P) and then compared the spatial locations of these two groups to known LGN anatomy. From human histology, about 20% of the volume of the human LGN is magnocellular, while about 80% is parvocellular (Andrews et al., 1997; Selemon and Begovic, 2007). Therefore, for each LGN, we classified the 20% of voxels with the highest M-P values as "more M" and the remaining 80% as "more P". We then calculated the 3-dimensional spatial center of each of these voxel groups (Figure 17A). If the distribution of voxels between the two groups were random, we would expect their spatial centers to be identical, on average. However, consistent with the spatial layout of the M-P maps we observed, the M group and P group centers were significantly separated in space and had relative spatial positions that were consistent with known human LGN anatomy. Across sessions, the M group center was significantly more ventral and medial than the P group center (Figure 17B), as assessed by paired t-tests on the M and P group center positions. The mean separation between M and P group centers along the dorsal-ventral axis was 0.77 mm at 7T ($t(13) = 6.88$, $p < 0.0001$) and 1.07 mm at 3T ($t(7) = 4.85$, $p = 0.0018$). The mean separation along the medial-lateral axis was 0.83 mm at 7T ($t(13) = 3.38$, $p = 0.0049$) and 1.01 mm at 3T ($t(7) = 3.18$, $p = 0.0154$) (Figure 17B). The correspondence

between the layout of the M and P group centers and the known LGN anatomy was consistently observed in individual subjects and sessions (14/14 hemispheres acquired at 7T and 8/8 hemispheres acquired at 3T for the dorsal-ventral axis; 13/14 hemispheres acquired at 7T and 6/8 hemispheres acquired at 7T for the medial-lateral axis) (Figure 17B).

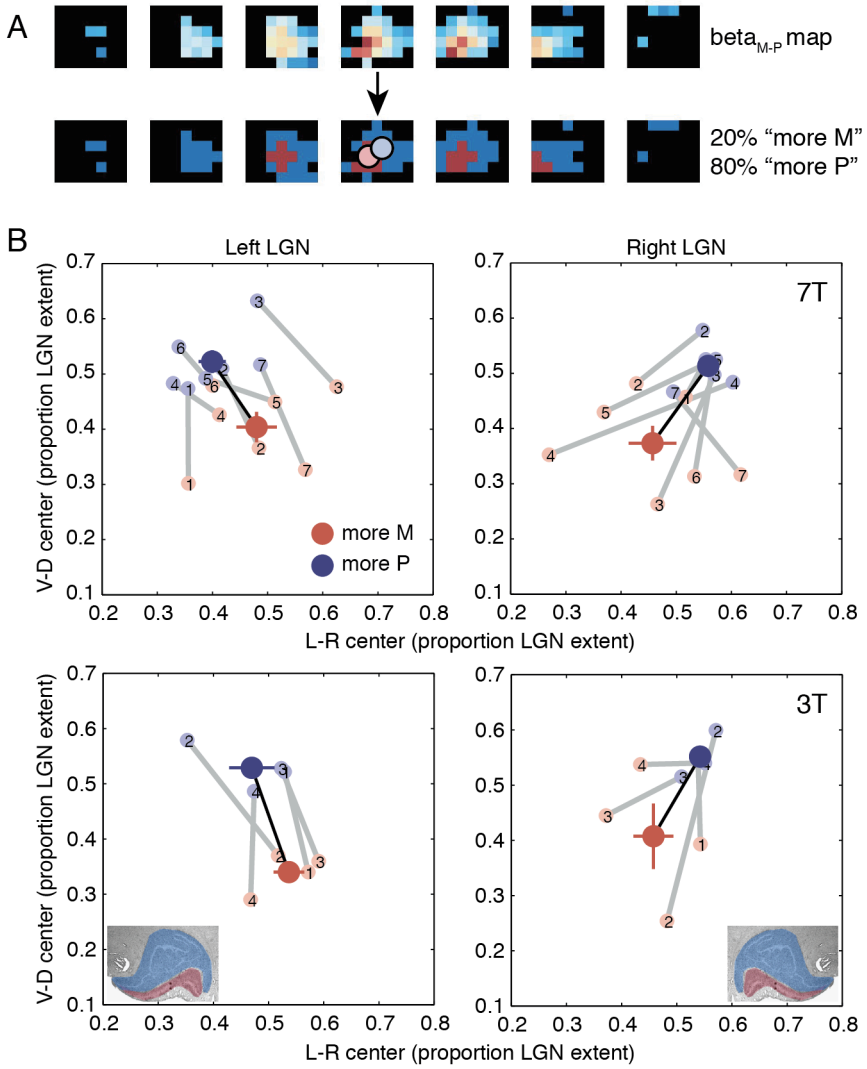

Figure 17. Spatial analysis of M-P maps. (A) Voxels were classified as "more M" or "more P" based on their betaM-P values. The 20% of voxels with the largest betaM-P values were assigned to the "more M" group, and the remaining 80% of voxels were assigned to the "more P" group, matching the volumetric proportions of the M and P subdivisions, as measured histologically. Spatial centers for the two groups, denoted by red and blue circles, are superimposed on the binarized map. An example right LGN (as in Figure 3) is shown. (B) Spatial centers of the M (red) and P (blue) voxel groups plotted for the medial-lateral and dorsal-ventral axes. Spatial centers were calculated in Talairach coordinates and are plotted as a proportion of the extent of each subject's LGN (based on the LGN localizer data from the same scanning session) along a given axis. Light circles connected by gray lines show M and P spatial centers for individual scanning sessions. Dark circles connected by black lines show the group mean, with error bars corresponding to the s.e.m. for each axis. Top: 7T. Bottom: 3T. Left: Left LGN. Right: Right LGN. Reference histological coronal sections of human LGN are included in the bottom plots (modified from Selemon and Begovic, 2007).

To test the reliability of these findings, we repeated the spatial centers analysis on a subset of approximately 50% of LGN voxels that had the best fits to the GLM (highest variance explained by the model). The mean separation between M group and P group centers along the dorsal-ventral axis was greater than that computed for all localized LGN voxels (7T: 1.06 mm vs. 0.77 mm, $t(13) = 3.41$, $p = 0.0047$; 3T: 1.54 mm vs. 1.07 mm, $t(7) = 1.67$, $p = 0.14$), and there was a high degree of consistency in spatial center layout across individual subjects and sessions (Figure 18). This increase in map quality following thresholding based on explained variance is what we would expect for the subset of voxels best driven by the M and P stimuli.

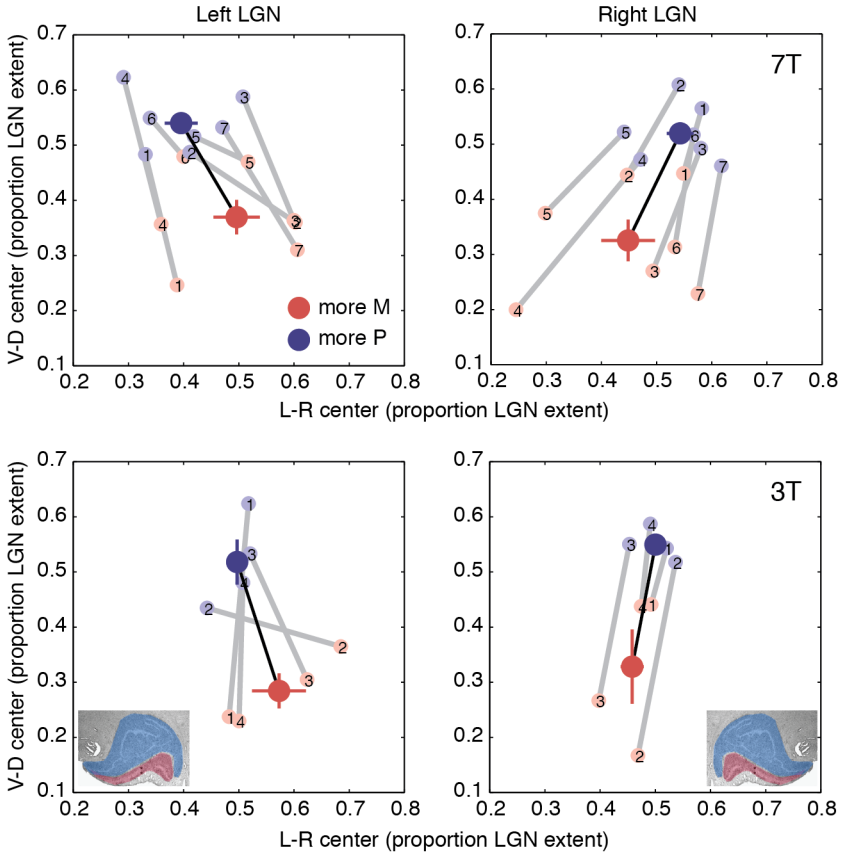

Figure 18. Spatial centers derived from the best-fit voxels. Spatial centers calculated as in Figure 17 for only those voxels with the highest proportions of variance explained by the M/P GLM (proportion > 2% for 7T and 0.4% for 3T, see Figure 19). These thresholds result in the inclusion of about half of all LGN ROI voxels across subjects. All other conventions as in Figure 17. Reference histological coronal sections of human LGN are included in the bottom plots (modified from Selemon and Begovic, 2007).

To ensure that the spatial center layout we observed did not depend on a particular choice of explained variance threshold, we calculated M and P group centers across a wide range of thresholds (Figure 19). The anatomically expected spatial arrangement of M and P group centers was consistently observed for both the dorsal-ventral and medial-lateral axes. Analysis of the anterior-posterior axis showed a tendency for the M group center to be more anterior than the P group center, but this did not reach significance at either field strength for the set of all localized LGN voxels and was less consistent across thresholds than the separations along the other two axes. Smaller separation along the anterior-posterior axis is expected from human LGN anatomy;

both M and P layers are present throughout the anterior-posterior extent of the structure (Hickey and Guillery, 1979).

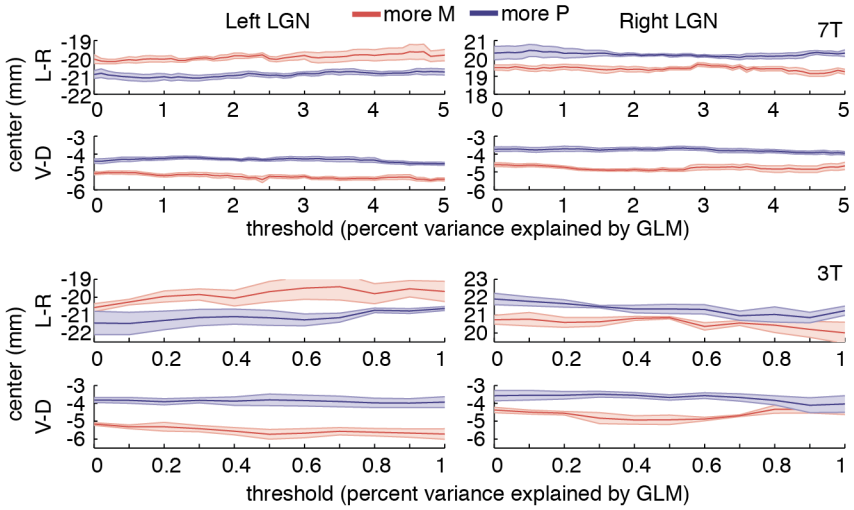

Figure 19. M/P map consistency across a range of LGN threshold values. Separation between spatial centers of "more M" group (red line) and "more P" group (blue line) along the medial-lateral and dorsal-ventral axes over a range of LGN threshold values. For a given threshold, an LGN voxel was included in the analysis if its proportion of variance explained by the GLM exceeded that threshold. Group data for all 7T (top) and 3T (bottom) sessions are shown in Talairach coordinates. Shaded regions show standard errors of the mean across sessions, after data points from each session were re-centered (via an additive shift) to the mean value across all sessions, voxel groups, and thresholds, in order to normalize for overall differences in LGN location across individual brains.

To evaluate the relative contributions of M and P responses to the M-P spatial gradient we observed, we repeated the spatial centers analysis on the M and P maps separately. For M responses, the 20% of voxels with the highest $beta_M$ values were defined as the "more M" group and the other 80% were the "less M" group. For P responses, the 80% of voxels with the highest $beta_P$ values comprised the "more P" group, and the other 20% were the "less P" group. We specifically considered the dorsal-ventral axis for this analysis, because this is the axis along which spatial separation of M and P voxels should be clearest based on anatomy (Hickey and Guillery, 1979). The ventrally-weighted gradient of $beta_{M-P}$ values we observed is consistent with two alternatives for the individual M and P gradients (Figure 20A): 1) opposing gradients (ventrally-weighted M and dorsally-weighted P) or 2) aligned gradients with different gains (e.g., strong ventrally-weighted M and weak ventrally-weighted P). Such aligned gradients could arise, for example, from an underlying gradient in vascular density across the LGN. Our results provide evidence for two gradients in opposing directions, with both M and P maps having the dorsal-ventral orientation expected from LGN anatomy in 12/14 7T hemispheres and 4/8 3T hemispheres (chance = 25%, Figure 20B). Our consistent finding of opposing directions of M and P gradients shows that the M-P map gradients we have found (Figures 16-19) are not driven exclusively by either the M or P stimulus but rather reflect anatomically correct maps for both stimulus types.

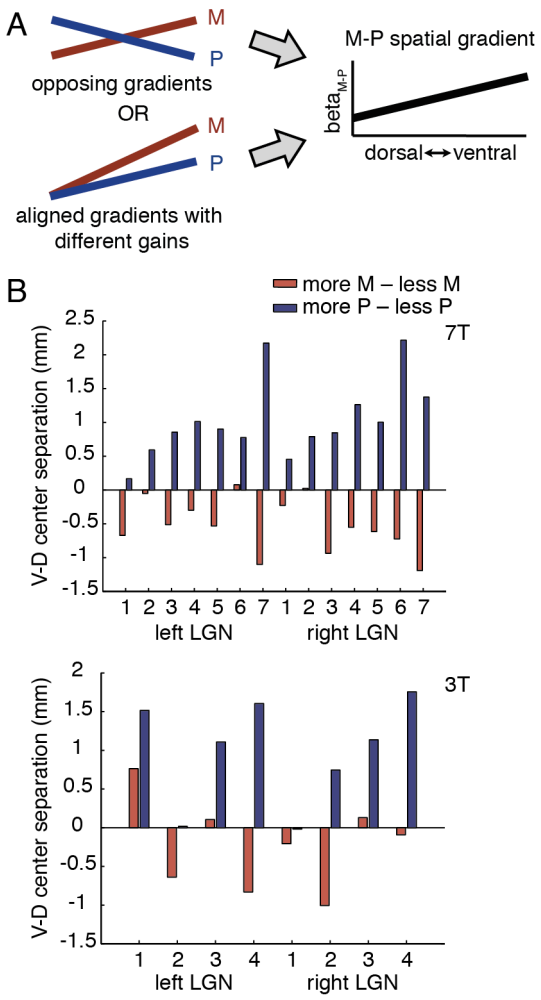

Figure 20. Components of the M-P spatial gradient. (A) Two possible arrangements of $beta_M$ and $beta_P$ gradients (left) that could give rise to a spatial gradient in the $beta_{M-P}$ map (right); only the dorsal-ventral axis is shown. (B) Separation of spatial centers along the dorsal-ventral axis in M maps (red bars) and P maps (blue bars) for the left and right LGN ROIs from each session. Separations between "more M" and "less M" centers from M maps and "more P" and "less P" centers from P maps (see Methods) are plotted, in Talairach coordinates. Ventrally-weighted maps are shown as negative values, and dorsally-weighted P maps are shown as positive values. Hemispheres with both ventrally-weighted M maps and dorsally-weighted P maps indicate two opposing gradients that are consistent with known anatomical organization. Top: 7T. Bottom: 3T.

Another test of the validity of our M/P localization procedure is consistency of M-P maps across experimental sessions. To quantify this consistency, we assessed individual subject M-P map reliability across scanning sessions on different days. We calculated the correlation of M-P values across voxels after the maps were projected onto a high-resolution anatomical volume and resampled to the resolution of that volume. We considered only the overlapping portion of the aligned LGN ROIs from the two sessions; the mean overlap (ROI intersection / ROI union) was 30% (SD 9%; range 13-44%). Some subjects were scanned multiple times at the same field strength (3T or 7T), and some were scanned at different field strengths. Significant positive cross-session correlations at the single-voxel level were observed in 6/6 same-field strength and 3/6 different-field strength comparisons, as assessed by randomization tests (all $p < 0.005$; Figure 21). The three comparisons that did not show positive correlations all involved a single session (Subject 2; 7T session 4) that had low overlap with the LGN ROIs from the comparison sessions (mean 18% overlap for this session vs. 34% for all other comparisons). This low overlap probably resulted from difficulty aligning functional images from 7T session 4 to the anatomical volume due to distortion and dropout in cortical regions that would ordinarily serve as landmarks for alignment.

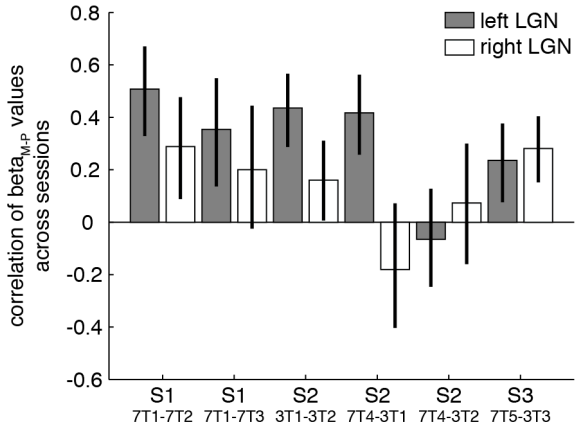

Figure 21. M-P map reliability across sessions. Correlations between LGN voxel betaM-P values across scanning sessions from the same subject, after aligning and resampling the functional maps to that subject's anatomical space. Each bar shows the test-retest correlation for one hemisphere. Error bars are bootstrapped 95% confidence intervals. Labels indicate subject and session numbers for the two sessions being compared (see Table 2).

The mean cross-session correlation across all comparison hemispheres was 0.23 (range -0.18 to 0.51) and was significantly greater than zero at the group level (one-sample t-test of Fisher z-transformed correlation coefficients, $t(11) = 3.78$, $p = 0.0031$; Figure 21). Taken together, these results demonstrate that the M-P maps were reliable across sessions for individual subjects. Examples of low test-retest reliability seemed to reflect different positions of the entire LGN ROI when aligned to the anatomical images rather than differences in map organization, suggesting that, at least within the parameter space we used, test-retest reliability does not strongly depend on field strength or specific scanning parameters.

In addition to cross-session reliability, we calculated reliability measures between pairs of 5-minute runs and across blocks within single runs. First, we calculated the inter-run correlation of M-P maps generated from individual runs within a single scanning session. This measure indicates the map quality of a single run and is therefore a useful measure of SNR. Second, we computed functional SNR across blocks within single runs as the F-statistic of a one-way ANOVA of mean response amplitudes in M, P, and blank stimulus blocks. Inter-run correlations differed between field strengths, with higher mean correlations for 7T (0.43 +/- 0.04) than for 3T (0.16 +/- 0.03). Likewise, mean F-statistic values were higher at 7T (6.86 +/- 0.52) than at 3T (2.37 +/- 0.16). Thus, in our study, functional SNR was 2.5-3 times as high for 7T as for 3T scans, even though voxel volume was smaller at 7T (1.875-3.375 mm^3) than at 3T (4.594 mm^3).

4.5 DISCUSSION

A critical step toward understanding the roles of the LGN in human vision in both health and disease is the ability to noninvasively measure functional signals from M and P subdivisions. This goal has proven elusive for two major reasons. The first is the challenge of measuring brain activity at the depth and spatial resolution required to segregate the M and P subdivisions within the LGN, a small brain structure that extends only 5-10 mm in any spatial dimension. The second has been the lack of a paradigm that differentially drives responses in LGN M and P subdivisions that can in turn be measured noninvasively. By using high-resolution fMRI to measure functional signals from the LGN combined with stimuli specially designed to differentially drive responses in M and P subdivisions, we found gradients of M and P voxel responses across human LGN with spatial organization in excellent agreement with known LGN anatomy. This is the first physiological evidence that the functional properties of human M and P subdivisions are similar to those of the monkey LGN.

In developing an fMRI M/P mapping paradigm guided by prior electrophysiological studies of M and P neurons, possible differences between electrophysiological and fMRI measurements from the LGN must be considered. One possible difference is the influence of neuronal feedback on the measured response. The BOLD signal likely reflects synaptic activity more than spiking output (Logothetis and Wandell, 2004). This, combined with the fact that the LGN receives about 90% of its input from sites other than the retina, including 30% from V1 (Van Horn et al., 2000; Sherman and Guillery, 2006), means that feedback projections are likely to contribute significantly to the BOLD response measured in the LGN. There is considerable evidence that feedback projections from V1 to LGN are M- and P-stream specific (Briggs and Usrey, 2009, 2010), but the functions of these projections and their possible influence on the BOLD signal is still not well understood. Our findings suggest that, even in the likely presence of feedback signals in the measured fMRI responses, the same stimuli that drive differential M and P neuron responses also evoke differential BOLD responses.

Previous studies have noninvasively measured activity in the human LGN using fMRI (Chen et al., 1999; Uğurbil et al., 1999; Chen and Zhu, 2001; O'Connor et al., 2002; Kastner et al., 2004; Parkes et al., 2004; Schneider et al., 2004; Haynes et al., 2005; Wunderlich et al., 2005; Mullen et al., 2008; Anderson et al., 2009; Schneider and Kastner, 2009; Mullen et al., 2010; D'Souza et al., 2011; Schneider, 2011), and there has been one attempt to localize the M and P subdivisions using fMRI (Schneider et al., 2004). In that study, stimulus contrast was manipulated (either 10% or 100% contrast-reversing checkerboard stimuli) to attempt to dissociate the M and P subdivisions. Voxels were classified as M if they responded similarly to the two contrast levels and P if they responded more to the high contrast checkerboard. This classification was based on the logic that M neuronal responses saturate at low contrasts, while P neuronal responses continue to increase across a greater contrast range in the macaque (Kaplan and Shapley, 1982; Derrington and Lennie, 1984). The resulting M and P classification maps were presented for two subjects. However, these maps do not appear to exhibit the 3D spatial organization expected from anatomy – perhaps because the manipulation of only a single stimulus dimension limited map quality – and no attempt was made to quantify the spatial organization of the maps or establish their consistency across subjects. We show here that simultaneous manipulation of multiple stimulus dimensions selected to differentially drive M and P layers provides a robust approach to M and P mapping with fMRI, in which the anatomically expected map organization could be observed and quantified in nearly every hemisphere we studied.

Although our localizer effectively and reliably generates M-P maps, the small size of the LGN relative to voxel size as well as variability across subjects leave at least two aspects of M/P localization that could be improved. First, the M-P maps we observed were more like gradients across the structure than bimodal maps with separate M and P peaks. The distribution of $beta_{M-P}$ values in a given hemisphere was also typically unimodal. A likely contributor to this unimodality is partial voluming: single voxels that straddle the M/P border will contain both M and P neurons. Future studies may employ even higher spatial resolution to reduce partial volume effects, thereby improving mapping and voxel classification. Another possible contributor to the unimodality of response amplitude distributions is the mixing of M- and P-related BOLD signals in common vascular networks.

A second area for improvement is the classification of M and P voxels in a way that better accounts for individual differences. In our study, we defined M and P subdivisions according to a

fixed 20/80 volumetric ratio of M and P layers. However, this ratio has been shown to vary across individuals (Hickey and Guillery, 1979; Andrews et al., 1997; Selemon and Begovic, 2007), adding uncertainty to the voxel classification, especially for those voxels with M-P values near the classification boundary. This means that, in its current form, the classification method we have employed is not suitable for measuring the absolute volumes of the M and P subdivisions. In the future, more sophisticated voxel classification approaches combining functional and structural information could generate more accurate classification boundaries. For functional studies, both partial volume effects and classification limitations can be overcome to some extent by selecting only the most M-like and P-like voxels for subsequent analyses, based on the distribution of M-P values that are calculated for each voxel.

Our results suggest that both 7T and 3T field strengths can provide sufficient signal and spatial resolution for consistent M/P mapping of human LGN. We also found advantages of 7T over 3T, including: higher functional SNR; more variance explained by the GLM; higher reliability across runs; and more consistent dorsal-ventral gradients in both M and P maps across hemispheres. As all these advantages were evident for 7T voxel sizes that were similar to or smaller than the 3T voxel sizes used, they likely arise from a combination of higher MR signal at 7T and reduced partial volume effects at smaller voxel sizes. The higher SNR and reliability across runs at 7T also enable M/P localization using fewer runs compared to 3T. Therefore, researchers seeking to localize the M and P subdivisions and then conduct other experimental tasks investigating the functions of the subdivisions would benefit from the use of 7T.

The ability to noninvasively map the M and P subdivisions of human LGN presents opportunities to study the roles of these subdivisions in normal human vision as well as in clinical disorders. Since fMRI is an excellent tool for the study of large-scale brain networks, M/P mapping of the LGN enables functional investigations of parallel thalamocortical processing pathways. Modulations of LGN activity have also been observed during selective visual attention (Vanduffel et al., 2000; O'Connor et al., 2002; McAlonan et al., 2008; Schneider and Kastner, 2009; Schneider, 2011) and perceptual fluctuations during binocular rivalry (Haynes et al., 2005; Wunderlich et al., 2005), supporting the idea that the human LGN may support higher-level aspects of vision, as opposed to operating as a simple sensory relay (Kastner et al., 2006). Indeed, reciprocal interactions between cortex and thalamus are increasingly recognized as central to sensory system function (Sherman and Guillery, 2002; Briggs and Usrey, 2008). The differential roles of the M and P subdivisions in such higher-level visual functions are currently not well understood, but behavioral studies suggest different contributions from the two pathways to spatial attention (Theeuwes, 1995; Yeshurun and Levy, 2003; Cheng et al., 2004; Yeshurun, 2004; Yeshurun and Sabo, 2012) and perceptual selection (Denison and Silver, 2012). Measuring human M and P responses with fMRI during a variety of behavioral tasks is an exciting direction for future work.

Functional studies of the M and P subdivisions in healthy individuals and patient populations may additionally further our understanding of human disorders. In particular, dysfunction of the M system has been implicated in dyslexia (Demb et al., 1998) and schizophrenia (Butler and Javitt, 2005; Kandil et al., 2013), but clear physiological tests of the hypothesized links between M stream abnormalities and specific diseases have not yet materialized. Stream-specific abnormalities have also been associated with albinism (Guillery et al., 1975) and degenerative disorders including multiple sclerosis, Parkinson’s disease, and Alzheimer’s disease (Yoonessi

and Yoonessi, 2011), and better understanding of these relationships offers the potential for simple visual tests that could aid diagnosis of these disorders.

In conclusion, we have shown that high spatial resolution fMRI using optimized stimuli reliably maps the M and P subdivisions of human LGN, advancing the noninvasive study of these parallel processing pathways in the human visual system.

References

Alais D, Blake R, eds (2005) Binocular rivalry. Cambridge, MA: MIT Press.

Alais D, Parker A (2006) Independent binocular rivalry processes for motion and form. Neuron 52:911-920.

Alais D, O'Shea RP, Mesana-Alais C, Wilson IG (2000) On binocular alternation. Perception 29:1437-1445.

Alink A, Schwiedrzik CM, Kohler A, Singer W, Muckli L (2010) Stimulus predictability reduces responses in primary visual cortex. J Neurosci 30:2960-2966.

Anderson EJ, Dakin SC, Rees G (2009) Monocular signals in human lateral geniculate nucleus reflect the Craik-Cornsweet-O'Brien effect. J Vis 9:14 11-18.

Andrews TJ, Blakemore C (1999) Form and motion have independent access to consciousness. Nat Neurosci 2:405-406.

Andrews TJ, Blakemore C (2002) Integration of motion information during binocular rivalry. Vision Res 42:301-309.

Andrews TJ, Halpern SD, Purves D (1997) Correlated size variations in human visual cortex, lateral geniculate nucleus, and optic tract. J Neurosci 17:2859-2868.

Andrews TJ, Schluppeck D, Homfray D, Matthews P, Blakemore C (2002) Activity in the fusiform gyrus predicts conscious perception of Rubin's vase-face illusion. NeuroImage 17:890-901.

Baker CL, Jr., Braddick OJ (1985) Temporal properties of the short-range process in apparent motion. Perception 14:181-192.

Baker D, Graf E (2009) Natural images dominate in binocular rivalry. Proc Natl Acad Sci USA 106:5436-5441.

Blake R, Fox R (1974) Adaptation to invisible gratings and the site of binocular rivalry suppression. Nature 249:488-490.

Blake R, Overton R (1979) The site of binocular rivalry suppression. Perception 8:143-152.

Blake R, Logothetis NK (2002) Visual competition. Nat Rev Neurosci 3:13-21.

Blake R, Westendorf DH, Overton R (1980) What is suppressed during binocular rivalry? Perception 9:223-231.

Blake R, Yu K, Lokey M, Norman H (1998) Binocular rivalry and motion perception. J Cogn Neurosci 10:46-60.

Blakemore C, Nachmias J (1971) The orientation specificity of two visual after-effects. J Physiol (Lond) 213:157-174.

Bonneh Y, Sagi D, Karni A (2001) A transition between eye and object rivalry determined by stimulus coherence. Vision Res 41:981-989.

Bours RJ, Stuur S, Lankheet MJ (2007) Tuning for temporal interval in human apparent motion detection. J Vis 7:2.

Boynton GM, Engel SA, Glover GH, Heeger DJ (1996) Linear systems analysis of functional magnetic resonance imaging in human V1. J Neurosci 16:4207-4221.
Brainard DH (1997) The Psychophysics Toolbox. Spat Vis 10:433-436.
Brascamp JW, van Ee R, Pestman WR, van den Berg AV (2005) Distributions of alternation rates in various forms of bistable perception. J Vis 5:287-298.
Brascamp JW, Knapen THJ, Kanai R, van Ee R, van den Berg AV (2007) Flash suppression and flash facilitation in binocular rivalry. J Vis 7:12.11-12.
Bressler DW, Denison RN, Silver MA (2013) Effects of stimulus configuration, stimulus context, and observer state on binocular rivalry. In: The constitution of visual consciousness: lessons from binocular rivalry (Miller S, ed). Philadelphia: John Benjamins Publishing Company.
Briggs F, Usrey WM (2008) Emerging views of corticothalamic function. Curr Opin Neurobiol 18:403-407.
Briggs F, Usrey WM (2009) Parallel processing in the corticogeniculate pathway of the macaque monkey. Neuron 62:135-146.
Briggs F, Usrey WM (2011) Corticogeniculate feedback and visual processing in the primate. J Physiol 589.1:33-40.
Butler PD, Javitt DC (2005) Early-stage visual processing deficits in schizophrenia. Curr Opin Psychiatry 18:151-157.
Carlson TA, He S (2000) Visible binocular beats from invisible monocular stimuli during binocular rivalry. Curr Biol 10:1055-1058.
Carney T, Shadlen M, Switkes E (1987) Parallel processing of motion and colour information. Nature 328:647-649.
Carrasco M (2011) Visual attention: The past 25 years. Vision Res 51:1484-1525.
Chen W, Zhu XH (2001) Correlation of activation sizes between lateral geniculate nucleus and primary visual cortex in humans. Magn Reson Med 45:202-205.
Chen W, Zhu XH, Thulborn KR, Uğurbil K (1999) Retinotopic mapping of lateral geniculate nucleus in humans using functional magnetic resonance imaging. Proc Natl Acad Sci USA 96:2430-2434.
Cheng A, Eysel UT, Vidyasagar TR (2004) The role of the magnocellular pathway in serial deployment of visual attention. Eur J Neurosci 20:2188-2192.
Chong SC, Blake R (2006) Exogenous attention and endogenous attention influence initial dominance in binocular rivalry. Vision Res 46:1794-1803.
D'Souza DV, Auer T, Strasburger H, Frahm J, Lee BB (2011) Temporal frequency and chromatic processing in humans: An fMRI study of the cortical visual areas. J Vis 11:8-8.
Dayan P (1998) A hierarchical model of binocular rivalry. Neural Comput 10:1119-1135.
de Courten C, Garey LJ (1982) Morphology of the neurons in the human lateral geniculate nucleus and their normal development. A Golgi study. Exp Brain Res 47:159-171.
De Valois K, De Valois RL (2000) Color Vision. In: Seeing (De Valois K, ed), pp 129-176. San Diego, CA: Academic Press.
De Valois RL, Morgan H, Snodderly DM (1974a) Psychophysical studies of monkey vision. 3. Spatial luminance contrast sensitivity tests of macaque and human observers. Vision Res 14:75-81.
De Valois RL, Morgan HC, Polson MC, Mead WR, Hull EM (1974b) Psychophysical studies of monkey vision. I. Macaque luminosity and color vision tests. Vision Res 14:53-67.

Demb JB, Boynton GM, Best M, Heeger DJ (1998) Psychophysical evidence for a magnocellular pathway deficit in dyslexia. Vision Res 38:1555-1559.
Denison RN, Silver MA (2012) Distinct contributions of the magnocellular and parvocellular visual streams to perceptual selection. J Cogn Neurosci 24:246-259.
Denison RN, Piazza EA, Silver MA (2011) Predictive context influences perceptual selection during binocular rivalry. Front Hum Neurosci 5:166.
Denison RN, Vu A, Yacoub E, Feinberg DA, Silver MA (under review) Functional mapping of the magnocellular and parvocellular subdivisions of human LGN.
Derrington AM, Lennie P (1984) Spatial and temporal contrast sensitivities of neurones in lateral geniculate nucleus of macaque. J Physiol 357:219-240.
Diaz-Caneja E (1928) Sur l'alternance binoculaire [On binocular alternation]. Annal Ocul 165:721–731.
Doherty JR, Rao A, Mesulam MM, Nobre AC (2005) Synergistic effect of combined temporal and spatial expectations on visual attention. J Neurosci 25:8259-8266.
Dolan RJ, Fink GR, Rolls E, Booth M, Holmes A, Frackowiak RS, Friston KJ (1997) How the brain learns to see objects and faces in an impoverished context. Nature 389:596-599.
Eger E, Henson RN, Driver J, Dolan RJ (2007) Mechanisms of top-down facilitation in perception of visual objects studied by fMRI. Cereb Cortex 17:2123-2133.
Engel E (1956) The role of content in binocular resolution. Am J Psychol 69:87-91.
Enoksson P (1963) Binocular rivalry and monocular dominance studied with optokinetic nystagmus. Acta Ophthalmol (Copenh) 41:544-563.
Esterman M, Yantis S (2010) Perceptual expectation evokes category-selective cortical activity. Cereb Cortex 20:1245-1253.
Feinberg DA, Moeller S, Smith SM, Auerbach E, Ramanna S, Gunther M, Glasser MF, Miller KL, Ugurbil K, Yacoub E (2010) Multiplexed echo planar imaging for sub-second whole brain FMRI and fast diffusion imaging. PLoS ONE 5:e15710.
Fox R, Check R (1966) Forced-choice form recognition during binocular rivalry. Psychon Sci 6:471-472.
Fox R, Herrmann J (1967) Stochastic properties of binocular rivalry alternations. Percept Psychophys 2:432-436.
Fox R, Check R (1968) Detection of motion during binocular rivalry suppression. J Exp Psychol 78:388-395.
Freeman AW (2005) Multistage model for binocular rivalry. J Neurophysiol 94:4412-4420.
Freyd JJ, Finke RA (1984) Facilitation of length discrimination using real and imaged context frames. Am J Psychol 97:323-341.
Freyd JJ, Johnson JQ (1987) Probing the time course of representational momentum. J Exp Psychol Learn Mem Cogn 13:259-268.
Friston K (2005) A theory of cortical responses. Phil Trans R Soc Lond B Biol Sci 360:815-836.
Friston K, Kiebel S (2009) Predictive coding under the free-energy principle. Phil Trans R Soc Lond B Biol Sci 364:1211-1221.
Garrido MI, Kilner JM, Stephan KE, Friston KJ (2009) The mismatch negativity: a review of underlying mechanisms. Clin Neurophysiol 120:453-463.
Gershman S, Vul E, Tenenbaum J (2009) Perceptual multistability as Markov chain Monte Carlo inference. Adv Neural Inf Process Syst 22:611–619.
Gregory RL (1997) Knowledge in perception and illusion. Phil Trans R Soc Lond B Biol Sci 352:1121-1127.

Grunewald A, Bradley DC, Andersen RA (2002) Neural correlates of structure-from-motion perception in macaque V1 and MT. J Neurosci 22:6195-6207.
Guillery RW, Okoro AN, Witkop CJ (1975) Abnormal visual pathways in the brain of a human albino. Brain Res 96:373-377.
Haijiang Q, Saunders JA, Stone RW, Backus BT (2006) Demonstration of cue recruitment: change in visual appearance by means of Pavlovian conditioning. Proc Natl Acad Sci USA 103:483-488.
Hancock S, Andrews TJ (2007) The role of voluntary and involuntary attention in selecting perceptual dominance during binocular rivalry. Perception 36:288-298.
Haynes J-D, Deichmann R, Rees G (2005) Eye-specific effects of binocular rivalry in the human lateral geniculate nucleus. Nature 438:496-499.
He S, Carlson T, Chen X (2005) Parallel pathways and temporal dynamics in binocular rivalry. In: Binocular rivalry (Alais D, Blake R, eds), pp 81-100. Cambridge, MA: MIT Press.
Helmholtz, H. von (1866). *Treatise on Physiological Optics*, Vol. 3. (J.P. Southall, Ed.) New York: Dover. (English translation, 1924)
Hickey TL, Guillery RW (1979) Variability of laminar patterns in the human lateral geniculate nucleus. J Comp Neurol 183:221-246.
Hicks TP, Lee BB, Vidyasagar TR (1983) The responses of cells in macaque lateral geniculate nucleus to sinusoidal gratings. J Physiol 337:183-200.
Hohwy J, Roepstorff A, Friston K (2008) Predictive coding explains binocular rivalry: an epistemological review. Cognition 108:687-701.
Hubbard TL (2005) Representational momentum and related displacements in spatial memory: A review of the findings. Psychon Bull Rev 12:822-851.
Hubel DH, Livingstone MS (1990) Color and contrast sensitivity in the lateral geniculate body and primary visual cortex of the macaque monkey. J Neurosci 10:2223-2237.
James TW, Humphrey GK, Gati JS, Menon RS, Goodale MA (2000) The effects of visual object priming on brain activation before and after recognition. Curr Biol 10:1017-1024.
Jenkinson M, Bannister P, Brady M, Smith S (2002) Improved optimization for the robust and accurate linear registration and motion correction of brain images. NeuroImage 17:825-841.
Julesz B, Miller JE (1975) Independent spatial-frequency-tuned channels in binocular fusion and rivalry. Perception 4:125–143.
Kandil FI, Pedersen A, Wehnes J, Ohrmann P (2013) High-level, but not low-level, motion perception is impaired in patients with schizophrenia. Neuropsychology 27:60-68.
Kang M-S, Blake R (2008) Enhancement of bistable perception associated with visual stimulus rivalry. Psychon Bull Rev 15:586-591.
Kaplan E, Shapley RM (1982) X and Y cells in the lateral geniculate nucleus of macaque monkeys. J Physiol 330:125-143.
Kastner S, Schneider KA, Wunderlich K (2006) Beyond a relay nucleus: neuroimaging views on the human LGN. Prog Brain Res 155:125-143.
Kastner S, O'Connor DH, Fukui MM, Fehd HM, Herwig U, Pinsk MA (2004) Functional imaging of the human lateral geniculate nucleus and pulvinar. J Neurophysiol 91:438-448.
Kersten D, Mamassian P, Yuille A (2004) Object perception as Bayesian inference. Annu Rev Psychol 55:271-304.

Kim CY, Blake R (2005) Psychophysical magic: rendering the visible 'invisible'. Trends Cogn Sci 9:381-388.
Kleinschmidt A, Lee BB, Requardt M, Frahm J (1996) Functional mapping of color processing by magnetic resonance imaging of responses to selective P- and M-pathway stimulation. Exp Brain Res 110:279-288.
Knapen T, Paffen C, Kanai R, van Ee R (2007) Stimulus flicker alters interocular grouping during binocular rivalry. Vision Res 47:1-7.
Knill DC, Pouget A (2004) The Bayesian brain: the role of uncertainty in neural coding and computation. Trends Neurosci 27:712-719.
Kovács I, Papathomas TV, Yang M, Fehér A (1996) When the brain changes its mind: interocular grouping during binocular rivalry. Proc Natl Acad Sci USA 93:15508-15511.
Kveraga K, Ghuman AS, Bar M (2007) Top-down predictions in the cognitive brain. Brain Cogn 65:145-168.
Lee SH, Blake R (1999) Rival ideas about binocular rivalry. Vision Res 39:1447-1454.
Lee SH, Blake R (2002) V1 activity is reduced during binocular rivalry. J Vis 2:618-626.
Lee SH, Blake R (2004) A fresh look at interocular grouping during binocular rivalry. Vision Res 44:983-991.
Lee SH, Blake R, Heeger DJ (2005) Traveling waves of activity in primary visual cortex during binocular rivalry. Nat Neurosci 8:22-23.
Lehky SR, Maunsell JH (1996) No binocular rivalry in the LGN of alert macaque monkeys. Vision Res 36:1225-1234.
Leopold DA, Logothetis NK (1996) Activity changes in early visual cortex reflect monkeys' percepts during binocular rivalry. Nature 379:549-553.
Leopold DA, Wilke M, Maier A, Logothetis NK (2002) Stable perception of visually ambiguous patterns. Nat Neurosci 5:605-609.
Levelt WJ (1967) Note on the distribution of dominance times in binocular rivalry. Brit J Psychol 58:143-145.
Liebert RM, Burk B (1985) Voluntary control of reversible figures. Percept Motor Skills 61:1307-1310.
Liu C-SJ, Bryan RN, Miki A, Woo JH, Liu GT, Elliott MA (2006) Magnocellular and parvocellular visual pathways have different blood oxygen level-dependent signal time courses in human primary visual cortex. Am J Neuroradiol 27:1628-1634.
Livingstone MS, Hubel DH (1987) Psychophysical evidence for separate channels for the perception of form, color, movement, and depth. J Neurosci 7:3416-3468.
Livingstone MS, Hubel DH (1988) Segregation of form, color, movement, and depth: anatomy, physiology, and perception. Science 240:740-749.
Logothetis NK (1998) Single units and conscious vision. Phil Trans R Soc Lond B Biol Sci 353:1801-1818.
Logothetis NK (2008) What we can do and what we cannot do with fMRI. Nature 453:869-878.
Logothetis NK, Schall JD (1989) Neuronal correlates of subjective visual perception. Science 245:761-763.
Logothetis NK, Schall JD (1990) Binocular motion rivalry in macaque monkeys: eye dominance and tracking eye movements. Vision Res 30:1409-1419.
Logothetis NK, Wandell BA (2004) Interpreting the BOLD signal. Annu Rev Physiol 66:735-769.

Logothetis NK, Leopold DA, Sheinberg DL (1996) What is rivalling during binocular rivalry? Nature 380:621-624.
Logothetis NK, Schiller PH, Charles ER, Hurlbert AC (1990) Perceptual deficits and the activity of the color-opponent and broad-band pathways at isoluminance. Science 247:214-217.
Logothetis NK, Pauls J, Augath M, Trinath T, Oeltermann A (2001) Neurophysiological investigation of the basis of the fMRI signal. Nature 412:150-157.
Long GM, Toppino TC (2004) Enduring interest in perceptual ambiguity: alternating views of reversible figures. Psychol Bull 130:748-768.
Maloney LT, Dal Martello MF, Sahm C, Spillmann L (2005) Past trials influence perception of ambiguous motion quartets through pattern completion. Proc Natl Acad Sci USA 102:3164-3169.
Maunsell JH, Ghose GM, Assad JA, McAdams CJ, Boudreau CE, Noerager BD (1999) Visual response latencies of magnocellular and parvocellular LGN neurons in macaque monkeys. Vis Neurosci 16:1-14.
McAlonan K, Cavanaugh J, Wurtz RH (2008) Guarding the gateway to cortex with attention in visual thalamus. Nature 456:391-394.
Melloni L, Schwiedrzik CM, Müller N, Rodriguez E, Singer W (2011) Expectations change the signatures and timing of electrophysiological correlates of perceptual awareness. J Neurosci 31:1386-1396.
Meng M, Tong F (2004) Can attention selectively bias bistable perception? Differences between binocular rivalry and ambiguous figures. J Vis 4:539-551.
Merigan WH (1989) Chromatic and achromatic vision of macaques: role of the P pathway. J Neurosci 9:776-783.
Merigan WH, Maunsell JH (1990) Macaque vision after magnocellular lateral geniculate lesions. Vis Neurosci 5:347-352.
Merigan WH, Maunsell JH (1993) How parallel are the primate visual pathways? Annu Rev Neurosci 16:369-402.
Merigan WH, Katz LM, Maunsell JH (1991) The effects of parvocellular lateral geniculate lesions on the acuity and contrast sensitivity of macaque monkeys. J Neurosci 11:994-1001.
Mitchell JF, Stoner GR, Reynolds JH (2004) Object-based attention determines dominance in binocular rivalry. Nature 429:410-413.
Moeller S, Yacoub E, Olman CA, Auerbach E, Strupp J, Harel N, Ugurbil K (2010) Multiband multislice GE-EPI at 7 tesla, with 16-fold acceleration using partial parallel imaging with application to high spatial and temporal whole-brain fMRI. Magn Reson Med 63:1144-1153.
Moreno-Bote R, Knill DC, Pouget A (2011) Bayesian sampling in visual perception. Proc Natl Acad Sci USA 108:12491-12496.
Mullen KT, Dumoulin SO, Hess RF (2008) Color responses of the human lateral geniculate nucleus: selective amplification of S-cone signals between the lateral geniculate nucleus and primary visual cortex measured with high-field fMRI. Eur J Neurosci 28:1911-1923.
Mullen KT, Thompson B, Hess RF (2010) Responses of the human visual cortex and LGN to achromatic and chromatic temporal modulations: an fMRI study. J Vis 10:13.
Mumford D (1992) On the computational architecture of the neocortex. II. The role of cortico-cortical loops. Biol Cybern 66:241-251.

Murray SO, Kersten D, Olshausen BA, Schrater P, Woods DL (2002) Shape perception reduces activity in human primary visual cortex. Proc Natl Acad Sci USA 99:15164-15169.
Nassi JJ, Callaway EM (2009) Parallel processing strategies of the primate visual system. Nat Rev Neurosci 10:360-372.
Nestares O, Heeger DJ (2000) Robust multiresolution alignment of MRI brain volumes. Magn Reson Med 43:705-715.
Nguyen VA, Freeman AW, Alais D (2003) Increasing depth of binocular rivalry suppression along two visual pathways. Vision Res 43:2003-2008.
O'Connor DH, Fukui MM, Pinsk MA, Kastner S (2002) Attention modulates responses in the human lateral geniculate nucleus. Nat Neurosci 5:1203-1209.
Ooi TL, He ZJ (1999) Binocular rivalry and visual awareness: the role of attention. Perception 28:551-574.
Ozkan K, Braunstein ML (2009) Predominance of ground over ceiling surfaces in binocular rivalry. Atten Percept Psychophys 71:1305-1312.
Parker AJ, Krug K (2003) Neuronal mechanisms for the perception of ambiguous stimuli. Curr Opin Neurobiol 13:433-439.
Parkes LM, Fries P, Kerskens CM, Norris DG (2004) Reduced BOLD response to periodic visual stimulation. NeuroImage 21:236-243.
Pearson J, Brascamp J (2008) Sensory memory for ambiguous vision. Trends Cogn Sci 12:334-341.
Pearson J, Tadin D, Blake R (2007) The effects of transcranial magnetic stimulation on visual rivalry. J Vis 7:2 1-11.
Pearson J, Clifford CW, Tong F (2008) The functional impact of mental imagery on conscious perception. Curr Biol 18:982-986.
Pelli DG (1997) The VideoToolbox software for visual psychophysics: transforming numbers into movies. Spat Vis 10:437-442.
Perrett DI, Xiao D, Barraclough NE, Keysers C, Oram MW (2009) Seeing the future: Natural image sequences produce "anticipatory" neuronal activity and bias perceptual report. Q J Exp Psychol 62:2081-2104.
Perry VH, Oehler R, Cowey A (1984) Retinal ganglion cells that project to the dorsal lateral geniculate nucleus in the macaque monkey. Neuroscience 12:1101-1123.
Peterson MA (1986) Illusory concomitant motion in ambiguous stereograms: evidence for nonstimulus contributions to perceptual organization. J Exp Psychol Hum Percept Perform 12:50-60.
Polonsky A, Blake R, Braun J, Heeger DJ (2000) Neuronal activity in human primary visual cortex correlates with perception during binocular rivalry. Nat Neurosci 3:1153-1159.
Power JD, Barnes KA, Snyder AZ, Schlaggar BL, Petersen SE (2012) Spurious but systematic correlations in functional connectivity MRI networks arise from subject motion. NeuroImage 59:2142-2154.
Rao RP, Ballard DH (1999) Predictive coding in the visual cortex: a functional interpretation of some extra-classical receptive-field effects. Nat Neurosci 2:79-87.
Reid RC, Shapley RM (2002) Space and time maps of cone photoreceptor signals in macaque lateral geniculate nucleus. J Neurosci 22:6158-6175.
Roach NW, McGraw PV, Johnston A (2011) Visual motion induces a forward prediction of spatial pattern. Curr Biol 21:740-745.

Robson JG (1966) Spatial and temporal contrast-sensitivity functions of the visual system. J Opt Soc Am 56:1141-1142.
Rubin E (1915) Synsoplevede Figurer. Copenhagen: Gyldenhal.
Schiller PH, Malpeli JG (1978) Functional specificity of lateral geniculate nucleus laminae of the rhesus monkey. J Neurophysiol 41:788-797.
Schiller PH, Logothetis NK, Charles ER (1990) Functions of the colour-opponent and broad-band channels of the visual system. Nature 343:68-70.
Schneider KA (2011) Subcortical mechanisms of feature-based attention. J Neurosci 31:8643-8653.
Schneider KA, Kastner S (2009) Effects of sustained spatial attention in the human lateral geniculate nucleus and superior colliculus. J Neurosci 29:1784-1795.
Schneider KA, Richter MC, Kastner S (2004) Retinotopic organization and functional subdivisions of the human lateral geniculate nucleus: a high-resolution functional magnetic resonance imaging study. J Neurosci 24:8975-8985.
Schrater PR, Sundareswara R (2007) Theory and dynamics of perceptual bistability. Adv Neural Inf Process Syst 19:1217-1224.
Sekuler R, Ball K (1977) Mental set alters visibility of moving targets. Science 198:60-62.
Selemon LD, Begovic A (2007) Stereologic analysis of the lateral geniculate nucleus of the thalamus in normal and schizophrenic subjects. Psychiat Res 151:1-10.
Sengpiel F (1997) Binocular rivalry: ambiguities resolved. Curr Biol 7:R447-450.
Setsompop K, Gagoski BA, Polimeni JR, Witzel T, Wedeen VJ, Wald LL (2012) Blipped-controlled aliasing in parallel imaging for simultaneous multislice echo planar imaging with reduced g-factor penalty. Magn Reson Med 67:1210-1224.
Shapley R (1990) Visual sensitivity and parallel retinocortical channels. Annu Rev Psychol 41:635-658.
Sheinberg DL, Logothetis NK (1997) The role of temporal cortical areas in perceptual organization. Proc Natl Acad Sci USA 94:3408-3413.
Sherman SM, Guillery RW (2002) The role of the thalamus in the flow of information to the cortex. Phil Trans R Soc Lond B Biol Sci 357:1695-1708.
Sherman SM, Guillery RW (2006) Exploring the thalamus and its role in cortical function. Cambridge, MA: The MIT Press.
Shimono M, Kitajo K, Takeda T (2011) Neural processes for intentional control of perceptual switching: a magnetoencephalography study. Hum Brain Mapp 32:397-412.
Silver MA, Logothetis N (2007) Temporal frequency and contrast tagging bias the type of competition in interocular switch rivalry. Vision Res 47:532-543.
Sincich LC, Horton JC (2005) The circuitry of V1 and V2: integration of color, form, and motion. Annu Rev Neurosci 28:303-326.
Smith AM, Lewis BK, Ruttimann UE, Ye FQ, Sinnwell TM, Yang Y, Duyn JH, Frank JA (1999) Investigation of low frequency drift in fMRI signal. NeuroImage 9:526-533.
Spratling MW (2008) Predictive coding as a model of biased competition in visual attention. Vision Res 48:1391-1408.
Spratling MW (2010) Predictive coding as a model of response properties in cortical area V1. J Neurosci 30:3531-3543.
Stein J, Walsh V (1997) To see but not to read; the magnocellular theory of dyslexia. Trends Neurosci.

Sterzer P, Frith C, Petrovic P (2008) Believing is seeing: expectations alter visual awareness. Curr Biol 18:R697-698.
Straw AD (2008) Vision egg: an open-source library for realtime visual stimulus generation. Front Neuroinform 2:4.
Summerfield C, Koechlin E (2008) A neural representation of prior information during perceptual inference. Neuron 59:336-347.
Summerfield C, Egner T (2009) Expectation (and attention) in visual cognition. Trends Cogn Sci 13:403-409.
Summerfield C, Egner T, Greene M, Koechlin E, Mangels J, Hirsch J (2006) Predictive codes for forthcoming perception in the frontal cortex. Science 314:1311-1314.
Sundareswara R, Schrater PR (2008) Perceptual multistability predicted by search model for Bayesian decisions. J Vis 8:12.11-19.
Theeuwes J (1995) Abrupt luminance change pops out; abrupt color change does not. Percept Psychophys 57:637-644.
Tong F, Engel SA (2001) Interocular rivalry revealed in the human cortical blind-spot representation. Nature 411:195-199.
Tong F, Meng M, Blake R (2006) Neural bases of binocular rivalry. Trends Cogn Sci 10:502-511.
Toppino TC (2003) Reversible-figure perception: mechanisms of intentional control. Percept Psychophys 65:1285-1295.
Treue S, Husain M, Andersen RA (1991) Human perception of structure from motion. Vision Res 31:59-75.
Uğurbil K, Hu X, Chen W, Zhu XH, Kim SG, Georgopoulos A (1999) Functional mapping in the human brain using high magnetic fields. Phil Trans R Soc Lond B Biol Sci 354:1195-1213.
Ungerleider LG, Mishkin M (1982) Two cortical visual systems. In: Analysis of visual behaviour (Ingle DJ, Goodale M, Mansfield RJW, eds), pp 549-586. Cambridge, MA: MIT Press.
van Boxtel JJA, Knapen T, Erkelens CJ, van Ee R (2008) Removal of monocular interactions equates rivalry behavior for monocular, binocular, and stimulus rivalries. J Vis 8:13.11-17.
van de Grind WA, van Hof P, van der Smagt MJ, Verstraten FA (2001) Slow and fast visual motion channels have independent binocular-rivalry stages. Proc R Soc Lond, Ser B: Biol Sci 268:437-443.
Van Horn SC, Erişir A, Sherman SM (2000) Relative distribution of synapses in the A-laminae of the lateral geniculate nucleus of the cat. J Comp Neurol 416:509-520.
Vanduffel W, Tootell RB, Orban GA (2000) Attention-dependent suppression of metabolic activity in the early stages of the macaque visual system. Cereb Cortex 10:109-126.
Wales R, Fox R (1970) Increment detection thresholds during binocular rivalry suppression. Percept Psychophys 8:90-94.
Watamaniuk SN, McKee SP (1995) Seeing motion behind occluders. Nature 377:729-730.
Weiss Y, Simoncelli EP, Adelson EH (2002) Motion illusions as optimal percepts. Nat Neurosci 5:598-604.
Wheatstone C (1838) On some remarkable, and hitherto unobserved, phenomena of binocular vision. Phil Trans R Soc Lond 128:371-394.
Wilke M, Logothetis NK, Leopold DA (2006) Local field potential reflects perceptual suppression in monkey visual cortex. Proc Natl Acad Sci USA 103:17507-17512.

Wilke M, Mueller K-M, Leopold DA (2009) Neural activity in the visual thalamus reflects perceptual suppression. Proc Natl Acad Sci USA 106:9465-9470.
Wilson HR (2003) Computational evidence for a rivalry hierarchy in vision. Proc Natl Acad Sci USA 100:14499-14503.
Wunderlich K, Schneider KA, Kastner S (2005) Neural correlates of binocular rivalry in the human lateral geniculate nucleus. Nat Neurosci 8:1595-1602.
Yang Y, Rose D, Blake R (1992) On the variety of percepts associated with dichoptic viewing of dissimilar monocular stimuli. Perception 21:47-62.
Yeshurun Y (2004) Isoluminant stimuli and red background attenuate the effects of transient spatial attention on temporal resolution. Vision Res 44:1375-1387.
Yeshurun Y, Levy L (2003) Transient spatial attention degrades temporal resolution. Psychol Sci 14:225-231.
Yeshurun Y, Sabo G (2012) Differential effects of transient attention on inferred parvocellular and magnocellular processing. Vision Res 74:21-29.
Yoonessi A, Yoonessi A (2011) Functional assessment of magno, parvo and konio-cellular pathways; current state and future clinical applications. J Opthalmic Vis Res 6:119-126.
Zarahn E, Aguirre GK, D'Esposito M (1997) Empirical analyses of BOLD fMRI statistics. I. Spatially unsmoothed data collected under null-hypothesis conditions. NeuroImage 5:179-197.
Zhou G, Zhang L, Liu J, Yang J, Qu Z (2010) Specificity of face processing without awareness. Conscious Cogn 19:408-412.